Fatigue Safety Factors for Dynamic Power Cables

A reliability based approach

Olivier de Jong

Master of Science Thesis

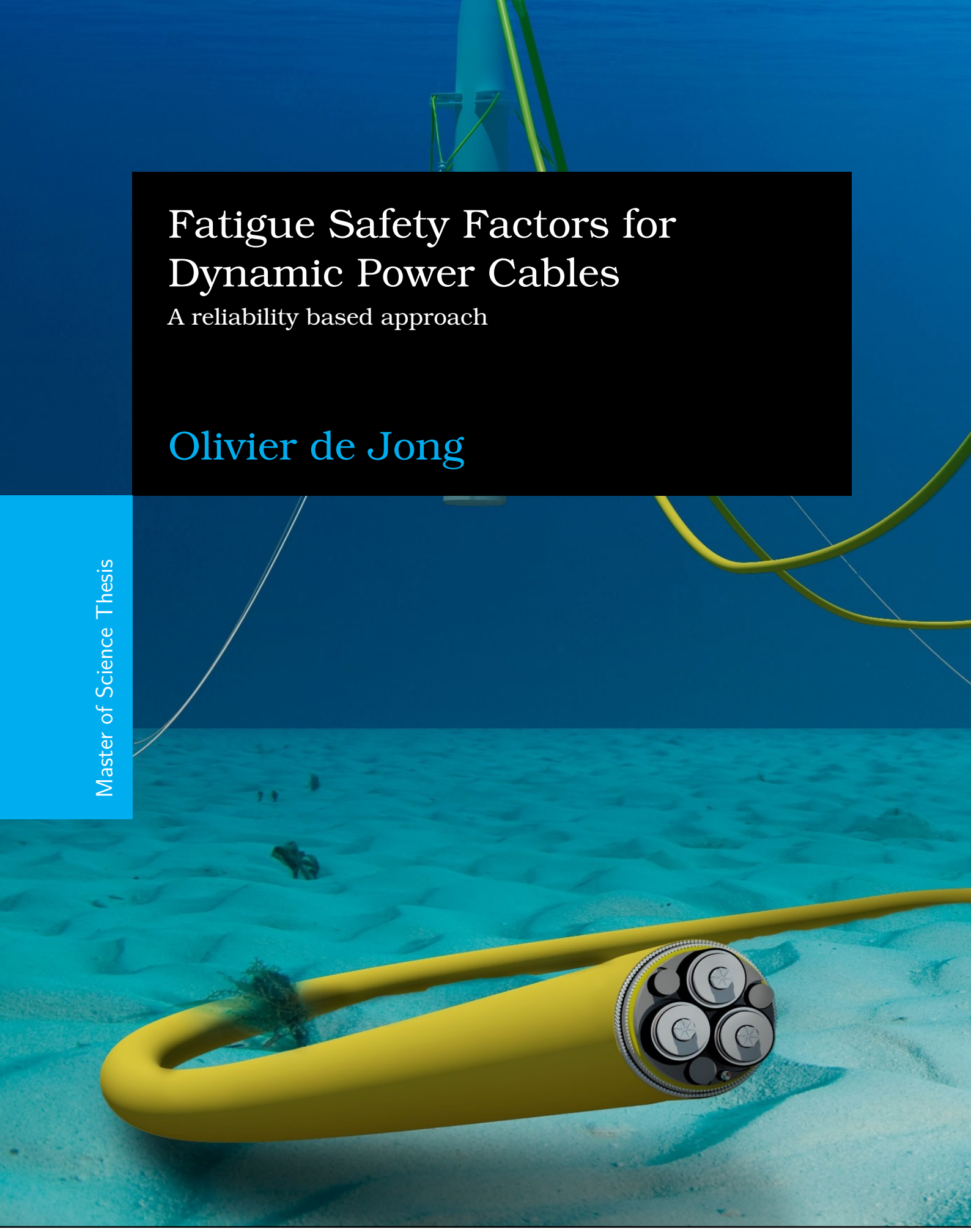

TU Delft Delft University of Technology

Offshore & Dredging Engineering

Fatigue Safety Factors for Dynamic Power Cables

A reliability based approach

Master of Science Thesis

For the degree of Master of Science in Offshore & Dredging Engineering
at Delft University of Technology

Olivier de Jong

August 10, 2022

Student number:	4551494	
Project duration:	November 2021 - August 2022	
Graduation committee:	Dr. O. J. Colomés Gené	TU Delft, Chair
	Dr. X. Jiang	TU Delft, Supervisor
	Dr. ir. S. Schreier	TU Delft, Quality control
	Ir. R. van Driel	Mocean Offshore, Company supervisor

Faculty of Mechanical, Maritime and Materials Engineering (3mE) · Delft University of Technology

Cover: Illustration by Joshua Bauer, NREL 49065

Abstract

In contrast to traditional power cables for bottom-founded offshore wind turbines, power cables for floating wind turbines penetrate the water column and are exposed to cyclic loading. Due to the dynamic nature of the cable loading, the cables are prone to fatigue failure. Since the evaluation of the fatigue life of complex structures, like power cables, has to deal with a certain degree of uncertainty, fatigue safety factors are introduced. These factors ensure a desired probability of failure based on the degree of uncertainty present in the modeling of the fatigue life. Limited experience in the evaluation of the fatigue life of dynamic power cables is found in the literature, and no sources have been found attempting to calibrate the prescribed fatigue safety factor. Currently, a fatigue safety factor of 10 is advised. This implies that there is much room for reduction in the uncertainties, meaning that there is a potential for making the cables cheaper and more reliable, which will in turn make floating wind energy more competitive with other (renewable) energy sources.

Due to the lack of available literature, comparisons with umbilicals and flexible risers are made. Different methods for the evaluation of fatigue safety factors for flexible risers are evaluated, and judged on how applicable they are to use on dynamic power cables. It is found that a reliability based approach is most suitable for this purpose.

A case study is carried out for a presently relevant scenario to put the proposed method into practice. It is concluded that for a safety class corresponding to a required maximum probability of failure of 10^{-3} in the last operational year, a fatigue safety factor of 3.5 is needed. This safety factor is required for the wave-load induced fatigue, as opposed to the seabed induced fatigue, to which the dynamic power cable is less vulnerable nearby the touch-down zone.

The main parameter driving the uncertainty in the fatigue analysis is the sensitivity of the local stress analysis, which is in line with what has been found for similar studies for the oil & gas industry. In order to bring down the cost of dynamic power cables, and make them more reliable, more accurate local stress analysis models need to be developed, being validated against test data, in order to reduce the standard deviation of the local stress computation.

Preface

I always heard horror storied about the master thesis, and before starting, I was expecting 9 long months ahead. The contrary turned out to be true, and I feel confident in saying these months have been the most fun and interesting ones of my academic career.
This was first and foremost due to the fact that Mocean Offshore gave me the unique opportunity to completely define my own topic. Starting with a very broad literature study into the floating wind industry, I gradually narrowed down the scope to meet my personal interests. My supervisors were of invaluable help in this process, having great sparring sessions about what a feasible scope would be. I would like to thank Oriol, Robert and Xiaoli for their time and effort spent on helping my thesis become what it is now.
Next, a big thanks goes out to all of the other people at Mocean Offshore, who have really been amazing. Apart from being a fun group of people, everybody was always more than happy to help me out when I was stuck.
Lastly, a special thanks is in order to the engineers at Femto Engineering, for putting me back on the path through the forest, that is finite element analysis.
All in all, it has been a great experience, on which I can look back with pride and joy.

Thank all!!

Table of Contents

List of Figures

List of Tables

Chapter 1

Introduction

1-1 Background

In the present day, much focus is being put on the generation of clean and sustainable energy. The offshore sector lends itself well to accommodate this need, since the available offshore space is vast and there is much energy to be captured. Traditional offshore wind energy is already a well established technology, and more turbines are being installed every day. However, due to the ever growing demand for energy, the offshore wind industry is forced to expand its scope to deeper waters, making traditional monopiles or jacket sub-structures less feasible. The current solution to overcome this, is the deployment of floating wind turbines. This enables the industry to deploy turbines in a much larger portion of the sea, not being limited to shallow, near-shore areas.
This new development brings with it new challenges. One of which is the power cable, transferring current from the turbines to offshore sub-stations. Cable related problems in bottom-founded wind farms are already commonly reported, even though these cables are not exposed to the motions of floaters, or wave induced forces. A study from Catapult [1] showed that 83% of the offshore wind farms constructed between 2007 and 2014 had cable related issues. With all of these cables being static ones, it is paramount that the industry learns to better understand cable failure before moving to the dynamically excited dynamic cables. This is not only vital from an operational point of view, but more so from an economic point of view. Floating offshore wind has much to gain in terms of Levelized Cost Of Energy (LCOE) to become competitive with traditional offshore wind. Figure 1-1 shows a prediction for the upcoming decades of the LCOE of onshore wind, bottom-founded wind and floating wind. It can be seen that not only floating wind has a higher expected median, but there is a much larger spread on the expected cost.

While many problems concerning offshore power cables have already been addressed in the development of traditional bottom-founded offshore wind energy, one of the new problems unique to dynamic power cables is fatigue. The fatigue lifetime prediction of cables and/or risers is a complex process. Despite the many years of experience in the oil & gas sector, it

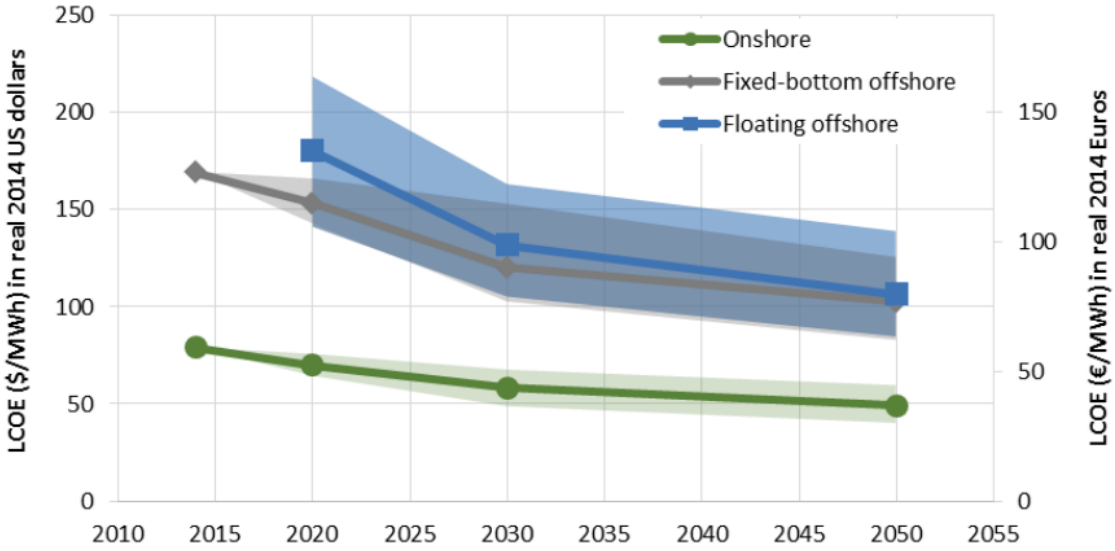

Figure 1-1: Levelized cost of energy of different types of wind energy [2]

is still a domain that deals with large uncertainties. Now that a shift is being made from offshore oil & gas to offshore renewables, also a different design philosophy for slender flexible sub-sea structures needs to be adopted. For oil rigs, these risers/umbilicals were one of a kind, unique to every platform. For floating wind, and other floating renewable energy sources, this is not the case. Hundreds of identical cables will be made, and a better ability to predict the internal mechanics can significantly bring down both the Operational Expenditure (OPEX) and the Capital Expenditure (CAPEX).
For now, in 2022, few floating wind farms are operational. However, Scotland, one of the front runners in offshore wind, recently announced that they aim to start the production of around 15 GW of floating offshore wind by 2030, putting a lot of pressure on the proper understanding of dynamic power cables.
In the rest of this chapter, the background information regarding dynamic power cables, fatigue and fatigue safety factors will be discussed.

1-1-1 Dynamic power cables

In this section the different types and aspects of Dynamic Power Cable (DPC)'s will be discussed.

1-1-1-1 Components in dynamic cables

The two most common sub-sea power cables are three phase Alternating Current (AC) cables and single core Direct Current (DC) cables. These are both widely used in static applications, and have also found their use in more recent dynamic purposes. In figure 1-2 a cross section of both of these cables is shown.

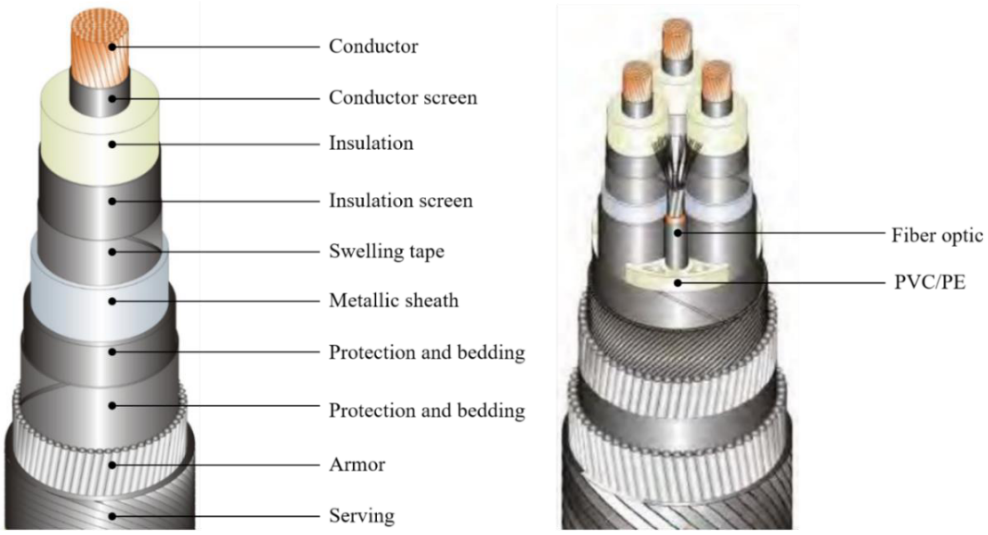

Figure 1-2: Cross section of DC (left) and AC (right) cable [3]

Since the sub-sea environment is much harsher and less predictable than the land environment, many layers, with different purposes, are required for a proper sub-sea cable design. Below, each layer is listed, with its purpose.

- **Conductor**: The conductor is the part of the cable conducting the current. In sub-sea applications this part is usually made of multiple stranded conductors, making it more flexible. The conductor can be made out of aluminum or copper. Even though copper is more expensive, it is more conductive and thus needs a smaller diameter to transfer the same current. Because of this, less surrounding material is needed. Both materials are used in different sub-sea applications [4].
- **Conductor screen**: If the insulation would be added onto the conductor directly, the geometric imperfections would result in high local stresses. The conductor screen makes for a smooth outer diameter, preventing local stresses [4].
- **Insulation**: The insulation ensures that strands with potential differences do not get into contact and short-circuit. Cross-Linked Polyethylene (XLPE) is the most common material used for insulation [4]. A failure phenomenon for XLPE is so-called water-treeing. Under the presence of water and an electric field, a defect shaped like a tree can come to existence.
- **Insulation screen**: The insulation screen has the same function on the insulation as the conductor screen has on the conductor.
- **Swelling tape**: Swelling tape has two applications. It functions as a radial water buffer for moisture coming in via the outer diameter of the cable. This is done by absorbing the moisture, and delaying it from reaching the insulation material. This way the possibility of water treeing is delayed [5]. It also functions as a longitudinal water barrier. If water comes in at some point in the cable, and tries to travel along the cable, the swelling tape will absorb this water and expand. Because of it expansion, it blocks the water from further invasion of the cable.

- **Metallic sheath**: The metallic sheath is responsible for making the cable water tight. Different metals have been used for this. Lead was one of the first, making the cable completely impregnable for water . Lead is however susceptible to micro-cracking under bending, and thus vulnerable to fatigue loading [4].
  Aluminum is another material used for sheaths. Different ways of sealing aluminum around the cable exist like extruded, welded or laminated. Even though the aluminum is impermeable, the seems of the sheaths are weak points. Depending of the technique used, and the quality, some humidity might come in over the design life of the cable. Copper sheaths can be made by welding or from corrugated copper strips. Copper is very fatigue resistant, and is thus suitable for dynamic cables [4].

- **Protection and Bedding**: This part protects the metallic sheath from damage from the armor [3].

- **Armor**: The armor is the main load bearing component in sub-sea cables. It also functions as a shield against wear from external factors like the sea-bottom. The armor is wound around the cable to form a helical pattern. This way axial forces are translated into torsional forces, and reduce the bending stiffness. By winding two separate helical armors in opposing directions, the induced torsion is cancelled out by the two layers.

- **Serving**: The armor is usually coated to prevent corrosion from sea water. To prevent this coating form being scratched and damaged, a outer serving layer is added to protect the armor. This serving can be made from polymers or wound yarn. Wound yarn is designed to allow seawater into the armor, whereas a polymeric serving keeps seawater out [4].

Furthermore, auxiliaries like optical fibers can be added, and filler material in case of three strand cables to maintain a circular outer shape.

1-1-1-2 Design types

There is a distinction between different types of cable designs. There are "wet" and "dry" cable designs, and combinations of the two called semi-wet/semi-dry cable designs, see figure 1-3. According to Cigre, "A wet design allows water to migrate into the cable insulation and the conductor" [6]. This means that less/no effort is made to keep water out of the cable, making it cheaper and thinner, but also more prone to failure. The combination of water in the insulating layer and an electrical current can lead to water-treeing. Water-treeing, in turn, can lead to cable failure if gone undetected. In order to prevent this from happening, but still employing wet cable design, different requirements are necessary for the insulation material, making it more expensive.
In a dry cable design, a lead or corrugated copper/aluminum layer is formed around the insulating layer. This prevents water molecules from entering the cable. Since no water can enter, cheaper insulating materials can be used in comparison to the wet cable designs, because they do not need to be water retarding. For dynamic applications of power cables, lead is not suitable since it is prone to micro-cracking under bending [3].

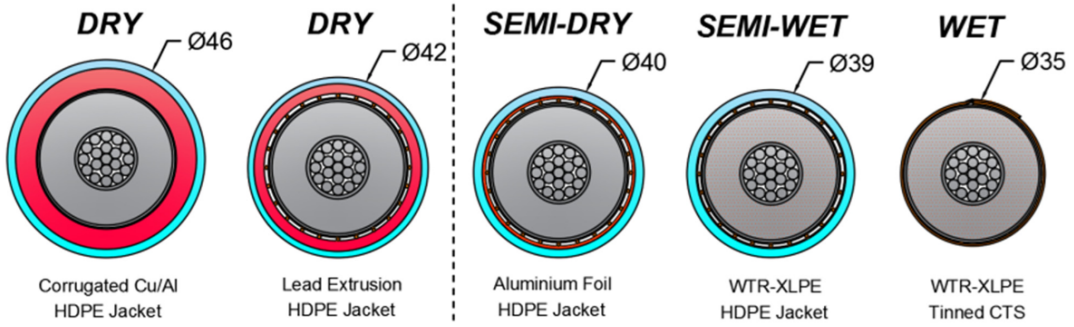

Figure 1-3: Different cable designs [7]

1-1-2 Fatigue

Fatigue analysis are mostly based on S-N curves. These curves show how many cycles N of load S can be survived until failure. An example of such a curve is shown in figure 1-4. A distinction is made between Low Cycle Fatigue (LCF) and High Cycle Fatigue (HCF). LCF corresponds to loads that should not happen too often like structural responses to hurricane conditions. HCF corresponds to daily loads like wave loads under common circumstances [8].

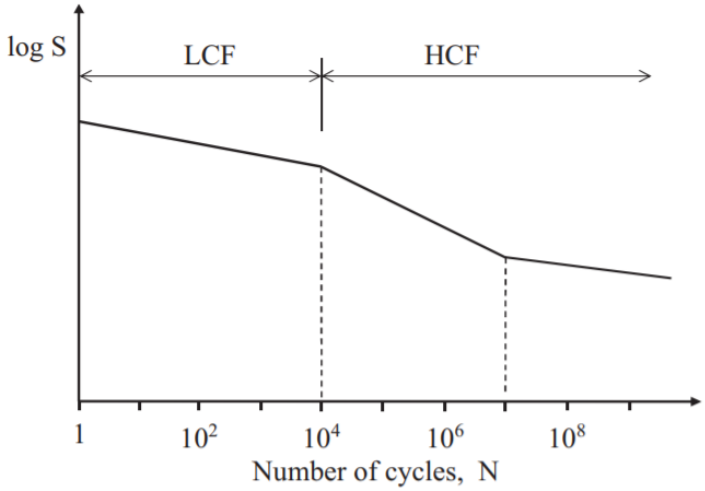

Figure 1-4: S-N curve example[8]

These curves only show how many cycles of a specific load can be resisted. The Palmgren-Miner rule assumes that the damage is linearly cumulative, and the fatigue life can thus be calculated according to equation 1-1 [8].

$$D = \sum_{i=1}^{k} \frac{n_i}{N_i} \leq \eta \tag{1-1}$$

Here D is the accumulated damage, n_i the number of experienced stress cycles in block i, and N_i the number of stress cycles in block i at failure. k indicates the amount of blocks into which the recorded stresses have been placed, with width $\Delta\sigma_i$. η is the usage factor, equal

to 1/Fatigue Safety Factor (FSF). According to [8], the Palmgren-Miner rule is not perfect, but since it is so simple to use, and gives an acceptable accuracy, it has become the standard in evaluating variable stress loadings. This method by itself would suffice if the system being evaluated were only subjected to constant sinusoidal loads. In reality, measurement data looks more like figure 1-5.

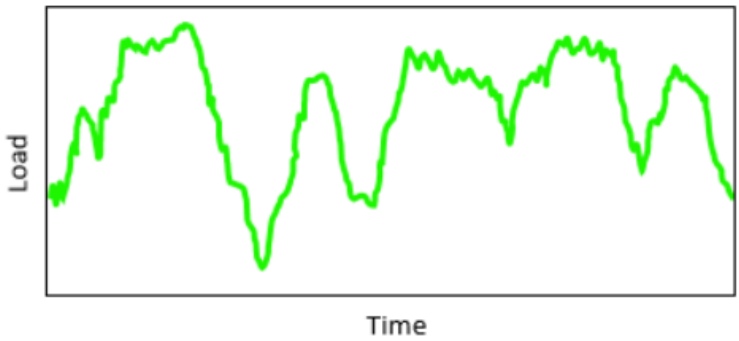

Figure 1-5: Example of raw measurement data [9]

To still be able to perform a fatigue analysis, a method called rainflow counting is used. The raw data gets filtered for hysteresis, and the peaks and valleys are identified, since only stress amplitude are of interest. What is left, is shown in figure 1-6.

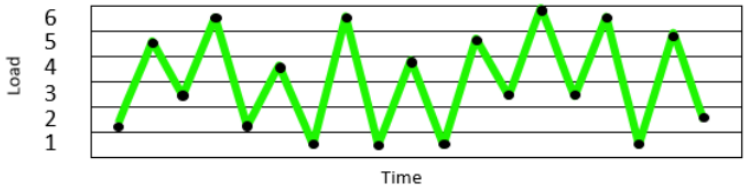

Figure 1-6: Peak-valley filtered data [9]

Different algorithms exist to evaluate the filtered results. All results can be recorded in a list with stress amplitudes and the corresponding number of cycles, which can be used in combination with equation 1-1 to evaluate the total damage.

1-1-3 Fatigue safety factor

DPC's will have to overcome the same problems as static cables, with the addition of problems related to motions, and wave induced forces. One of these problems is fatigue failure of dynamic power cables. Fatigue failure is a common topic of research, especially in the offshore industry, because of the periodic nature of the environmental loads. Fatigue is generally well understood, and for simple structures the fatigue life can be predicted rather accurately. However, as structures become more complex, and more assumptions need to be made when modelling fatigue, the accuracy of the fatigue life prediction drops. In order to account for uncertainties in the prediction of fatigue failure, or any kind of failure, safety factors are introduced. Models with a high degree of uncertainty require a high safety factor to ensure a desirable probability of failure.

For electrical power cables used in sub-sea applications, [10] states that the safety factor of the fatigue life "shall not be smaller than 10 unless otherwise agreed between manufacturer and purchaser". No further argumentation or proof for this is being given in the recommended practice. From private contact with DNV, it was clarified that the FSF for sub-sea power cables, originates from the FSF used for sub-sea umbilicals, as specified in [11] and [12]. Furthermore it was mentioned that "there has not been any calibration performed for the design fatigue factor for power cables", and that a joint industry project about the reliability of floating offshore wind is being initiated in the first half of 2022. The FSF of the power cables will be part of the scope [13].

Other slender flexible sub-sea structures which may have resemblance to dynamic power cables, are flexible risers. Despite being mostly hollow, and less complicated in cross-sectional build-up, loads and requirements might be comparable to that of dynamic power cables. [14] states 3 different FSF's, corresponding to different safety classes. These FSF's are 3, 6 and 10, corresponding to safety classes low, normal and high respectively. The safety classes are defined in [15] as follows:

- **Low:** "Where failure implies insignificant risk of human injury and minor environmental and economic consequences".
- **Medium:** "Where failure implies low risk of human injury, minor environmental pollution or high economic or political consequences"
- **High:** "Classification for operating conditions where failure implies risk of human injury, significant environmental pollution or very high economic or political consequences"

If dynamic power cables were to be classified in one of the safety classes, it would most likely be in the "low" class, corresponding to a FSF of 3. [15] offers no further substantiation for the values 3, 6 and 10.
In [16], the FSF of a flexible riser of "at least 10" is recommended, making reference to [17] and [11] , which in turn provides no argumentation for the FSF being 10.

As far as design codes and recommended practices for flexible sub-sea cables or pipelines go, there seems to be a large spread, 3 or 10, for the FSF that could apply for dynamic power cables. With neither value having any mathematical or physical backing-up.

According to [18], the value of 10 has an origin as safety factor in jacket design, and has now become industry standard. [19] is in line with this, arguing that in the early days of the offshore industry, 2 was a common FSF. As the industry moved to deeper waters, this safety factor was increased.

1-2 Problem statement

It is clear from section 1-1-3 that there is a poorly/no calibrated FSF available for DPC's, and comparable structures in the oil & gas industry, available in the recommended practices

provided by DNV. While this might not have been a big issue for the oil and gas industry, due to the uniqueness of every cable, and its small contribution to the LCOE, this is different for the offshore renewable energy sector. With cables expected to be around 13% of the total LCOE for floating wind [20] (compared to 11% for bottom founded), it is vital that the fatigue failure is better understood. Both in order to decrease the CAPEX by being able to produce cheaper cables, and reduce the OPEX by producing more reliable cables.
The industry currently seems to agree on the need for a (better) calibrated FSF for DPC's. As mentioned in section 1-1-3, a joint industry project is being initiated by DNV to address reliability in floating offshore wind. Part of the scope is the calibration of the FSF for inter array cables [13].

1-3 Scope

The assessment of fatigue in a DPC is a complex case, due to the many interactions between the different cross-sectional elements. A scope outline has been made in order to give the subjects at matter adequate attention.
The two main fatigue sensitive components in a DPC are the copper core, and the steel armor wiring, since they are the stiffest components, thus exposed to the highest stress. The focus of this research will be limited to the fatigue life of the armor. This is because the local effects in steel wires are better understood, since there is only in-line contact with the surrounding layers. In copper cores, there is also trellis contact between the different copper layers [21]. Because of this, a more grounded conclusion can be drawn from the analysis of steel wiring. For copper there are more uncertainties involved in the modeling due to its non-linear nature, the influence of the electric/magnetic field and the generation of heat along the copper core.
As for the external loading, distinction is made between Vortex Induced Vibration (VIV) and wave-induced fatigue in literature. The scope will only include wave-induced fatigue, and not consider VIV induced fatigue. This is done because mitigations for VIV loading exist, and it is thus considered to be more design related than concept related.
Furthermore, the model will be kept as simple as possible. Since many details about the cables and auxiliaries, like floatation modules and bend stiffeners, are unknown, a simple catenary DPC will be considered. This way, added uncertainties due to the unavailability of product information is omitted.
One case will be addressed in this study. This goes for floater type, location and cable type. Further work will have to show how sensitive the computed FSF is to a change in case selection. The case that will be investigated will be explained further in section 3.
Due to the simplifications that will be made for this research, attention must be paid to the validity of the outcome. Due to the reduced scope of the cross-section and the exclusion of auxiliaries along the power cable, less uncertainties will be taken into account when modeling the fatigue life. It is important that the results will be checked against future research, making use of more detailed models.

1-4 Research goal

In order to help reduce both the CAPEX and OPEX of dynamic power cables for the offshore renewable energy sector, this research will focus of providing credibility for the fatigue safety

factor used. By doing so, both a safety factor can be derived with confidence, and parameters that drive the uncertainty in the outcome of the model can be identified. The latter can be useful for further research. When it has been established what parameters are driving the required safety factor, more research can be done in order to reduce the uncertainty on that part of the model.
The main research question is:

How can the wave induced fatigue safety factor of the steel armoring of dynamic power cables be given credibility?

This question is split into the following sub-questions, trying to make a structured and logical research:

- What is a fatigue safety factor for a dynamic power cable?
- How are fatigue safety factors for steel catenary risers and dynamic umbilicals evaluated?
- How can a fatigue safety factor be evaluated for dynamic power cables?
- What is the fatigue safety factor for dynamic power cables in the NE7 floating wind project?
- What parameters are driving in the fatigue safety factor analysis, and (how) can the fatigue safety factor for dynamic cables in the offshore renewable sector be lowered?

1-5 Thesis outline

In the previous section the problem concerning an adequately calibrated FSF has been outlined. In section 2 the methodology for calibrating a FSF for a DPC will be outlined, and discussed in depth how the different parts of the models will be set up and calibrated. Using this proposed method, in section 3, details about the selected case study will be introduced. This case has been chosen to be relevant at the moment of research, to represent a case that might occur in the upcoming decade.
The results for this case study will be presented in section 4, and later on, in section 5, interpreted. In chapter 6 also the conclusions from the conducted research will be drawn.
The thesis will end with recommendations for further research in chapter 7.

Chapter 2

Methodology

2-1 Available methods

In this section, the state of the art for the evaluation of Fatigue Safety Factor's (FSF's) will be discussed. These methods have been applied to determine fatigue safety factors for steel catenary risers. Also the applicability of these methods to the offshore renewable sector will be discussed.

2-1-1 Enhanced risk based safety factor

2-1-1-1 Background

The enhanced risk based method, proposed in [16], aims to provide fatigue designs with a uniform safety level in line with [14]. The Fatigue Safety Factor (FSF) can be calculated using equation 2-1.

$$\log_{10}\gamma = (30+\gamma_{SC})\,T^{a(30+\gamma_{SC})+b}\,(c\sigma_{X_D}+d)\,(\sigma_{X_a})^{\left(e\sigma_{X_D}+f\right)} \tag{2-1}$$

Here γ is the fatigue safety factor, σ_{X_D} is the uncertainty in the fatigue damage, σ_{X_a} the uncertainty in the normalized fatigue constant on a log scale. σ_{X_a} equals 0.2 for a 2 slope S-N curve [22]. T the design lifetime in years, and a, b, c, d, e, f are empirical constants that have been calibrated for steel risers in [16]. σ_{X_D} can be calculated according to formula 2-2, where X_D is the normalized fatigue utilization (equation 2-3), X_i the stochastic variable i, and its standard deviations σ_{X_i}. $\sigma_{X_{mod}}$ is "a model uncertainty accounting for the uncertainty sources not accounted for in the assessment of X_D and reflects the confidence in the global analyses tools versus true life" [16].

$$\sigma_{X_D} = \sqrt{\sum \left(\frac{\partial X_D}{\partial X_i}\right)^2 \sigma_{X_i}^2 + \sigma_{X_{mod}}^2} \tag{2-2}$$

The normalized fatigue utilization's, X_D, is calculated as the log of the stochastic fatigue damage $D_s(X)$, divided by the best estimate fatigue damage $D(\mu_X)$, as seen in equation 2-3.

$$X_D = \log\left(\frac{D_s(X)}{D\left(\mu_X\right)}\right) \tag{2-3}$$

The stochastic fatigue damage for a bi-linear S-N curve can be calculated according to equation 2-4.

$$D_s(T) = \frac{Tf_v}{\bar{a}_1}\left[\int_{S_{SW}}^{\infty} s^{m_1} f_s(s)ds + \frac{\bar{a}_1}{\bar{a}_2}\int_0^{S_{SW}} s^{m_2} f_s(s)ds\right] \leq \frac{\alpha}{\gamma} \tag{2-4}$$

α is a bias factor, f_v is the mean frequency of the stress cycles, $f_S(S)$ is the probability density function of the stress cycles, m_i are fatigue exponents, a_i characteristic fatigue strength constants and S_{SW} is the stress at intersection of the two S-N curves.

2-1-1-2 Application

To apply the proposed method, the following steps will be required [16];

- A fatigue analysis with best estimate variables should be conducted. This analysis is site and project specific. This analysis is only needed to identify what sea-states are most damaging to the cable. A non-linear time-domain simulation is crucial for the proper assessment of non-linear effects in the structure [18]. The results of this analysis are the base case, denoted as $D(\mu_x)$.
- The contributions of individual short sea-states can be defined from $D(\mu_x)$. The most damaging sea-states should be used for sensitivity analysis.
- Identify the stochastic variables X_i that influence the uncertainty in the fatigue damage.
- Establish probabilistic models for all stochastic variables. This can be done based on measurements, literature sources, experts input or best estimates.
- Do a sensitivity analysis for the identified stochastic variables for the most governing sea-states. This sensitivity study should cover variations of 2 standard deviations from the mean ($\mu_{Xi} \pm 2\sigma_{Xi}$). This is noted as the stochastic fatigue damage $D_s(X)$.
- Generate response surfaces based on the stochastic fatigue damages.
- Establish numerical approximations for $\frac{\delta X_D}{\delta X_i}$.
- Establish the Std$[X_D]$, σ_{X_D}, as a function of a defined location along the cable using equation 2-2.
- Calculate the required safety factor γ using equation 2-1, based on the safety class, design lifetime and σ_{X_D}.

As mentioned, the above explained methodology has been proposed by [16], and has only been applied in three papers, [18], [23] and [24]. In all cases, the methodology was applied to (deep water) risers, but according to [18] the proposed method is applicable to all fatigue problems using the S-N curve approach. The methodology has been successfully bench-marks against level III reliability analysis by MARINTEK [24]. The conclusion of this bench-marking is that the safety factor can be calculated with good accuracy, and at lower computational costs.

2-1-1-3 Applicability to dynamic power cables

In the way the enhanced risk based method has been applied for risers, the main parameters that were expected to have a substantial effect on the fatigue damage due to waves were: transverse drag coefficient, floater heave motions, vertical soil stiffness and riser weight [23]. For Vortex Induced Vibration (VIV) induced damage, the Strouhal number, bandwidth, A/D factor and model uncertainty were used [24]. From talking to experts in the field of dynamic cables at Marin and Catapult, the conclusion was drawn that a large part of the uncertainty for dynamic cables was at local scale where the different strands interact with each other, and the internal friction coefficient. It would be interesting to incorporate parameters that are more cable specific into a model like this, to get a clear view on what the effect of these uncertainties are, and how they possibly effect a fatigue safety factor.

2-1-2 Reliability based safety factor

2-1-2-1 Background

Reliability refers to probability of not failing during the design lifetime of a component/structure. In structural reliability, one is interested in the probability that a predefined limit-state is violated. Violation of this limit state results into failure of a structure. Since most engineering cases involve certain degrees of uncertainty, two methods can be applied to ensure structural integrity. The first on is a deterministic approach with a safety factor that accounts for the uncertainties. The second method is a probabilistic approach, where stochastic variables are used to model the uncertainties.
In the studies that used a reliability based method for evaluating the FSF, a First Order Reliability Method (FORM) with a Rackwitz-Fiessler (RF) (transformation) algorithm to search for the design point is used [19], [25], [26], [27]. FORM is a First Order Second Moment (FOSM) method with a Hasofer-Lind (HL) safety index.

Limit state
A limit state function can be defined as the resistance $R(X)$ minus the load $S(X)$, as in equation 2-5.

$$g(X) = R(X) - S(X) \tag{2-5}$$

Where the probability of failure is defined as in equation 2-6.

$$P_f = P[g(\cdot) < 0] \tag{2-6}$$

Since the load and the resistance are both functions of stochastic variables, so is g(X).

The mean and standard deviation of of the limit state can be calculated according to equations 2-7 and 2-8 respectively.

$$\mu_g = \mu_R - \mu_S \tag{2-7}$$

Where μ_R is the mean of the resistance, and μ_S the mean of the load.

$$\sigma_g = \sqrt{\sigma_R^2 + \sigma_S^2 - 2 \cdot \rho_{RS}\sigma_R\sigma_S} \tag{2-8}$$

σ_R is the standard deviation of the resistance and σ_S is the standard deviation of the load. ρ_{RS} is the correlation factor between the load and the resistance. The safety index β is a degree of safety in the limit state function, and is calculated according to equation 2-9. This is visualized in figure 2-1 [28].

$$\beta = \frac{\mu_g}{\sigma_g} = \frac{\mu_R - \mu_S}{\sqrt{\sigma_R^2 + \sigma_S^2 - 2\rho_{RS}\sigma_R\sigma_S}} \tag{2-9}$$

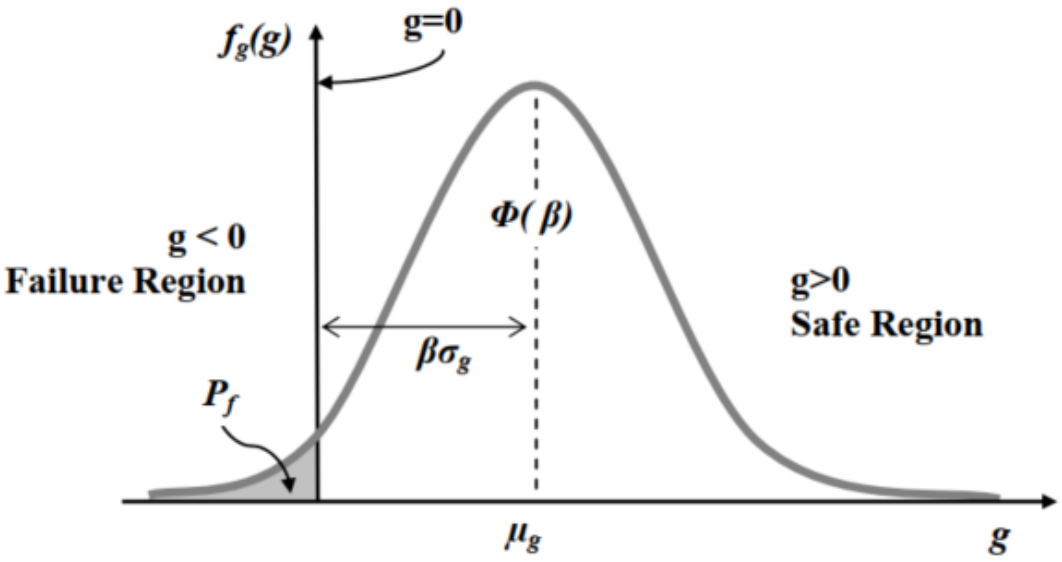

Figure 2-1: Limit state and safety index visualized [28]

FOSM

"First order" comes from the first order (Taylor) expansion used in this method. "Second moment" implies that only the mean and standard deviation are used, and higher moments

like skew and flatness are not considered [28]. The limit state for this method can thus be approximated as:

$$\widetilde{\mathrm{g}}(\mathrm{X}) \approx g\left(\mu_X\right) + \nabla g\left(\mu_X\right)^T \left(X_i - \mu_{X_i}\right) \tag{2-10}$$

Where the mean is approximately

$$\mu_{\tilde{g}} \approx E\left[g\left(\mu_X\right)\right] = g\left(\mu_X\right) \tag{2-11}$$

And the standard deviation;

$$\sigma_{\tilde{g}} = \left[\sum_{i=1}^{n} \left(\frac{\partial g\left(\mu_X\right)}{\partial x_i}\right)^2 \sigma_{x_i}^2\right]^{\frac{1}{2}} \tag{2-12}$$

The safety index can be calculated the same way in equation 2-13 as in equation 2-9. The two are equal if the limit state function is linear [28].

$$\beta = \frac{\mu_{\widetilde{g}}}{\sigma_{\widetilde{g}}} \tag{2-13}$$

Even though the FOSM method is easy to use, there are 2 drawbacks. Firstly, evaluating limit-state functions that are highly non-linear give large errors. Secondly, this method is not invariant, meaning that different mathematical formulations of the same problem can lead to different solutions [28].

HL safety index

The first step in the HL proposes is the transformation of the stochastic variables into standard normalized variables $\hat{R}$ and $\hat{S}$ according to equation 2-14.

$$\hat{R} = \frac{R - \mu_R}{\sigma_R}, \hat{S} = \frac{S - \mu_s}{\sigma_s} \tag{2-14}$$

Next, the limit state surface $g(R, S) = 0$ is transformed from the original (R,S) to the standard normalized $(\hat{R}, \hat{S})$ coordinate system:

$$g(R(\hat{R}), S(\hat{S})) = \hat{g}(\hat{R}, \hat{S}) = \hat{R}\sigma_R - \hat{S}\sigma_S + (\mu_R - \mu_S) = 0 \tag{2-15}$$

The point on $\hat{g}(\hat{R}, \hat{S}) = 0$ that has the shortest distance to $\hat{0}$ is known as the Most Probable Point (MPP), denoted as P^* in figure 2-2.

In general cases, the limit state is a function of n stochastic variables:

$$g(X) = g\left(\{x_1, x_2, \ldots x_n\}^T\right) \tag{2-16}$$

Which can be transformed to the standard normalized form (the u-space) with:

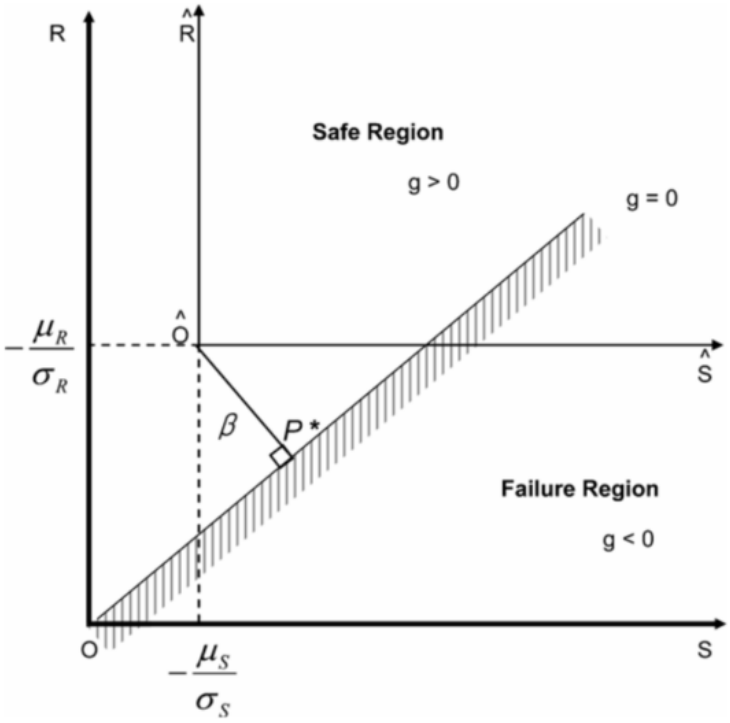

Figure 2-2: HL safety index [28]

$$u_i = \frac{x_i - \mu_{x_i}}{\sigma_{x_i}} \tag{2-17}$$

Giving

$$g(U) = g\left(\{\sigma_{x_1} u_1 + \mu_{x_1}, \sigma_{x_2} u_2 + \mu_{x_2}, \ldots, \sigma_{x_n} u_n + \mu_{x_n}\}^T\right) = 0 \tag{2-18}$$

This transformation from the X-space to the U-space is visualized in figure 2-3.

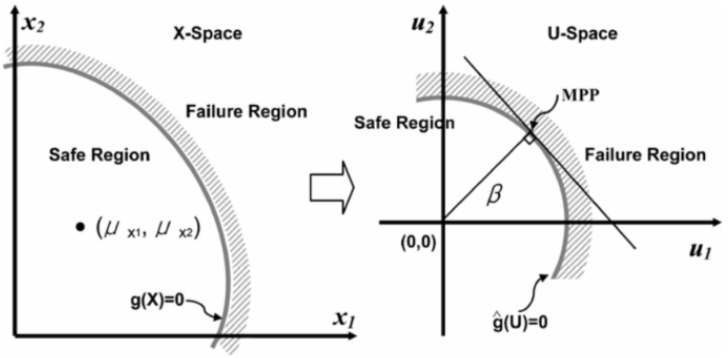

Figure 2-3: Transformation from X-space to U-space [28]

The safety index is again the shortest distance from the origin to the failure region. For the HL method in the u space, this is calculated according to equation 2-19.

$$\beta_{HL} = \min_{U \in g(U)=0} \left(U^T U\right)^{\frac{1}{2}} \tag{2-19}$$

To calculate the β_{HL}, an iterative process starting with an initial guess for the MPP to calculate an initial value for β_{HL}. This process can be repeated until the safety index has converged to give a desired error.

The difference between the FOSM and the FORM is that the FOSM uses a first order expansion at the mean value point, and the FORM expands at the design point X or U. The FOSM however does not need to iterate, whereas the FORM does need to iterate for non-linear problems, providing more accurate results. Important to note is that the FORM can only be used for Gaussian distributed random variables [28].

RF transformation

Stochastic variables involved in the modeling of a dynamic power cable or umbilical do not all follow a Gaussian distribution. In order to solve the limitation of the HL method of not being able to use non-Gaussian stochastic variables, the RF method can be used. It uses a simple normal distribution approximation.

$$u_i = \Phi^{-1}\left[F_{x_i}\left(x_i\right)\right] \tag{2-20}$$

Which is expanded at the MPP to the first order.

$$u_i = \Phi^{-1}\left[F_{x_i}\left(x_i^*\right)\right] + \frac{\partial}{\partial x_i}\left(\left[\Phi^{-1} F_{x_i}\left(x_i\right)\right]\right)\Big|_{x_i^*}\left(x_i - x_i^*\right) \tag{2-21}$$

With

$$\frac{\partial}{\partial x_i}\Phi^{-1}\left[F_{x_i}\left(x_i\right)\right] = \frac{f_{x_i}\left(x_i\right)}{\phi\left(\Phi^{-1}\left[F_{x_i}\left(x_i\right)\right]\right)} \tag{2-22}$$

Giving

$$u_i = \frac{x_i - \left[x_i^* - \Phi^{-1}\left[F_{x_i}\left(x_i^*\right)\right]\phi\left(\Phi^{-1}\left[F_{x_i}\left(x_i^*\right)\right]\right)/f_{x_i}\left(x_i^*\right)\right]}{\phi\left(\Phi^{-1}\left[F_{x_i}\left(x_i^*\right)\right]\right)/f_{x_i}\left(x_i^*\right)} \tag{2-23}$$

Which can be written as

$$u_i = \frac{x_i - \mu_{x_i'}}{\sigma_{x_i'}} \tag{2-24}$$

Resulting in the approximate normal distribution values in equation 2-25.

$$\sigma_{x_i'} = \frac{\phi\left(\Phi^{-1}\left[F_{x_i}\left(x_i^*\right)\right]\right)}{f_{x_i}\left(x_i^*\right)} \tag{2-25a}$$

$$\mu_{x_i'} = x_i^* - \Phi^{-1}\left[F_{x_i}\left(x_i^*\right)\right]\sigma_{x_i'} \tag{2-25b}$$

This normal equivalent has to be re-calculated in every iteration of the FORM. The effect of the normal approximation is visualized in figure 2-4.

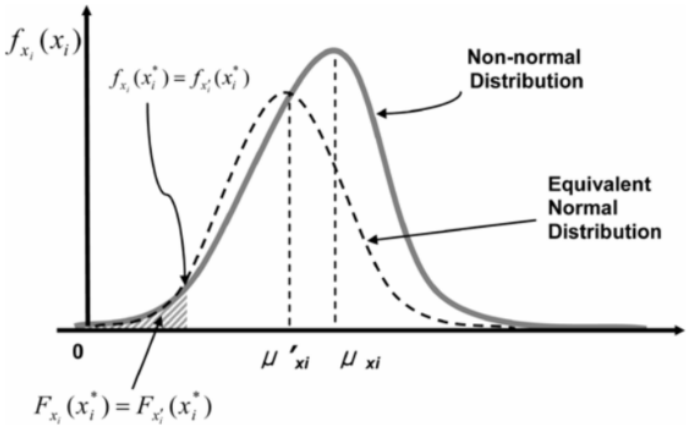

Figure 2-4: Normal distribution approximation [28]

2-1-2-2 Other methods

Higher order reliability methods exist, generally leading to more accurate results. In [29], the FORM is compared to the Second Order Reliability Method (SORM) and a Monte Carlo simulation for evaluating the FSF of flexible pipes. Depending on the allowable probability of failure, the effect of the different methods is shown in table 2-1.

	Safety Factor for T_{op} = 20 years		
Pf	FORM	FOSM	Monte Carlo
10^{-3}	1.14	1.12	1.11
10^{-4}	2.56	2.51	2.45
10^{-5}	4.84	4.77	4.69

Table 2-1: Effect of higher order reliability method and Monte Carlo [29]

It is observed that the use of a more expensive model does not significantly influence the outcome of the reliability analysis.

2-1-2-3 Application

[30] describes a framework for a reliability-based fatigue safety factor for flexible rises. This paper includes a (more than Leira's other papers) detailed description of the steps taken in the analysis performed.

The procedure using irregular waves starts by dividing the wave scatter diagram into blocks, typically in the order of 30 blocks, as seen in figure 2-5. Next, create a time series of the mean top-angle, angle range and corresponding tension by performing a non-linear time domain simulation of each block, in all multiple directions using a global Finite Element (FE) model. Then, in a local FE model, convert the obtained time series into local stresses and calculate the damage from each block. When this has been performed for all blocks, the total damage can be obtained.

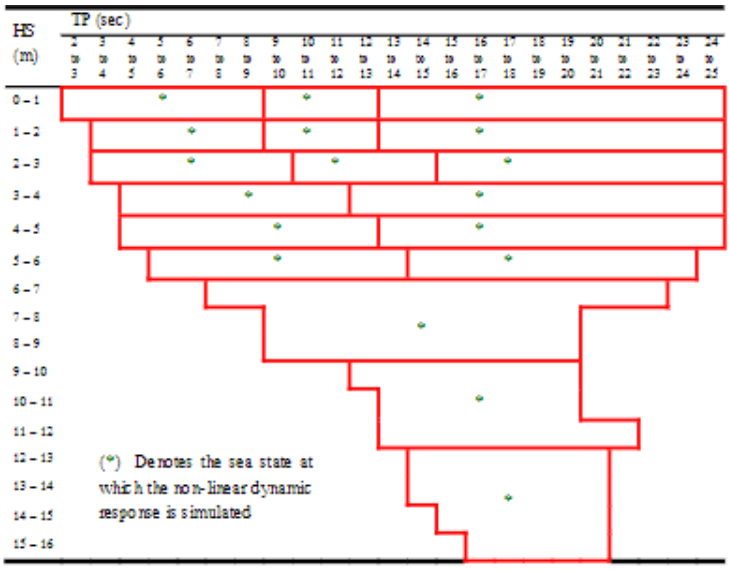

Figure 2-5: Wave scatter diagram split up into blocks [30]

Reliability analysis

The reliability assessment performed in the literature [26] starts with a basic failure criterion as seen in equation 2-26.

$$\mathrm{D_{Tref}}\ (\mathrm{T_{op}}/\mathrm{T_{ref}}) = 1 \tag{2-26}$$

Here T_{op} is the operating life time, and T_{ref} the reference duration. D_{Tref} is the damage during this time. Since we are considering a stochastic process, and not a deterministic one, the value "1" can be replaced by X_{fail}, which is the stochastic variable for the resistance of the system, and D_{ref}, which is the stochastic damage, dependent on multiple stochastic variables; $\mathrm{D_{Tref}}\ (\mathrm{X_1}, \mathrm{X_2}, \cdots, \mathrm{X_N})$. Here X_i signifies random variables. With this stochastic expression, equation 2-27 is obtained.

$$\mathrm{g}(\mathbf{X}) = \mathrm{X_{Fail}} - \mathrm{D_{Tref}}\ (\mathrm{X_1}, \mathrm{X_{2,}}, \cdots, \mathrm{X_N}) \cdot (\mathrm{T_{op}}/\mathrm{T_{ref}}) \tag{2-27}$$

When this function becomes negative, failure occurs.
We are not only interested in the probability of failure, but more so the FSF associated with this probability of failure. By reformulating equation 2-27, equation 2-28 is obtained.

$$\mathrm{g}(\mathbf{X}) = \mathrm{Y_1} - (1/\mathrm{SF}) \cdot \mathrm{f}\,(\mathrm{Y_2}, \mathrm{Y_3} \ldots, \mathrm{Y_N}) \tag{2-28}$$

Here $Y_i = X_i/(X_i)_{Basecase}$, which is a dimensionless variable.
Having determined the limit state, a modeling choice has to be made as to what stochastic variables to include in the study. Ideally, the most relevant ones need to be identified and used. After having done so, and ran the model, the influence on the fatigue damage of each random variable, based on their statistical properties, can be determined. Usually the mean value, and the mean value plus/minus 2 times the standard deviation are evaluated. This

way a second order polynomial can be fitted. If the curvature is very high, more points can be calculated, and a higher order polynomial can be fitted [26].

The stochastic variables used in [26] are the drag coefficient, floater surge amplitude, floater pitch amplitude, three dimensional effect, friction coefficient, internal pressure, global analysis method, local analysis method, environmental description, Miner-Palmgren sum at failure and intercept of SN-curves.

2-1-2-4 Applicability to cables

Similarly to section 2-1-1-3, the parameters used in this model can be altered to represent cable specific parameters that are uncertain when evaluating fatigue. According to [23], this method is more computationally expensive, but has the potential for being more accurate. Moreover, no empirical constants need to be calibrated, meaning the reliability based method can directly be applied.

2-2 Implementation

Of the two methods proposed in the previous section, the reliability based method is deemed more feasible to apply for the calibration of a FSF for Dynamic Power Cable's (DPC's). This is because it does not involve the calibration of the riser specific empirical constants.
In this section, a more detailed description of the implementation of the proposed method will be discussed. Firstly, a local FE model is discussed, which is used to determine a bending stiffness of the cable, as well as a relationship between the applied bending moment and the stress in the armoring. Secondly, a global FE model is explained. Here environmental loads are applied to the model to generate a stress time-series of the power cable. Thirdly, the stress time-series are used to calculate a fatigue damage. Lastly, the reliability method is used to calculate the FSF and importance factors. The workflow is summarized in figure 2-6.

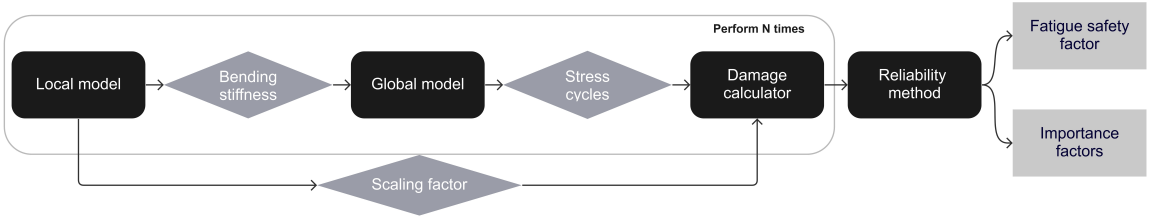

Figure 2-6: Workflow

2-2-1 Local model

In this section the local (FEMAP) model will be discussed. Simcenter FEMAP (Finite Element Modeling and Post-processing), is "an advanced simulation application for creating, editing, and inspecting finite element models of complex products or systems" [31] developed

by Siemens. It uses the Simcenter Nastran as FE solver, which is seen as one of the industry leading solvers. Background information and modeling choices will be discussed, as well as the way the analysis will be performed.

2-2-1-1 Background

The use of commercial FE software to model local interactions in cable like structures in the offshore industry is not a novelty in itself. Studies have been carried out to investigate flexible pipelines and risers in the oil & gas industry, [32] and [33] are some examples of this. A similar modeling techniques has been applied in [34] to model a Dynamic Power Cable (DPC). Only in [32] the models are used to obtain hysteric bending curves for the flexible riser. This curve can then serve as input for the global model. Figure 2-7 shows the workflow that will be adopted.

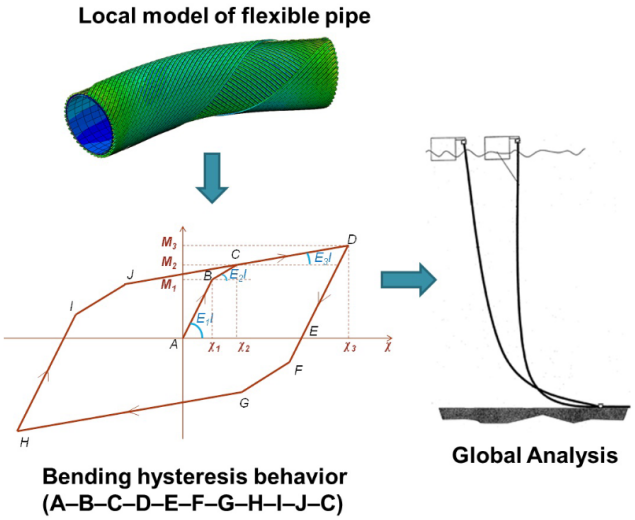

Figure 2-7: Flow local model [32]

2-2-1-2 Model

Since 3D FE models can quickly become too expensive to run, only part of the cable will be modeled. [32] uses a model length that is equal to one pitch length, the distance covered by an armor wire fully rotating around the core once. In [33] use is made of the periodic nature of the helical strands in a 3D periodic model. Here the model length is equal to the pitch length divided by the amount of strands in the layer. By setting up periodic conditions between nodes A1 and B1, A2 and B2 and so on (see figure 2-8), only a very small length has to be modeled. Also a full model is discussed in the paper, where the length is also dependent on the model that is being analyzed. This full model is described as "more realistic" than the periodic model. For the sake of this research, one pitch length is deemed to be long enough. This will be confirmed by a convergence of the bending stiffness later on.

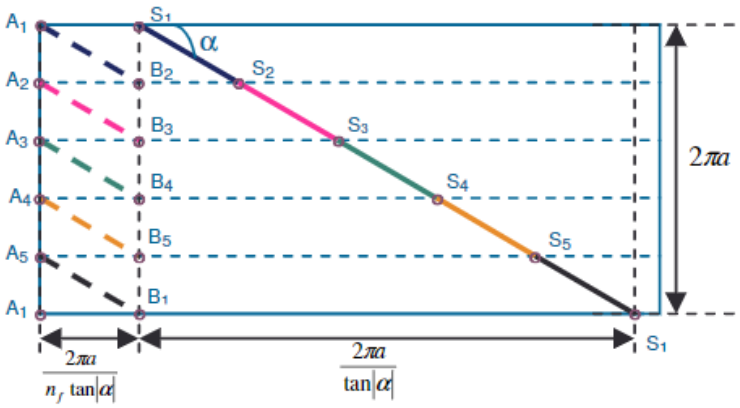

Figure 2-8: Periodicity of helical strands [33]

In [35], a lay angle of 35 degrees is used. For the model in this research, also a lay angle of 35 degrees is taken, giving a pitch length of 1.62m.
Another important modeling choice is the element types used in the model. Since contact between elements is very important in the model, only 2D and 3D elements can be used, since 1D elements do not have contact surfaces. For the strands, [33] and [36] propose the use of 8 node brick elements. Similarly to the goal of this research, in [33] the focus is on the strands, and the other layers are modeled with less detail.
[37] proposes the use of beam elements to model (copper) wires. This allows for a reduction in elements required, relying on the assumption that the fatigue damage is governed by axial loading. Since beam elements are one dimensional, they cannot be used for contact modeling. To resolve this, [37] sets up contact elements between the nodes of different strands to model the contact, as can be seen in figure 2-9. Wire to wire contacts are given an elastic stiffness in the normal direction, and friction is modeled as an elastic-plastic model. Despite the reduction in the required elements, for the model for this research, 8 node brick elements will be used for the strands, and 2D shell elements to model the sheaths. This is done in order to keep the model as simple and intuitive as possible.

As for the core, in order to reduce computational time, an equivalent 2D element will be calculated in section 3-4-1-2 that properly matches the global bending properties of the core, but does not require the use of solid elements.

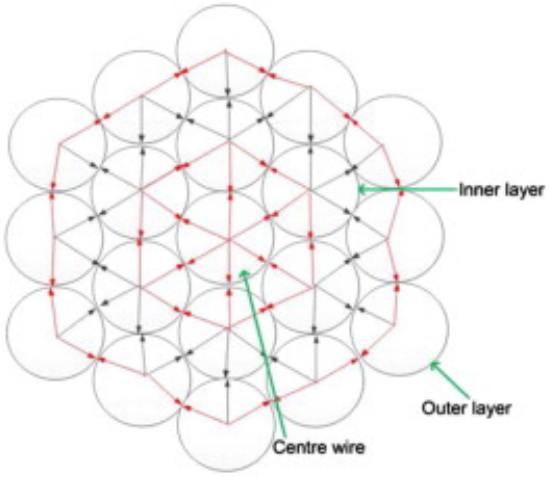

Figure 2-9: Inter layer coupling between beam elements [37]

2-2-1-3 Analysis

In this section, the way the model is loaded and constrained, and the post-processing of the data will be discussed.
Similar to literature [35], use is made of reference nodes at both ends of the cable, as shown in figure 2-10. Here the white web represents a rigid connection from the center node to all other end nodes. This center node is constrained in all 6 degrees of freedom. A similar rigid connection is made at the top of the model, where all loads are applied instead of an imposed constraint.

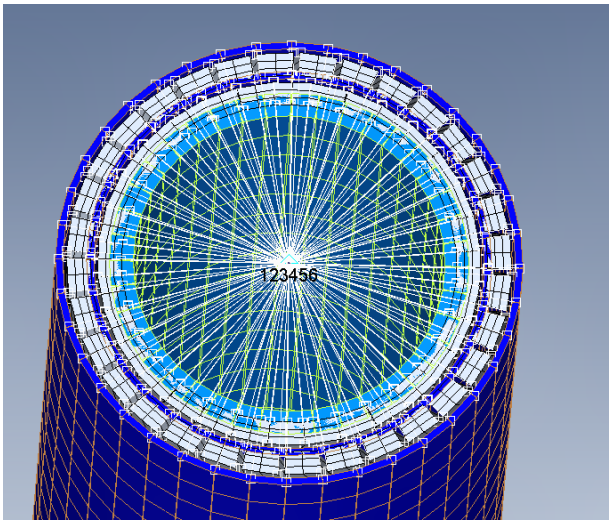

Figure 2-10: Reference node

Since Femap does not include a means to calculate or visualize curvatures, nodal positions are exported to Python at every time-step for post-processing. In Python, ghost coordinates are

generated, being the center-line of the cable. This is done by averaging x, y and z coordinates of all nodes in the core that have the same z value at t=0 as shown in figure 2-11. For every load step, a curvature κ is calculated using equation 2-29.

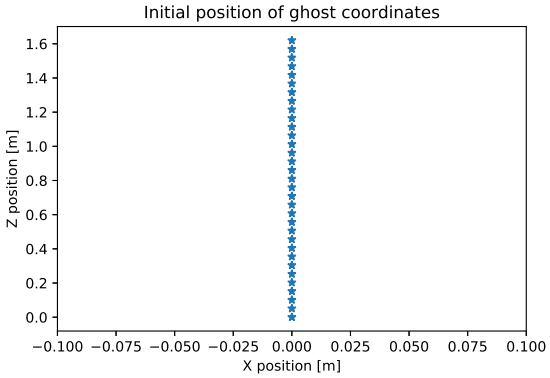

Figure 2-11: Ghost coordinates at t=0

$$\kappa = \frac{1}{\rho} = \frac{z''}{\left[1 + (z')^2\right]^{3/2}} \tag{2-29}$$

Important to note here is that since a flexible cable, with the assumption of large deformations, the common simplification $\frac{1}{\rho} \approx z''$ is assumed not to hold. Bending curves are then obtained by plotting the applied moment against the corresponding curvatures, an example of which is shown in figure 2-12, which will serve as input for the global model. Here the maximum applied bending moment can be observed to be 2kNm, which is about two times the applied moment form which point on the cable is fully in slip regime. This is in correspondence with what is observed in related literature.

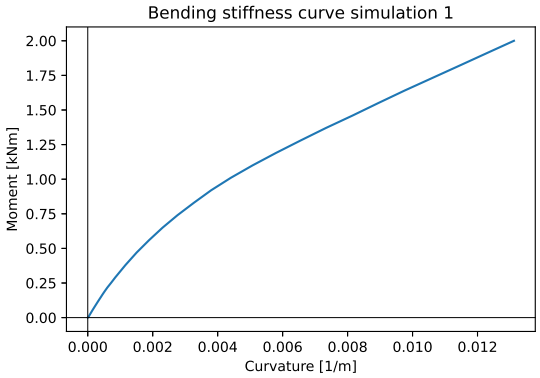

Figure 2-12: Example of a bending curve as obtained from the local model

2-2-2 Global model

For the global model, use will be made of Orcaflex. Orcaflex is an analysis software, designed by Orcina, that can perform global static and dynamic analysis for offshore systems. It has been designed to accommodate a wide range of applications, including riser systems and pipelines, and is deemed suitable to serve as the global model for this research [38].
In this section the Orcaflex model setup and modeling choices to analyze a DPC will be discussed.

2-2-2-1 Model setup

The global model consists of several components. In this section the implementation of each component will be discussed.

Floater
For the floater motions, the full equation of motion (equation 2-30) is solved for each time-step. In order to do this, a diffraction analysis is required to determine the (frequency dependent) coefficients. These are the added mass ($a_{i,j}$), the damping ($b_{i,j}$), and the stiffness ($c_{i,j}$) as shown in the equation. Furthermore, coefficients having to do with the external forces (F_{ext}) are determined. These are the wave load RAO's, wave drift QTF's, wave drift damping coefficients, and quadratic damping coefficients. Forces on the floater caused by the mooring lines and power cable are included in F_{ext}.

$$\begin{aligned} &\sum_{j=1}^{6} \left\{ \left(m_{i,j} + a_{i,j}\left(\omega_e\right) \right) \cdot \ddot{x}_j\left(\omega_e, t\right) + b_{i,j}\left(\omega_e\right) \cdot \dot{x}_j\left(\omega_e, t\right) + c_{i,j} \cdot x_j\left(\omega_e, t\right) \right\} \\ &= \sum F_{ext}\left(\omega_e\right) \qquad \text{for } i = 1, \ldots 6 \end{aligned} \tag{2-30}$$

Lines
For both the mooring lines and the power cables, line types will be used in Orcaflex. The general line type is used, since this provides most control over all individual line data. By performing a mesh convergence study in section 3-12, an appropriate mesh can be defined for the power cable. This allows for an adequately refined mesh, whilst not wasting computational power. This will be done for the region of interest, the touch-down zone. The rest of the cable will be modeled with a coarser mesh, since stresses are not evaluated there.
The bending stiffness of the power cable will be based on the results obtained from Femap. A bending curve as shown in figure 2-12 is read by Orcaflex, and can be interpreted as being hysteric. The "Orcina bending hysteresis model uses the basic non-linear curve and uses it to calculate the bending moment history that results from any given curvature history."[39] This method is used, instead of exporting and importing the full hysteresis curve, in order to eliminate small numerical errors from the local model, causing duplicate values in Orcaflex. The curve describes the same path twice in part of the first and second loading cycle. These lines are theoretically identical, but in practice vary slightly. In order for Orcaflex to be able to read these curves, these lines must be identical. In figure 2-13 the corresponding full bending stiffness curve, as interpreted by Orcaflex, is shown. This curve is compared to a full

loading cycle in Femap, and is deemed appropriate.

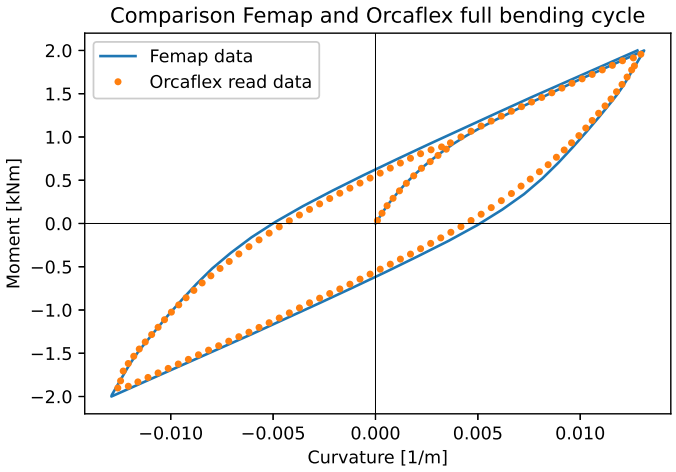

Figure 2-13: Comparison between the hysteresis curve from Femap, and the curve interpreted by Orcaflex

Environmental conditions

For the environmental conditions, the two most important parameters for this analysis will be the sea-state, and the soil modeling. The sea-state will be modeled using a Joint North Sea Wave Project (JONSWAP) spectrum, defined by a Significant Wave-height (Hs) and a Peak Period (Tp). Since this is a stochastic distribution, an adequate simulation time is required. According to [30] the standard deviation of the response converges after 1.14 hours. This will be taken as a simulation time for this research as well.
The soil stiffness influences the stress in the power cable around the touch-down zone, since this is where there is contact between the seabed and the cable. For the sake of this research, the soil will be modeled as a linear spring.

2-2-2-2 Analysis

Due to the environmental loading, motions in the DPC are caused. Because of these motions, variations of stress due to bending, tension and contact are present in the cable. These variations in stress, or stress cycles, are used for the calculation of the fatigue damage.

Loading

In order to calculate how much damage is accumulated in a year, different environmental loadings need to be evaluated. Location specific scatter diagrams, specifying the occurrence of a Hs and a Tp can be found. An example of such a scatter diagram is shown in figure 2-14.

For every combination of Hs and Tp a simulation is run for a certain amount of time. This gives a time series of the stress in the power cable, which is used to calculate the cumulative fatigue damage for the simulated time. Dividing this damage by the fraction of a year that

	lower	01	02	03	04	05	06	07	08	09	10	11	12	13	14	15	16	17	18	19	20	21	22	23	24	25	26	
lower	upper	02	03	04	05	06	07	08	09	10	11	12	13	14	15	16	17	18	19	20	21	22	23	24	25	26	27	total
0.0	0.5	0	0	1.0	0.5	0.8	0.4	0.4	0.4	0.3	0.3	0.2	0.2	0.1	0.1	0.1	0.0	0.0	0.1	0.1	0.0	0.0	0.0	0.0	0	0.0	0	5.0
0.5	1.0	0	0.1	4.1	2.4	2.2	3.4	1.6	1.6	1.7	1.1	0.5	0.4	0.3	0.1	0.0	0.0	0.1	0.1	0.1	0.0	0.0	0	0.0	0	0	0	19.7
1.0	1.5	0	0	0.4	7.3	1.6	3.2	2.4	3.8	1.6	1.5	1.1	0.4	0.2	0.2	0.1	0	0.0	0.0	0.0	0.0	0.0	0.0	0.0	0	0	0	23.9
1.5	2.0	0	0	0	4.1	3.4	1.5	3.4	1.9	1.2	1.4	1.4	0.7	0	0.2	0.1	0	0.0	0.0	0	0.0	0	0.0	0	0	0	0	19.3
2.0	2.5	0	0	0	0.4	3.6	1.2	2.4	1.6	1.0	0.9	0.8	0.7	0	0.3	0.1	0.0	0.0	0.0	0	0.0	0	0	0	0	0	0	12.9
2.5	3.0	0	0	0	0.0	1.3	1.0	1.9	1.1	0.8	0.5	0.4	0.4	0.2	0.0	0.0	0.0	0	0	0	0.0	0	0	0	0	0	0	7.8
3.0	3.5	0	0	0	0	0.2	0.7	1.3	0.8	0.8	0.4	0.2	0.2	0.1	0	0.0	0.0	0	0.0	0	0	0	0	0	0	0	0	4.7
3.5	4.0	0	0	0	0	0.0	0.2	0.7	0.6	0.6	0.3	0.1	0.1	0.1	0	0.0	0.0	0	0	0	0	0	0	0	0	0	0	2.7
4.0	4.5	0	0	0	0	0	0.0	0.2	0.3	0.5	0.3	0.1	0.1	0.1	0	0.0	0	0	0	0	0	0	0	0	0	0	0	1.6
4.5	5.0	0	0	0	0	0	0	0.1	0.1	0.3	0.3	0.1	0.0	0.0	0	0.0	0.0	0	0	0	0	0	0	0	0	0	0	0.9
5.0	5.5	0	0	0	0	0	0	0.0	0.0	0.2	0.2	0.1	0.0	0.0	0	0.0	0.0	0	0	0	0	0	0	0	0	0	0	0.6
5.5	6.0	0	0	0	0	0	0	0.0	0.0	0.1	0.2	0.1	0.0	0.0	0	0.0	0.0	0	0	0	0	0	0	0	0	0	0	0.3
6.0	6.5	0	0	0	0	0	0	0.0	0.0	0.0	0.1	0.1	0.0	0.0	0	0	0	0	0	0	0	0	0	0	0	0	0	0.2
6.5	7.0	0	0	0	0	0	0	0	0.0	0.0	0.1	0.1	0.0	0	0	0	0	0	0	0	0	0	0	0	0	0	0	0.1
7.0	7.5	0	0	0	0	0	0	0	0	0.0	0.0	0.1	0.0	0	0	0	0	0	0	0	0	0	0	0	0	0	0	0.1
7.5	8.0	0	0	0	0	0	0	0	0	0	0.0	0.0	0.0	0	0	0	0	0	0	0	0	0	0	0	0	0	0	0.1
8.0	8.5	0	0	0	0	0	0	0	0	0	0	0.0	0.0	0	0	0	0	0	0	0	0	0	0	0	0	0	0	0.0
8.5	9.0	0	0	0	0	0	0	0	0	0	0	0.0	0.0	0	0	0	0	0	0	0	0	0	0	0	0	0	0	0.0
9.0	9.5	0	0	0	0	0	0	0	0	0	0	0	0.0	0	0	0	0	0	0	0	0	0	0	0	0	0	0	0.0
9.5	10.0	0	0	0	0	0	0	0	0	0	0	0	0	0	0	0	0	0	0	0	0	0	0	0	0	0	0	0.0
total		0.0	0.1	5.5	14.5	13.1	11.5	14.3	12.3	9.2	7.5	5.3	3.3	1.1	0.9	0.4	0.1	0.2	0.2	0.2	0.1	0.1	0.0	0.0	0.0	0.0	0.0	100.0

Figure 2-14: Example wave-scatter [40]

has been simulated, gives the yearly damage of the simulated combination of Hs and Tp. By multiplying the yearly fatigue damage by the yearly occurrence, and adding up all the resulting products, a total yearly fatigue damage is obtained, according to equation 2-31.

$$D_{1year} = \sum_{n=1}^{N} D_n \cdot P_n \tag{2-31}$$

Here D_n and P_n are the damage and occurrence of combination n respectively.

2-2-3 Damage calculation

Orcaflex offers a built in damage calculator for the evaluation of fatigue lives. Due to the fact that Orcaflex uses 1D elements to model cables, the resulting cross-section is in essence homogeneous. For tensile and bending loading, the resulting stress is calculated as follows.

$$\sigma_{vm} = \frac{T}{A} + \frac{M \cdot y}{I} \tag{2-32}$$

Here T is the tension, A the cross-sectional area, M the bending moment, y the distance to the bending axis and I the moment of inertia.
Because the DPC is not homogeneous in cross-section, the resulting stresses obtained from Orcaflex would be too low for the steel armor, resulting in an underestimation of the fatigue damage, and thus an overestimation of the fatigue life. In order to solve this problem, the stresses obtained by Orcaflex are compared to that obtained by Femap, for the same applied bending moments. A ratio of the two stresses in the steel armoring is defined as a scaling factor, according to equation 2-33.

$$SF = \frac{\sigma_{Femap}}{\sigma_{Orcaflex}} \tag{2-33}$$

Because this ratio varies per applied moment, a different scaling factor is needed for every calculated homogeneous stress in Orcaflex. By multiplying the stresses from Orcaflex by the corresponding scaling factor, equivalent non-homogeneous stresses are obtained, as Femap would give. These stresses are then used for the fatigue analysis.

For the fatigue analysis, the Python package Fatpack will be used. Fatpack allows for the damage calculation using the Miner's sum, as explained in section 1-1-2. The scaled stress obtained by Orcaflex serves as input, and is analysed for stress ranges. By defining an SN curve, the corresponding fatigue life can be calculated. Since not only the stress range amplitude, but also the mean stress influences the fatigue damage, a correction is made for the mean stress to account for this, using the Goodman's mean stress model. [41] shows the effect of the mean stress correction in figure 2-15. It can be observed that neglecting the mean stress correction would give an underestimation of the fatigue damage. The Goodman stress correction can be calculated according to equation 2-34 [42].

$$\Delta\sigma_0 = \frac{\Delta\sigma}{1 - \left(\frac{\bar{\sigma}}{\sigma_u}\right)} \tag{2-34}$$

Here $\Delta\sigma_0$ is the stress range at zero mean, $\Delta\sigma$ is the calculated stress range, $\bar{\sigma}$ is the mean stress level and σ_u is the ultimate stress level [42].

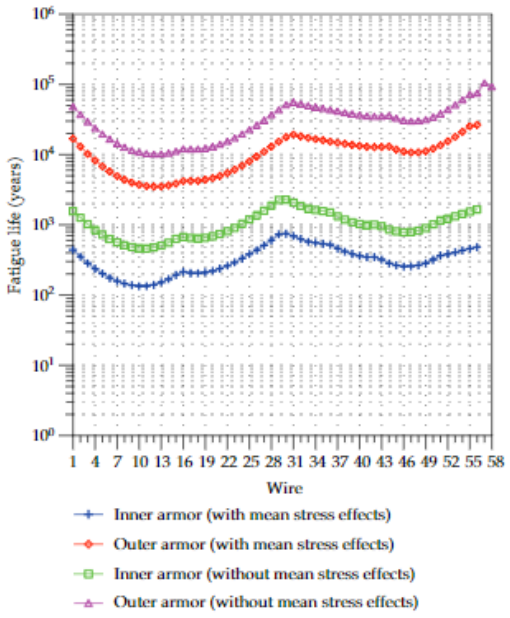

Figure 2-15: The effect of the Goodman correction factor [41]

2-2-4 Reliability method

In the previous section, it has been explained how the fatigue damage can be calculated for a certain situation. Since the goal is to investigate the FSF, a multitude of situations need to be evaluated for different values of stochastic parameters. These parameters will be put forward in section 3. In this section, it will be explained how the FORM will be applied to calculate a FSF. In [30], a clear explanation of this is put forward. Similar methods, has been used in more literature. [19], [26], [27], [43] and [44] all use this method for determining different safety factors for different cases of steel catenary risers. The method and its application to the case is summarized below.

2-2-4-1 Application

The first step is setting up a limit-state function $g(\mathbf{X})$. This function consists of a resistance and a load, X_{Fail} and D in equation 2-35 respectively.

$$g(\mathbf{X}) = \mathrm{X_{Fail}} - \mathrm{D}\left(\mathrm{T_{op}}, \mathrm{X_1}, \mathrm{X_2} \cdots \mathrm{X_N}\right) \tag{2-35}$$

This can be simplified to equation 2-36, since only a reference time T_{Ref} is modeled, instead of the full lifetime T_{Op}. X_{Fail} is a stochastic parameter taking into account uncertainties in the Miner's sum. This will not be included in the analysis of this case, since it is not specific to a DPC, and is thus assumed to have a deterministic value of 1.

$$g(\mathbf{X}) = 1 - \mathrm{D_{Tref}}\ \left(\mathrm{X_1}, \mathrm{X_2}, \cdots, \mathrm{X_N}\right) \cdot \left(\mathrm{T_{op}}/\mathrm{T_{ref}}\right) \tag{2-36}$$

Here X_i denotes the stochastic variable i, and $\mathbf{X}$ a vector containing all stochastic variables. When the limit-state function becomes smaller than zero, failure occurs. As explained in the previous section, a damage per year (D_1) can be calculated. This means $T_{ref} = 1\,year$ and $T_{op} = 20\,years$. Formula 2-36 assumes a linear relation between the cumulative damage and time. This implies that the structural properties do not change per year. With the limit-state function the Probability of failure (Pf) can be calculated, and introducing a FSF into the equation allows us to achieve a desired Pf, which can be satisfied by changing the FSF. This leaves equation 2-37, relating the FSF with the Pf.

$$g(\mathbf{X}) = 1 - \frac{1}{FSF} \cdot \mathrm{D_1}\left(\mathrm{X_1}, \mathrm{X_2}, \cdots, \mathrm{X_N}\right) \cdot 20 \tag{2-37}$$

In order to implement the FORM, it is necessary to be able to evaluate the limit-state function not only at the mean of all stochastic parameters, but at a new design point in every iteration of the reliability analysis. Since the resulting damage to the DPC is the output of a FE model, the answer to the limit-state function, as it stands right now, is discrete, meaning it cannot be evaluated at any point. [43] states that evaluating each stochastic parameter at its mean μ_i and its mean plus and minus two times its standard deviation $\mu_i \pm 2\sigma_i$ is sufficient, since it will "cover the relevant variation range with a very high probability". A second order polynomial can then be fitted through the three points. Through private communication with prof. Leira, he explained that second order polynomials worked best for the cases he evaluated. By fitting a curve through the evaluated points, a continuous relation between the individual random variables, and the corresponding damage can be determined. Normalizing all of the resulting damages, as well as the stochastic variables makes it easier to calculate the total damage [30]. For every parameter, plots like figure 2-16 will be made.

Now that a continuous relation has been formed between the normalized stochastic parameters, and the normalized damage, the total normalized damage can be calculated according to equation 2-38.

$$D_{total} = D(\mu) \cdot \prod_{i=0}^{nVar} D_{i,norm} \tag{2-38}$$

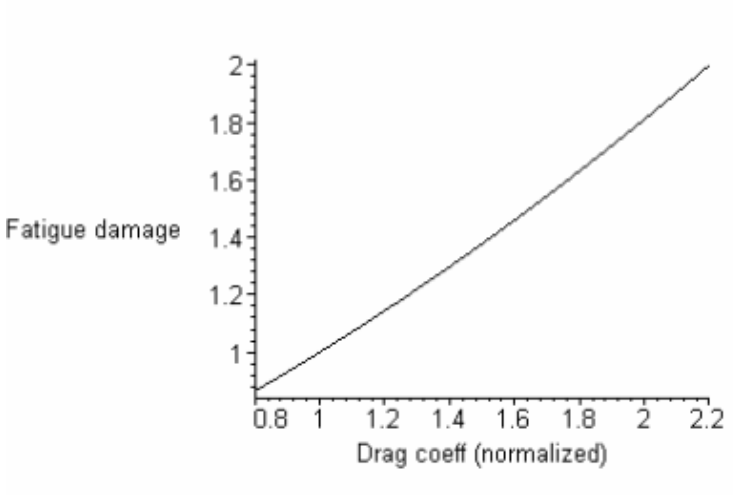

Figure 2-16: Curve fit through the evaluated points at the limit-state function [30]

Here $D(\mu)$ is the damage at the mean of all stochastic parameters, against which all other damages have been normalized. Since all parameters are normalized, they represent a percentage of change of the normalized damage. Because of this, the product of all individual terms represent the total change in normalized damage. By multiplying this by the damage against which all parameters have been normalized, the resulting real damage (D_{Total}) can be obtained.

According to [16], the desired Pf for flexible risers and umbilicals in safety class "low" (in which a DPC is assumed to be), in the last year of their design lifetime, should be a maximum of 10^{-3}. This value will be used as target Pf to calculate the FSF.

$$P_f = P[g(\mathbf{X}) \leq 0] \leq 10^{-3} \tag{2-39}$$

With the above information the safety index β_{HL} of the limit-state function can be calculated. This safety index can be related to the Pf as follows.

$$P_f = \Phi(-\beta_{HL}) \tag{2-40}$$

By evaluating equation 2-37 for a number of different safety factors, a continuous relationship between the FSF and the Pf is obtained. With this continuous relationship, it can be derived what FSF is required for a Pf of 10^{-3}.

The FORM allows for the determination of the influence of the individual random variables on the probability of failure of the limit-state function. This is the direction cosine of the unit outward normal vector [28], also referred to as the importance factor. The importance factors can be calculated according to equation 2-41.

$$\alpha_i = -\frac{\frac{\partial g(X^*)}{\partial x_i}\sigma_{x_i}}{\left[\sum_{i=1}^{n}\left(\frac{\partial g(X^*)}{\partial x_i}\sigma_{x_i}\right)^2\right]^{1/2}} \tag{2-41}$$

Here the asterisk denotes that the limit state function is zero ($g(X) = 0$). This is shown visually in figure 4-11.

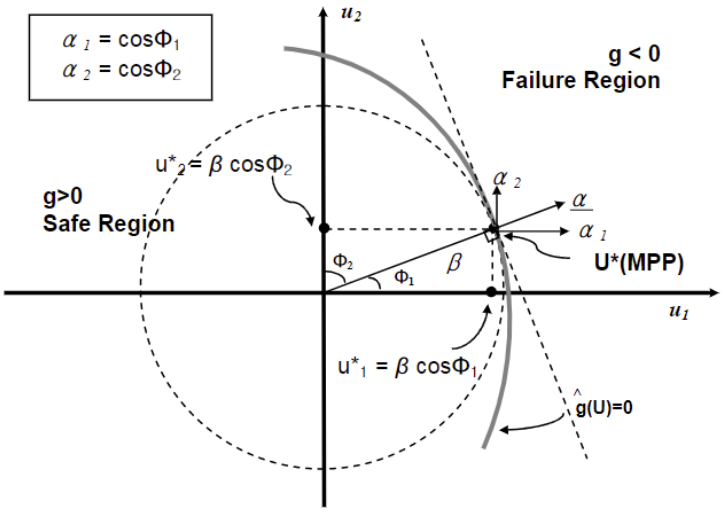

Figure 2-17: Visual representation of the importance factors [28]

For the evaluation of the FORM, a python package called OpenTURNS (open-sourced Treatment of Uncertainties, Risks'N Statistics) is used. By defining a limit-state function, stochastic models for all parameters, and an event ($g(X) < 0$), OpenTURNS returns requested outputs like the safety index or the importance factors.

Chapter 3

Case study

In the previous chapter, the methodology has been put forward. In this chapter, the information acquired for the case study will be presented, serving as input for the methodology. Location specific, cable, floater and fatigue data will be discussed. Lastly the stochastic model, used for the reliability method, is presented.

3-1 Location

In January 2022, Scotland made headlines by announcing 25GW of offshore wind to be installed in order to meet the climate goals of 2050. Most of these 17 wind farms will start construction around 2030. Of the 25GW, 15GW will be floating wind turbines. Seeing as it is a very recent development, the case study will be performed on one of the announced wind farms. The largest of the to be installed wind farms, is NE7, with lead applicant Scottish Power Renewables. The location of NE7 can be seen in the top right corner of figure 3-1, with the Scottish mainland in the left of the figure. A water depth corresponding to the chosen

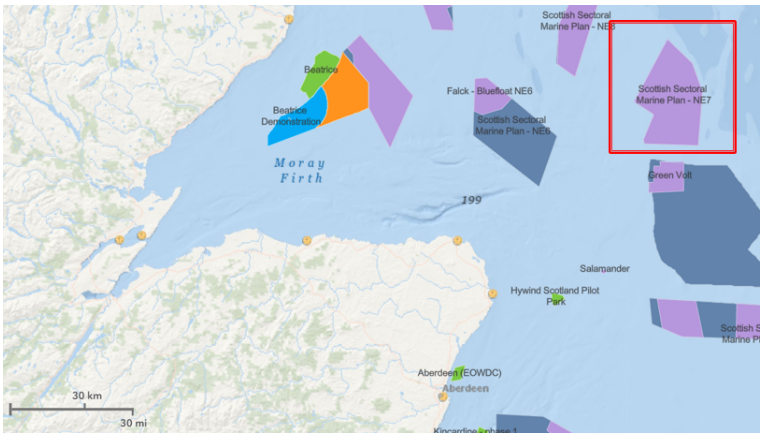

Figure 3-1: Offshore wind farm NE7 [45]

location can be identified in figure 3-2. Since the water depth varies slightly inside of the area, a value of 100m is chosen as an average.

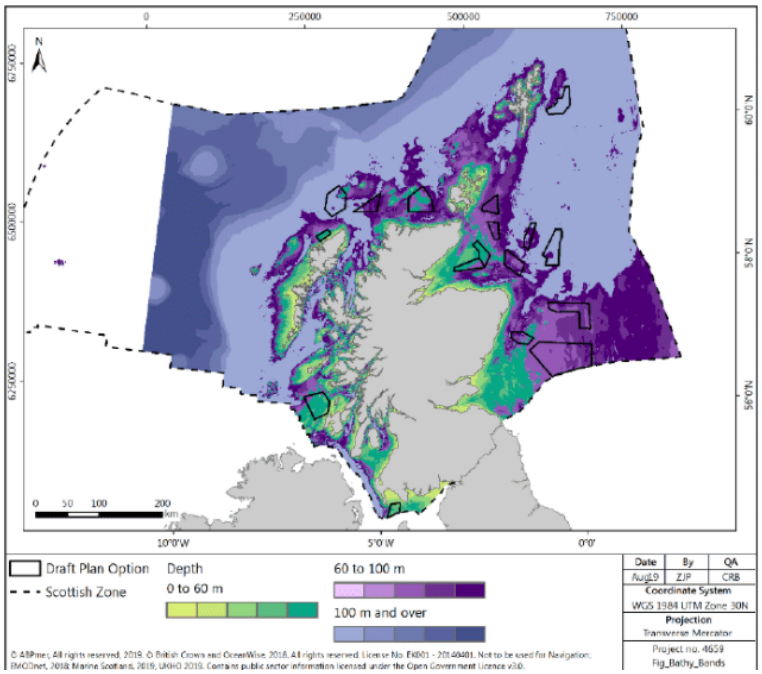

Figure 3-2: Farm NE7 water depth [46]

3-2 Wave data

For the wave climate data, use was made of [40]. This website "provides data for initial appraisal of metocean conditions", and is deemed suitable for the purpose of this research. The location, as outlined in section 3-1, was used to gather data for. For this research, wind and current loads are left outside the scope, so only data regarding the significant wave height, peak period and direction are of importance. For the analysis, the directionality will be split up into 9 bins of 40 deg will be used. Each bin has its own scatter diagram, similar to the example scatter diagram shown in figure 3-3. The shape factor of the JONSWAP spectrum γ is calculated in accordance with [47], as shown in equation 3-1. Here H_s is the significant wave height and T_P is the peak period. Important to note here, is that the occurrences gathered from [40], only has 1 decimal. Due to rounding off to 1 decimal, the sum of all the occurrences is less that 100 %, and the most severe cases (highest Significant Wave-height (Hs)), are not taken into account. In section 4-2 it will be explained how this is compensated for.

$$\gamma = \begin{cases} 5, & \text{for } T_p/\sqrt{H_s} \leq 3.6 \\ \exp\left(5.75 - 1.15\frac{T_p}{\sqrt{H_s}}\right), & \text{for } 3.6 < T_P/\sqrt{H_s} < 5 \\ 1, & \text{for } 5 \leq T_p/\sqrt{H_s} \end{cases} \tag{3-1}$$

	lower	01	02	03	04	05	06	07	08	09	10	11	12	13	14	15	16	17	18	19	20	21	22	23	24	25	26	
lower	upper	02	03	04	05	06	07	08	09	10	11	12	13	14	15	16	17	18	19	20	21	22	23	24	25	26	27	total
0.0	0.5	0	0	1.0	0.5	0.8	0.4	0.4	0.4	0.3	0.3	0.2	0.2	0.1	0.1	0.1	0.0	0.0	0.1	0.1	0.0	0.0	0.0	0.0	0	0.0	0	5.0
0.5	1.0	0	0.1	4.1	2.4	2.2	3.4	1.6	1.6	1.7	1.1	0.5	0.4	0.3	0.1	0.0	0.0	0.1	0.1	0.1	0.0	0.0	0	0.0	0	0	0	19.7
1.0	1.5	0	0	0.4	7.3	1.6	3.2	2.4	3.8	1.6	1.5	1.1	0.4	0.2	0.2	0.1	0	0.0	0.0	0.0	0.0	0.0	0.0	0.0	0	0	0	23.9
1.5	2.0	0	0	0	4.1	3.4	1.5	3.4	1.9	1.2	1.4	1.4	0.7	0	0.2	0.1	0	0.0	0.0	0	0.0	0	0.0	0	0	0	0	19.3
2.0	2.5	0	0	0	0.4	3.6	1.2	2.4	1.6	1.0	0.9	0.8	0.7	0	0.3	0.1	0.0	0.0	0.0	0	0.0	0	0	0	0	0	0	12.9
2.5	3.0	0	0	0	0.0	1.3	1.0	1.9	1.1	0.8	0.5	0.4	0.4	0.2	0.0	0.0	0.0	0	0	0	0.0	0	0	0	0	0	0	7.8
3.0	3.5	0	0	0	0	0.2	0.7	1.3	0.8	0.8	0.4	0.2	0.2	0.1	0	0.0	0.0	0	0.0	0	0	0	0	0	0	0	0	4.7
3.5	4.0	0	0	0	0	0.0	0.2	0.7	0.6	0.6	0.3	0.1	0.1	0.1	0	0.0	0.0	0	0	0	0	0	0	0	0	0	0	2.7
4.0	4.5	0	0	0	0	0	0.0	0.2	0.3	0.5	0.3	0.1	0.1	0.1	0	0.0	0	0	0	0	0	0	0	0	0	0	0	1.6
4.5	5.0	0	0	0	0	0	0	0.1	0.1	0.3	0.3	0.1	0.0	0.0	0	0.0	0.0	0	0	0	0	0	0	0	0	0	0	0.9
5.0	5.5	0	0	0	0	0	0	0.0	0.0	0.2	0.2	0.1	0.0	0.0	0	0.0	0.0	0	0	0	0	0	0	0	0	0	0	0.6
5.5	6.0	0	0	0	0	0	0	0.0	0.0	0.1	0.2	0.1	0.0	0.0	0	0.0	0.0	0	0	0	0	0	0	0	0	0	0	0.3
6.0	6.5	0	0	0	0	0	0	0.0	0.0	0.0	0.1	0.1	0.0	0.0	0	0	0	0	0	0	0	0	0	0	0	0	0	0.2
6.5	7.0	0	0	0	0	0	0	0	0.0	0.0	0.1	0.1	0.0	0	0	0	0	0	0	0	0	0	0	0	0	0	0	0.1
7.0	7.5	0	0	0	0	0	0	0	0	0.0	0.0	0.1	0.0	0	0	0	0	0	0	0	0	0	0	0	0	0	0	0.1
7.5	8.0	0	0	0	0	0	0	0	0	0	0.0	0.0	0.0	0	0	0	0	0	0	0	0	0	0	0	0	0	0	0.1
8.0	8.5	0	0	0	0	0	0	0	0	0	0	0.0	0.0	0	0	0	0	0	0	0	0	0	0	0	0	0	0	0.0
8.5	9.0	0	0	0	0	0	0	0	0	0	0	0.0	0.0	0	0	0	0	0	0	0	0	0	0	0	0	0	0	0.0
9.0	9.5	0	0	0	0	0	0	0	0	0	0	0	0.0	0	0	0	0	0	0	0	0	0	0	0	0	0	0	0.0
9.5	10.0	0	0	0	0	0	0	0	0	0	0	0	0	0	0	0	0	0	0	0	0	0	0	0	0	0	0	0.0
total		0.0	0.1	5.5	14.5	13.1	11.5	14.3	12.3	9.2	7.5	5.3	3.3	1.1	0.9	0.4	0.1	0.2	0.2	0.2	0.1	0.1	0.0	0.0	0.0	0.0	0.0	100.0

Figure 3-3: Wave scatter at NE7 [40]

3-3 Global configuration

Different configurations of a Dynamic Power Cable (DPC) in the water are possible. Three of the standard configurations, adopted from flexible riser technology, are the free hanging catenary, steep wave and the lazy wave configurations (figure 3-4). More configurations are possible, but these are the most common [48].

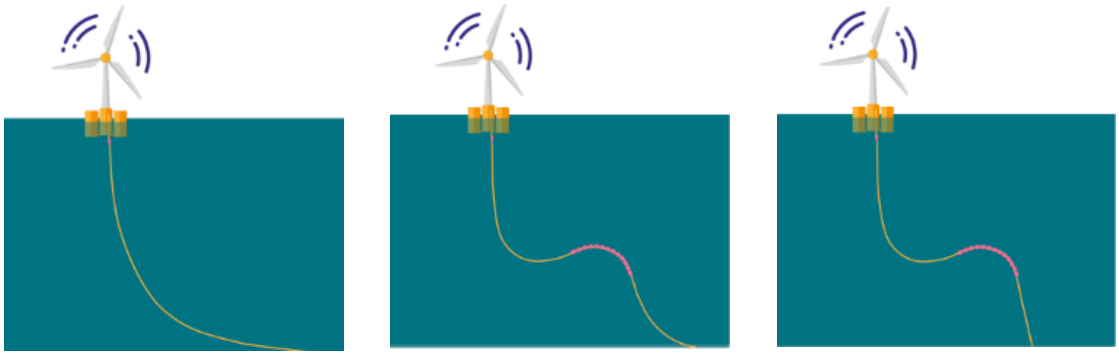

(a) Free hanging Catenary **(b)** Lazy wave **(c)** Steep wave

Figure 3-4: Standard dynamic cable configurations [49]

A free hanging catenary is the simplest configuration, as it does not require any additional buoyancy modules. It does not however decouple the floater motions, and requires a bend restrictor at the far-lead.
In the lazy wave configuration, buoyancy modules are added to the mid section of the cable, decoupling the motions of the floater and the bottom part of the cable. It changes shape if marine growth appears along the cable. This configuration is suitable for circumstances in which more motion of the floater is expected.
The steep wave is similar to the lazy wave, with the addition of a sub-sea bend stiffener. This extra bend stiffener prevents a change of shape due to marine growth, and limits the sub sea footprint of the dynamic cable. It does add more complexity to the configuration, and is only suitable if the advantages outweigh the added costs.
For this study, the case of a simple free hanging catenary dynamic power cable will be investigated. This is to avoid having to make additional assumptions about any buoyancy elements

that could influence the results.

3-3-1 Modeling choices

3-3-1-1 Initial properties

For setting up the global model, a hysteresis curve with initially best estimate properties is used. This initial case will be used to identify the critical regions along the cable, choose a mesh size and time step size, and investigate the effect of modeling a regular or irregular sea states. The most important initial values are summarized in table 3-1, and the hysteresis curve based on these values is shown in figure 3-5. These values are proposed by Orcaflex for an umbilical with a diameter of 0.18 meters.

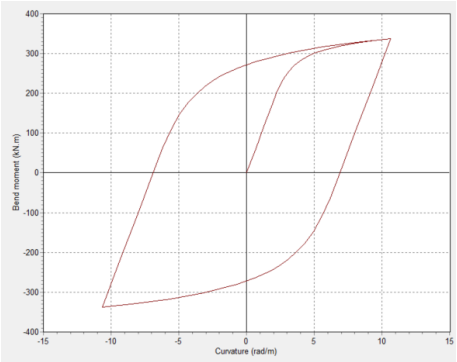

Figure 3-5: Hysteresis curve based on initial value estimation

Outer diameter [m]	Axial stiffness [MN]	Torsional stiffness [kNm^2]	Mass [kg/m]
0.192	800	600	72

Table 3-1: Summary of values used for the calibration of the global model

3-3-1-2 Critical region

For the identification of the most critical region of the DPC, a fatigue analysis is done for the entire length of the cable, using the built in damage calculator in Orcaflex, with an SN curve as put forward in section 3-5. First, the effect of the boundary condition at the off-lead position on the DPC in investigated. Figure 3-6 shows the normalized damages of a fixed and pinned boundary condition. It is clear that fixing the DPC moves the critical region of the cable towards the off-lead point. The cumulative damage at this point is largely influenced by the choice of bend-restrictor. Since data of such components is not readily available in open literature, and making an estimate of the properties of a bend-restrictor will introduce more uncertainties into the model, the scope of the study will be done with a pinned boundary condition at the hang-off point, thus focusing on the touch-down region.

To further investigate what part of the DPC is critical, analysis are performed for all wave directions and combinations of wave heights and peak periods that occur in the scatter di-

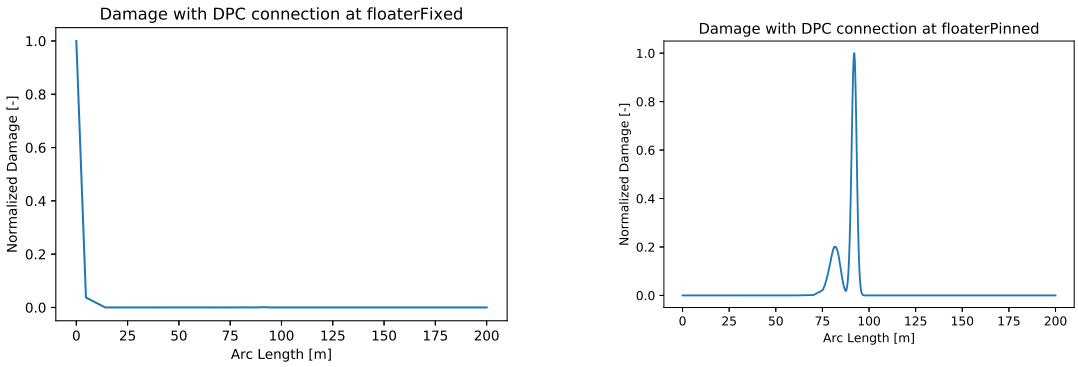

(a) DPC fixed at floater

(b) DPC pinned at floater

Figure 3-6: The effect of different boundary conditions at the floater end of the DPC

agram, since different directions/sea states can impact different locations on the cable. The results of all these analysis have been plotted in figure 3-7. Again, the damage has been normalized with respect to the most damaging case.

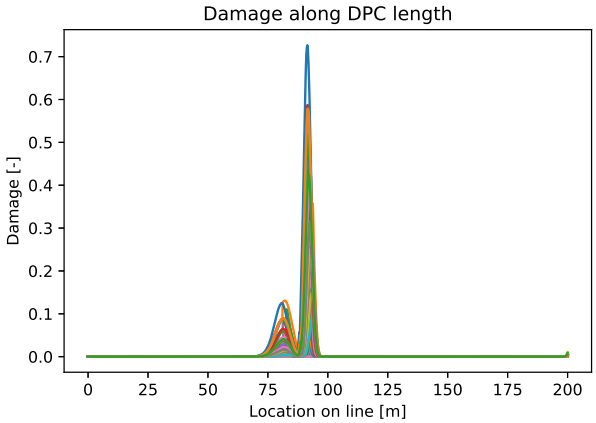

Figure 3-7: Critical location

In figure 3-7, 2 clear peaks can be distinguished from one another. This is a common observation when investigating the fatigue damage of flexible slender structures near their touchdown region. [50] and [32] observe similarly shaped damage plots along the arc length. The lowest of the two peaks in just a bit above the touchdown zone, and experiences most bending stress. The higher peak experiences less cycles, but the Von Mises stress has a higher standard deviation than that of the lower peak, as shown in figure 3-8.

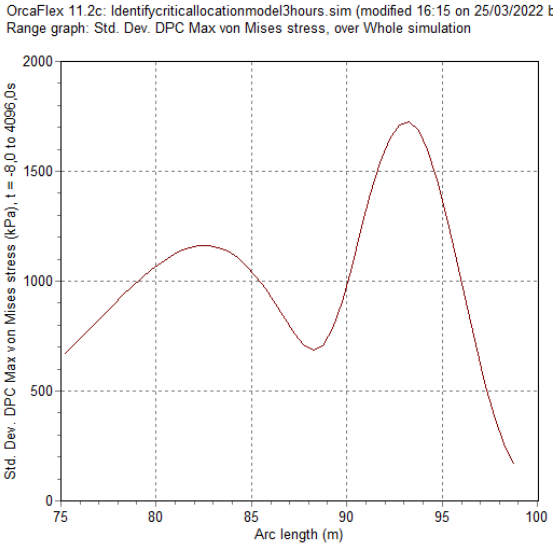

Figure 3-8: Standard deviation of the Von Mises stress between 75 and 100m arc length

Figure 3-9 clearly shows that more high-cycle-low-stress is encountered around the left peak, and more high-stress-low-cycle around the right peak.

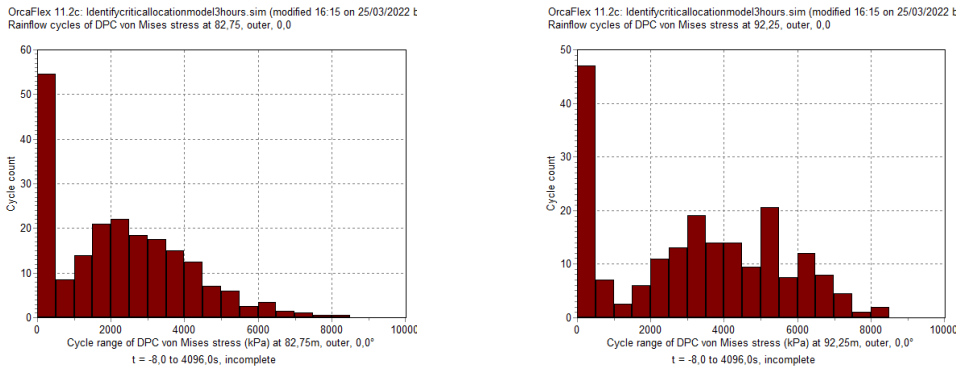

(a) Cycle range Von Mises stress at arc length=82.75m **(b)** Cycle range Von Mises stress at arc length=92.5m

Figure 3-9: Histograms of the Von Mises stress

According to [51], the left peak is a result of wave induced fatigue, and the right peak seabed induced fatigue. The amplitude of the right peak can be influenced by changing the soil stiffness, as can be seen in figure 3-10. Here the left peak stays constant, confirming the claim from [51].

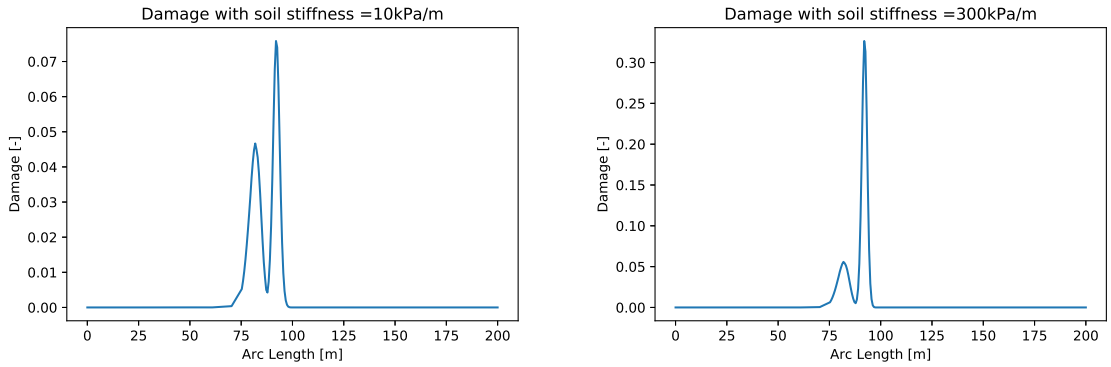

(a) Soil stiffness = 10 kpa/m **(b)** Soil stiffness = 300 kpa/m

Figure 3-10: Effect of soil stiffness on fatigue damage peaks

3-3-1-3 Critical sea state

From the data gathered in section 3-3-1-2, also the most critical sea state can be defined. This is defined as the sea-state that has the highest damage per time. This sea state will be used for the mesh convergence study and the determination of the required time-step. The most critical sea state for this initial cable lay-out occurs in a sea state with a significant wave height of 7.25m, a peak period of 11.50s, and with waves coming in under a 0 degree angle.

3-3-1-4 Mesh size

A study concerning the mesh size of the dynamic power cable was performed in order to determine a suitable segment length for the model. In the critical area, a finer mesh is required since there are higher stress variations, and this is the part of the cable that will be analyzed later on. Figure 3-11 shows the three different segments in different colors.

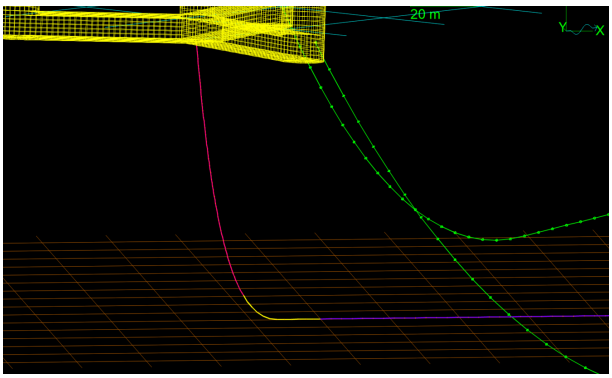

Figure 3-11: Segments in the DPC

The mesh convergence study was conducted only for the middle section of the cable, and the resulting damage is shown in figure 3-12. Figure 3-12a shows a large spread in damage for a mesh size of 5m to 0.1m. In figure 3-12b this spread in inspected between 1 and 0.1m. It is

observed that between 0.2m and 0.1m, a change of only 1% of the max damage is observed. From this it is concluded that a mesh size of 0.2m will suffice for the case at hand.

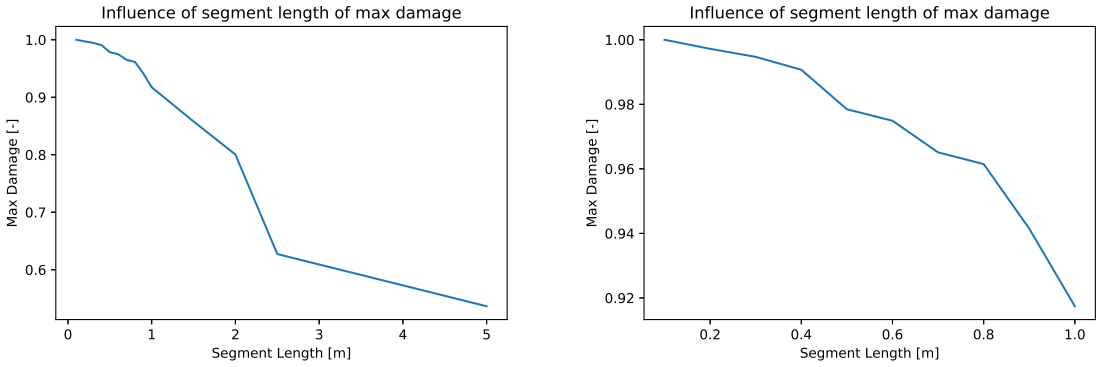

(a) Mesh convergence over the total analyzed range **(b)** Mesh convergence over the zoomed range

Figure 3-12: Results of the mesh convergence study

3-3-1-5 Time step

Similarly to the mesh size, also the time step influences the outcome of the fatigue calculation. The results from the time step study is shown in figure 3-13. Here, a clear convergence is visible, and an increase in computational time does not significantly influence the resulting damage at time steps smaller than 0.2s.

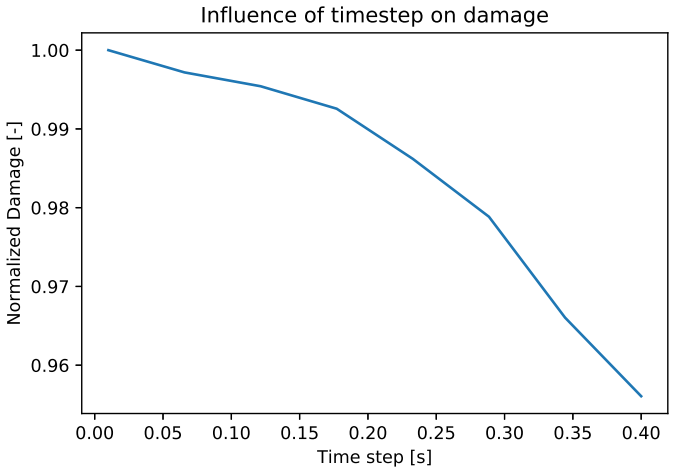

Figure 3-13: Time step convergence

3-3-1-6 Regular/irregular

In order to identify the effect of the type of sea-state used for the analysis, a comparison is made between regular and irregular (JONSWAP) seas. This is done in order to investigate

the possibility of reducing computational time. If regular seas give comparable results to irregular seas, the simulation time could be reduced significantly.
Both regular and irregular simulations are run for similar conditions, and the results are compared to see if a simplification of a regular sea can be made. For the previously identified critical sea state, the regular sea analysis has a 20 year fatigue damage of 0.32, whereas an irregular sea state has a 20 year damage of 0.47. Also the ratio between the height of the two peaks is not the same. It is therefore concluded that the simplification of a regular sea cannot be made.

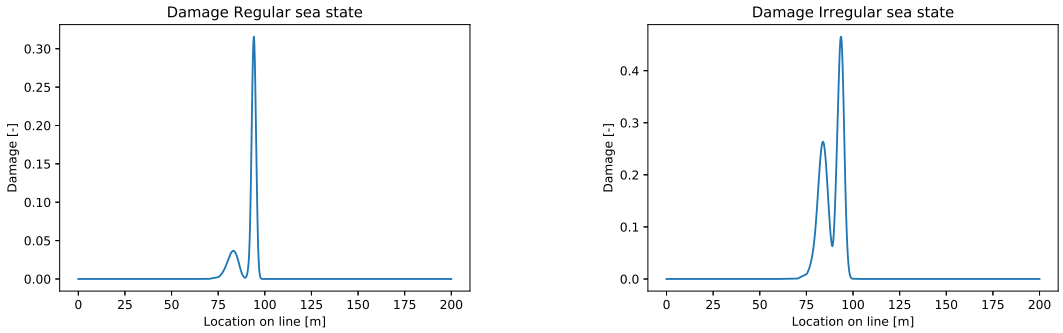

(a) Regular sea state damage **(b)** Irregular sea state damage

Figure 3-14: Difference in damage between a regular and irregular sea-state

3-4 Cable

Both CoreWind [49] and the Floating Offshore Wind reliability JIP of DNV [13] give a 66kV 3 core Alternating Current (AC) cable as a base case for design and cost reduction in upcoming studies. Mention is made that since this is a very new cable, not much documentation can be found on it. Comparisons can be made to the 33kV cables installed at the Kincardine floating offshore wind farm, and the 115kV dynamic cable installed at the floating oil & gas platform Gjøa [52]. Based on these 2 cases, a best estimate of a 66kV cable will be made.

The Gjøa cable, provided by NKT Cables, has 3x300mm^2 conductors, which is larger than the 240mm^2 static cable conductors. This is due to the fact that the dynamic cable is thermally limited at the bend stiffener at the upper end. The cable has a sheath of corrugated copper, and a double armoring, preventing water penetration. Two lead rods are present in the cross-section to increase the weight to diameter ratio. A polyethylene serving protects the armor from abrasion [52].
For the Kincardine project, the dynamic cables have been provided by Prysmian. Similar to the Gjøa cable, also these cables are 3 phase AC. They have a 500mm^2 total conductor area, an outside diameter of 170 mm and an in air weight of 57kg/m. A detailed cross-section is provided by [53], and can be seen in figure 3-15.
According to [49], the 66 kV base case has a copper conductor area of 800mm^2 and an outside diameter of 0.192 meters. In [54], Prysmian describes a static 66kv inter array cable having a 800mm^2 conductor of aluminum.

The main parameters of the discussed cables are summarized in table 3-2.

	Gjoa 115 kV	Kincardine 33 kV	Case study 66 kV
Conductor size [mm^2]	900	500	800
Diameter [m]	-	0.17	0.192

Table 3-2: Summarized data of the comparable cables

As previously stated, a dynamic cable needs a larger conductor area than a static cable, and an aluminum core a larger area than a copper one. Seeing as these two factor oppose each other, a $800mm^2$ copper conductor for a dynamic 66kv cable seems acceptable. As base case, the 33kv cable in figure 3-15 scaled to a diameter of 0.192 meters will be used.

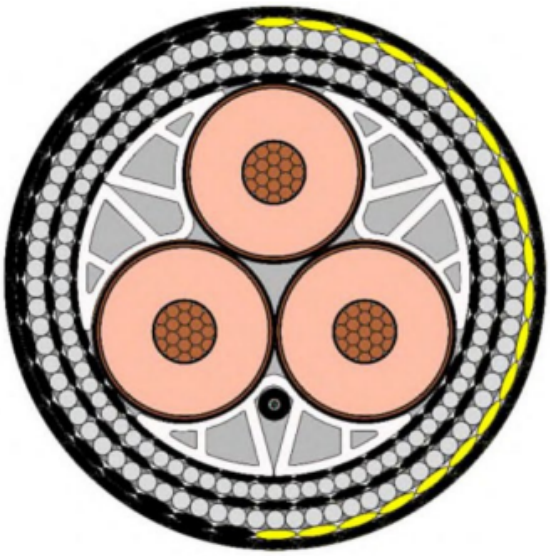

Figure 3-15: Cross-section of the 33kv inter-array cable used for the Kincardine project [53]

3-4-1 Model

Simplifications of the specified cable will be made to implement on the model. This is done based on the scope of this research.

3-4-1-1 Cross-section

As discussed, a similar cable to that used in the Kincardine floating wind farm will be used, but suitable for 66kV instead of 33kV. Diameters of the cable (shown schematically in figure 3-16) are shown in table 3-3. From outside to inside, the modeled layers are the outer sheath, outer strands, inner sheath, inner strands and the core.

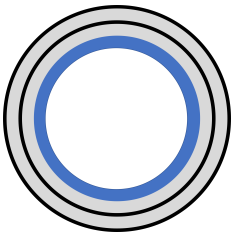

Figure 3-16: Schematic cable cross-section

Layer	Diameter [m]
Outer sheath	0.192
Outer strands	0.186
Inner sheath	0.166
Inner strands	0.16
Core	0.14

Table 3-3: Diameters of the individual layers

The initially modeled cable can be seen in figures 3-17a and 3-17b, showing a view of the two individual layers of strands, with two outer strands removed for the image, and a top view of all the layers respectively.

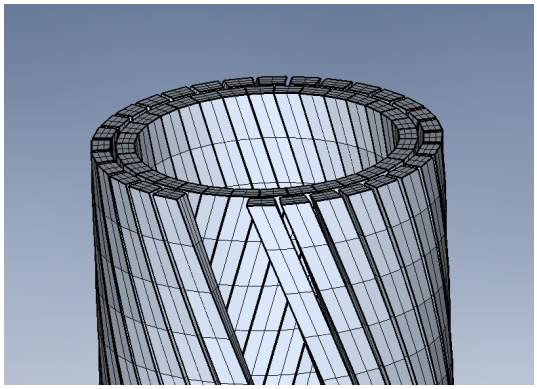

(a) Strands in the cable with 2 outer strands removed

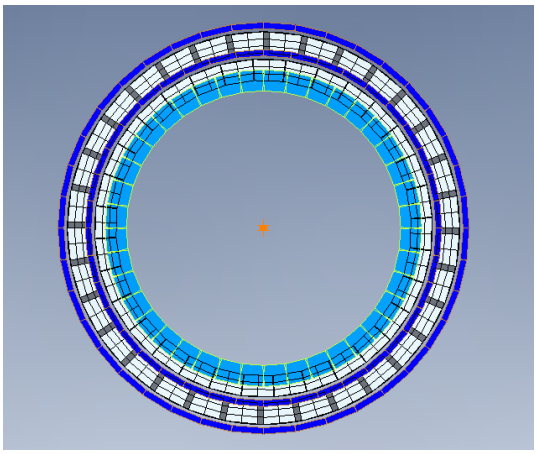

(b) Cross sectional view of the cable

Figure 3-17: Initial cable model

3-4-1-2 Properties

Material properties for the different layers in the cross section are adopted from [36], and summarized in table 3-4.

Layer	Core	Strand	Sheath
Material	Copper/XLPE	Steel	PE
Young's modulus [GPa]	20.2	207	0.18
Poisson's ratio [-]	0.35	0.3	0.38

Table 3-4: Material properties

Core equivalent

As mentioned before, the solid core will be modeled using shell elements to reduce computational time. Thus, equivalent material properties for the core elements need to be calculated.

This is done in two steps. First a homogeneous equivalent of the core is calculated according to the area ratio between the conductor and the filler (equation 3-2). With this equivalent stiffness, a model stiffness can be calculated by equating the bending stiffness of the homogeneous core to that of a shell core with a thickness of 10mm (equation 3-3).

$$E_{eq} = \frac{E_{copper} \cdot A_{conductor} + E_{xlpe} \cdot A_{xlpe}}{A_{core}} \tag{3-2}$$

Then equating the bending stiffness of the equivalent core with the modeled plate core of 1cm thickness;

$$E_{mod} = \frac{E_{eq} \cdot I_{core}}{I_{mod}} \tag{3-3}$$

Here I_{core} and I_{mod} are known since the core is a solid cylinder with an area of 0.015 m^2 and the modeled core a tube with a thickness of 0.01 m and a diameter of 0.14 m. Then with $E_{copper} = 120GPa$ and $E_{xlpe} = 0.1Gpa$, the Young's modulus used in the model, $E_{mod} = 20.2GPa$.

Strands

For the modeling of the strands, rectangular shaped (10x14.5 mm) cross sections are used in order to make for a better contact surface between the different layers, and reduce the computational cost. Since a solid rectangular beam does not have the same axial and bending stiffness as the wire it is meant to represent, an equivalent stiffness is determined. From a typical 10mm steel wire, shown in figure 3-18, it is estimated that there is steel in about 65 % of the cross-sectional area. Furthermore, the bending stiffness of the steel wire and the rectangular block, that is modeled, should be equal.

$$E_{strand} = \frac{0.65 \cdot E_{steel} \cdot I_{wire}}{I_{rectangle}} \tag{3-4}$$

With $I_{wire} = \frac{\pi \cdot D^4}{32} = \frac{\pi \cdot 0.01^4}{32}$ and $I_{rectangle} = \frac{b \cdot h^3}{12} = \frac{0.01 \cdot 0.0145^3}{12}$, it results in $E_{strand} \approx 0.25 \cdot E_{steel}$.

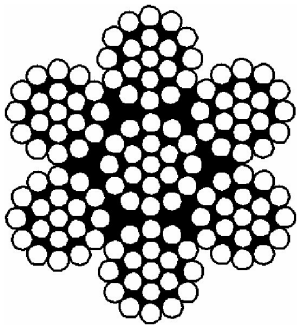

Figure 3-18: Cross-section of a 10mm steel wire [55]

3-4-1-3 Hysteresis curve

As explained in section 2-2-1, the curvature is calculated at every (ghost) node along the length of the cable, and at every iteration. This gives a hysteresis curve for every node. In figure 3-19 the hysteresis curves of all nodes in the cable are plotted. Here it can be observed

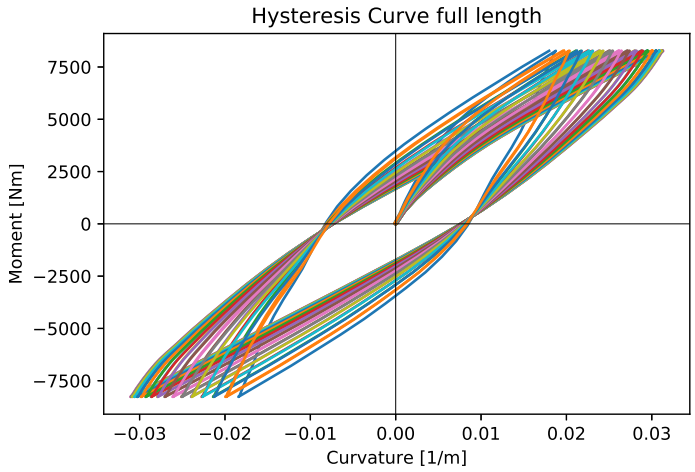

Figure 3-19: Hysteresis curves full length

that significant deviations exist between the different curves. The applied moment and the curvature are related to each other by the bending stiffness EI, according to equation 3-5.

$$\kappa = \frac{M}{EI} \tag{3-5}$$

Here EI is assumed to be constant, which is not in line with the results from figure 3-19. The differences in the curves is expected to be the result of the influence of the boundary conditions, by adding stiffness and causing the strands not to transition from stick to slip at the same instance. Results near the ends of the cable are therefore not expected to be accurate. Figure 3-20a shows the same curves, now excluding the top and bottom part of the cable. Of the 34 ghost nodes, only the hysteresis curves for nodes 12 to 24 are plotted.

Here there is a clear convergence to a single hysteresis curve visible. From this convergence, it can be concluded that an adequate length of the model has been selected, since a far enough distance form the boundary conditions can be reached to evaluate the bending stiffness at. This confirms the claim made in [32] that one pitch length is enough to model. In order to get one consistent hysteresis curve as output, the hysteresis curves of the middle 10 nodes are averaged. This can be seen in figure 3-20b.

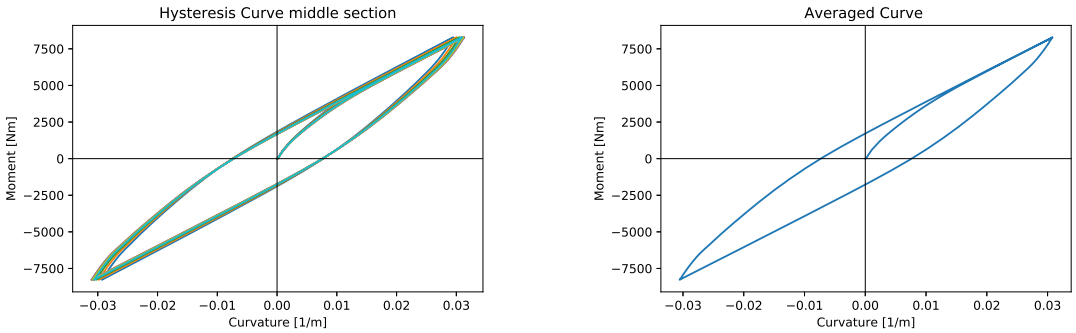

(a) Hysteresis curves middle section **(b)** Averaged hysteresis curve

Figure 3-20: Hysteresis curves

3-4-2 Mesh convergence

In this section the effect of increasing the amount of elements used in the model on the hysteresis curve is investigated. This is useful to determining an adequate mesh size that gives accurate results, without being unnecessarily computationally expensive. In order to be able to compare different mesh sizes with one another, the area under the hysteresis curve is evaluated, see figure 3-21.

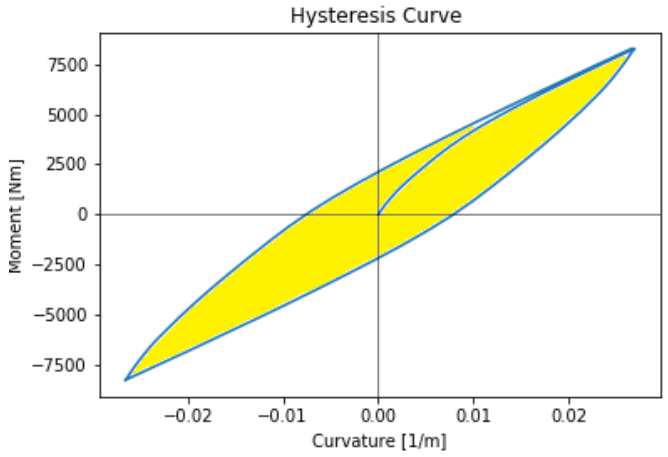

Figure 3-21: Area inside the hysteresis curve

This way both energy dissipating effects and maximum curvatures are taken into account. In order to reduce computational time, only 6 strands per layer are modeled for the mesh convergence study, as opposed to the 32 in the full model. In the initial model, 3074 elements are used. This is gradually increased until no large (<1%) change is observed between the successive models. In figure 3-22 the absolute error with respect to the model containing the most amount of elements (equation 3-6) evaluated is plotted. It can be seen that increasing the amount of elements to more than 20784 does not have a significant impact on the dissipated energy.

$$\epsilon_{abs} = \left| \frac{E_n - E_{max}}{E_{max}} \right| \tag{3-6}$$

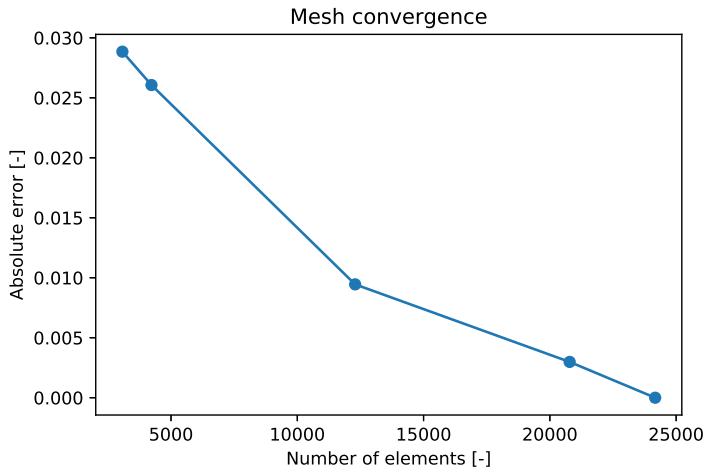

Figure 3-22: Absolute error of mesh convergence

3-4-3 Validation

The local model is very complex, with many variables at play. Especially the way contact can be defined in Femap is very elaborate. Therefore, a validation model has been made to be compared against data from literature. This way, the way the model is being set up can be validated. For validation, [35] is used. In this paper an un-bonded flexible riser is modeled in Abaqus. A cross-section of the riser is seen in figure 3-23.

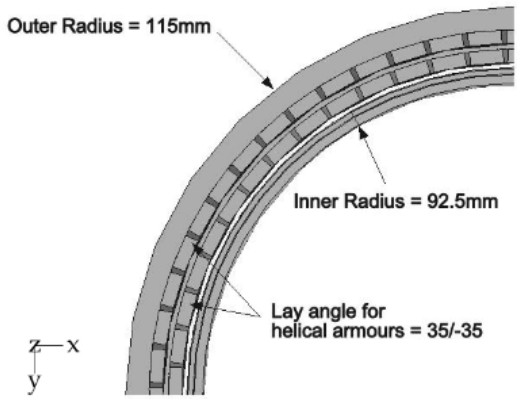

Figure 3-23: Cross section validation riser [35]

To better match this case, a model of the DPC is altered to match the diameter of the riser in [35]. Since the lay-angles of the DPC and the riser are already the same, this scaled model

is expected to have a good resemblance to the riser. This validation case is then used to tune properties that were uncertain before. One of these uncertainties is the bonding pressure. This value tells us how tightly the cable is bonded by the outer sheath during production, and gives an initial radial pressure in the cable. This largely influences the amount of traction between the different layers in the cable, and thus the stiffness. In the model, this parameter is changed by altering the offset of the plate elements in the outer sheath. In figure 3-24 it can be observed how the outer sheath has some initial penetration into the outer layer of strands. The same is done for the initial penetration of the core into the inner layer of strands. By setting up the model this way, and running a Femap simulation without external load, the outer sheath will essentially be pushed out of the outer strands, creating pressure. An other parameter of interest is the Young's modulus of the modeled strands. In section 3-4-1-2 an initial estimation of this has been made. In the validation, this estimate can be validated.

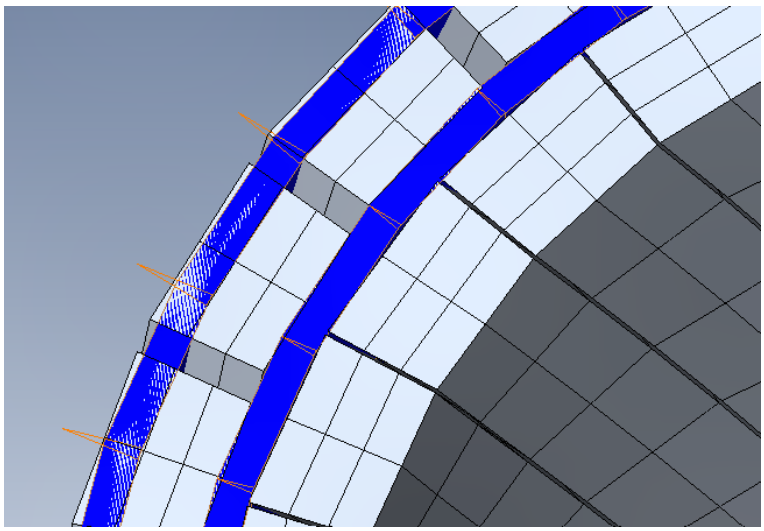

Figure 3-24: Initial penetration

Figure 3-25 shows the comparison between the Femap model and the validation case. Two aspects to the plot are influenced by changing the bonding pressure. Firstly, the stiffness is influenced. With a higher bonding pressure, a higher stiffness will be obtained due to the fact that there is more traction between the layers. Secondly, the width of the curve (distance between the loading and unloading cycle) is affected. With higher bonding pressure and traction, there will be a larger difference between the stick and the slip stiffness. This is because only the slip stiffness is increased by increasing the traction, and the cable will be in the stick regime for a larger portion. Because of this, a larger area is created inside the curve, meaning more energy is being dissipated. For the validation the goal was to match the bending stiffness of [35] as good as possible. The Young's modulus of the strands did not largely influence the results, while keeping this parameter in an acceptable range. Changing the bonding pressure influenced both the width and the stiffness. The aim was to get the individual stiffnesses as close to the validation stiffnesses as possible. In figure 3-25 it can be seen that the slip stiffness lines are almost parallel, and that the stick stiffness in the first loading cycle is also very close to the validation case. The biggest difference between the two is the transition phase from stick to slip.This is expected to be due to the presence of a pressure

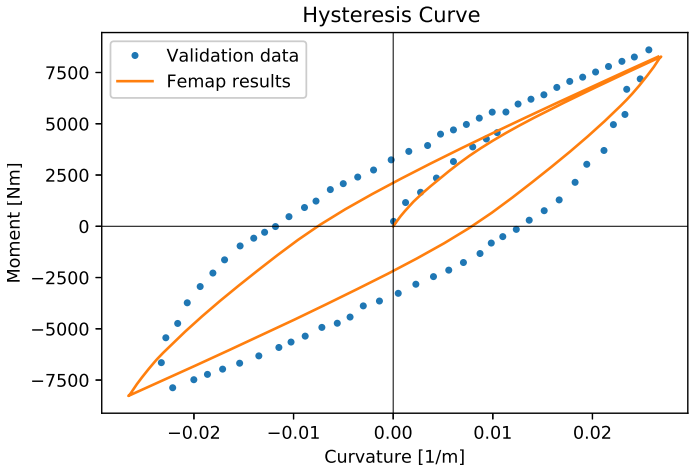

Figure 3-25: Comparison between the Femap model and the validation data

armoring in the validation case, adding radial stiffness to the riser, that is not present in the power cable. Due to the flexibility, not the entire circumference of the cable transitions from from stick to slip at the same time. Therefore this kink in the line is smoother. Since the change in Young's modulus for the stands, within an acceptable range, does not largely affect the outcome, the initial estimate for the equivalent Young's modulus of the strands accepted to be good.

The resulting parameters from comparing the model to the validation data are summarized in table 3-5. These values will be adopted for the model of the DPC.

Outer sheath penetration [m]	Core penetration [m]	Strands Young's modulus [Gpa]
0.005	0.005	51.8

Table 3-5: Validated parameters

3-5 S-N curve

S-N curves for umbilical and riser armoring are manufacturer specific, and not a lot is freely available in the open literature [16]. Each manufacturer tests and establishes its own curves. In [41], a theoretical approach for determining the fatigue life of flexible pipes is put forward. In this paper, an S-N curve proposed by [22] is used. This is a curve for high strength steel, in the presence of seawater. This curve will also be adopted for this case, and is deemed to be accurate enough, given the lack of manufacturer information. This is a single slope S-N curve with m=4.7 and log(A)=17.446, seen in figure 3-26. Similar to [41], the Goodman mean stress model will be used, as explained in section 2-2-3.

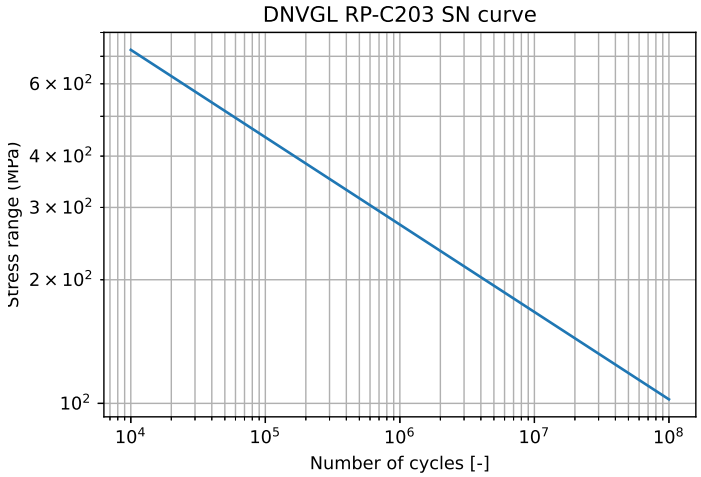

Figure 3-26: High strength steel S-N curve

3-6 Floater

Many different floater types exist at this moment, as the industry has not converged to a single concept yet. The floaters can mainly be classified into three categories. The spar, semi-submersible and the Tension Leg Platform (TLP). Typically, due to its large draft, spar type floaters are suitable for deeper waters (>120m), whereas semi-submersibles and TLP's are also suitable for shallower waters. Since the modeling of a floater is not part of the scope of this study, an example floating wind turbine model, provided by Orcina, will be used. This is the K03 15MW semi-sub FOWT [38], seen in figure 3-27. This model contains a 15 MW turbine, developed as part of the International Energy Agency's (IEA) Wind Task 37 [56]. The floater, the Volturn US-S reference semi-submersible platform, was developed by the University of Maine [57]. This includes the mooring design.

Figure 3-27: K03 15MW semi-sub FOWT

3-7 Stochastic models

For the evaluated case, literature has been consulted to come up with the right stochastic models. It should be noted that all of the available literature on the subject at hand is considering risers. Therefore, no parameters that are unique to power cables can be considered in this research, since there are no available stochastic models for there parameters. The stochastic parameters used were deemed most interesting for the evaluation of dynamic power cables specifically, and parameters having to do with uncertainties in the fatigue analysis are kept outside the scope of this research. The normalized stochastic models are summarized in table 3-6.

In the Orcaflex model, the soil stiffness is modeled as being linear. This parameter is more complex in reality, and many studies have been done to better understand the dynamic interaction with soil, [58] for example. The complex modelling of this interaction is considered beyond the scope of this research. To determine the stiffness, a static situation where the cable is submerged by half its diameter into the soil is evaluated. Using the underwater weight of the cable, and its diameter, the soil stiffness is determined.

Variable	Distribution type	Mean	Standard Deviation	Source
Friction coefficient (Cf)	LN	1	0.1	[30]
Local analysis sensitivity (LAS)	N	1	0.15	[30]
Soil stiffness (Es)	LN	1	0.35	[16]
Drag coefficient (Cd)	LN	1	0.175	[16]
Global analysis sensitivity (GAS)	N	1	0.05	[44]

Table 3-6: Normalized stochastic models

In table 3-7, all combinations of variables are outlined, and the corresponding simulation ID's.

Simulation ID	Friction coefficient[-]	Local analysis sensitivity[-]	Soil stiffness $[kN/m^3]$	Drag coefficient [-]	Global analysis sensitivity [-]
1	0.1	1	39	1.05	1
2	0.08	1	39	1.05	1
3	0.12	1	39	1.05	1
4	0.1	0.7	39	1.05	1
5	0.1	1.3	39	1.05	1
6	0.1	1	11.7	1.05	1
7	0.1	1	66.3	1.05	1
8	0.1	1	39	0.6825	1
9	0.1	1	39	1.4175	1
10	0.1	1	39	1.05	0.9
11	0.1	1	39	1.05	1.1

Table 3-7: Summary of the simulations

Chapter 4

Results

In this chapter, the results obtained for the case study will be presented and evaluated on their validity. In chapter 5 the results will be discussed further, and compared to other literature. In chapter 6, conclusions will be drawn.

4-1 Local model

The local model was used to determine the global bending stiffness of the cable, as explained in section 2-2-1. One of the bending stiffness curves obtained from local can be seen in figure 4-1.

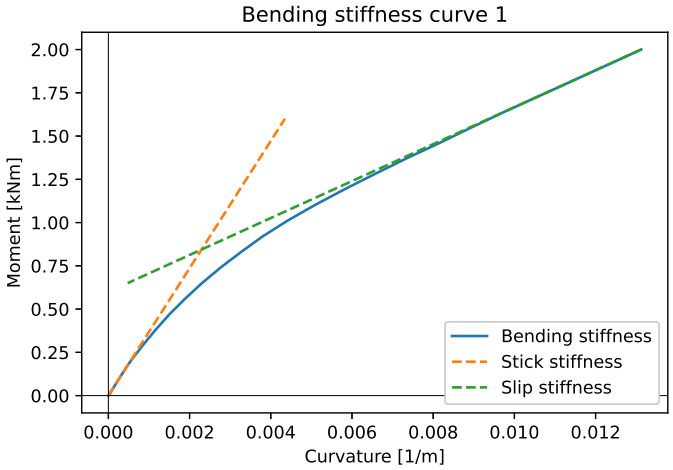

Figure 4-1: Bending curve from Femap

Here a clear distinction between the stick- and slip stiffness can be observed. The fact that the transition from stick- to slip stiffness is smooth, and not a pointy kink, can be explained

by the fact that not all strands in the cross-section of the cable slip at the same moment. Figure 4-2 shows all of the 5 stiffnesses corresponding to simulations 1 till 5. Clear differences are visible both for the stiffness, as well as for the maximum curvatures.

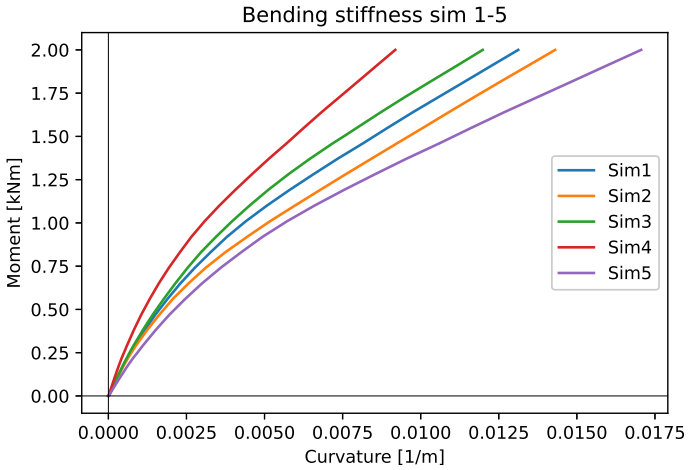

Figure 4-2: All bending stiffnesses for simulations 1-5

As expected, the maximum curvature of ID 2 is higher than that of ID 1, since it becomes less stiff due to the reduction in friction coefficient. This holds vice versa for ID 3. This effect can be seen in figure 4-3. Here a cross-section of the cable in the center for (from left to right) simulation 2, 1 and 3 are shown. Higher traction can be seen for higher friction coefficients, leading to a stiffer cable.

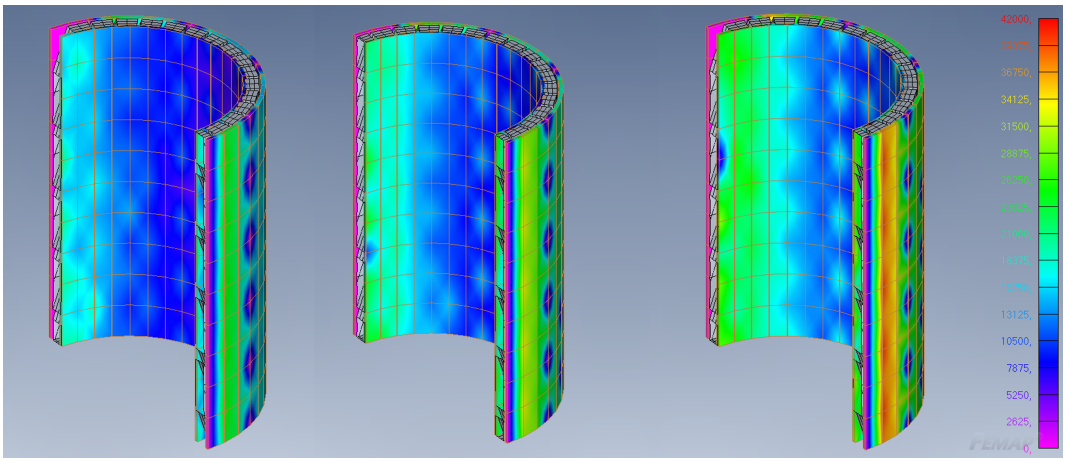

Figure 4-3: Traction [N] for simulation 2, 1 and 3 (from left to right)

For ID 4 and 5, the final result of the local model is multiplied by 0.7 and 1.3 respectively. This is in line with the results in the table. Important to note is that only 5 different cases for the local model need to be evaluated, as opposed to the total of 11 simulations. This is because for simulations ID 6-11, all local parameters are evaluated at their mean, which is identical to ID 1.

4-2 Global model

In this section, the results obtained from the global analysis method will be discussed. Section 2-2-2-2 explained how damage is calculated for a given combination of a significant wave-height and a peak-period. By performing this damage calculation for every combination in the wave scatter diagram, and multiplying the resulting damage by the yearly occurrence, the total damage per year can be obtained. As explained in section 3-2, the scatter diagrams used for this research only have 1 decimal. Because of this, due to rounding off, the most severe sea-states appear to have 0 occurrence, whereas in reality they have an occurrence between 0 and 0.049. These sea-states are the most damaging ones, and completely neglecting them would result in an underestimation of the yearly damage. The total damage for every simulation is therefore multiplied by a factor of 1.25 in order to get a more realistic fatigue life, approximately matching the fatigue life calculated in [42]. The resulting data is summarized in table 4-1, showing the damage per year.

	Wave-induced peak	Seabed-induced peak	Total
Sim ID	Damage per year [-]	Damage per year [-]	Damage per year [-]
1	4,54E-02	4,06E-02	4,54E-02
2	3,27E-02	3,05E-02	3,27E-02
3	5,98E-02	5,43E-02	5,98E-02
4	1,61E-01	1,90E-01	1,90E-01
5	1,99E-02	9,51E-03	1,99E-02
6	4,14E-02	3,03E-02	4,14E-02
7	4,63E-02	4,19E-02	4,63E-02
8	3,92E-02	3,91E-02	3,92E-02
9	5,95E-02	4,29E-02	5,95E-02
10	1,19E-02	1,18E-02	1,19E-02
11	1,46E-01	1,16E-01	1,46E-01

Table 4-1: Results from the global model

Simulation 1 is the reference case, at which all stochastic parameters are evaluated at their mean. For every stochastic parameter the effect on its fatigue damage along the cable is plotted in figures 4-5 to 4-9. There are two distinct peaks visible for each case, as previously discussed in section 3-7. In line with [59], the right peak corresponds to seabed induced fatigue, and the left one is related to wave induced fatigue. The location corresponding to the peaks are shown in red in figure 4-4. Table 4-1 also shows the overall damage, which is the maximum of the two peaks. Underlined are the values that are the maximum in every simulation. It can be seen that the wave-induced peak is dominant in all but one simulation.

Figure 4-4: Critical points around the touch-down zone

Friction coefficient

Simulation 2 and 3 correspond to a friction coefficient of 0.08 and 0.12 respectively. For these simulations, the change in bending stiffness is discussed in paragraph 4-1. For a lower friction coefficient, a lower bending stiffness is calculated because there is less traction between the layers, and vice versa. The effect of the change in bending stiffness on the results of the global analysis is shown in figure 4-5. Increasing the stiffness means higher stresses are present in the cable than for a lower stiffness. Higher stresses result in a higher cumulative damage.

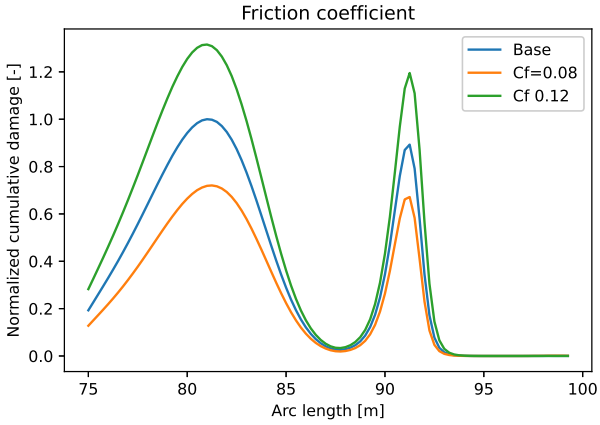

Figure 4-5: Damage along the DPC due to a variation in friction coefficient

Local analysis sensitivity

In the factor accounting for the sensitivity of the local analysis method, the resulting curvatures from the local model are varied. This is comparable to varying the calculated stiffness, as is discussed in section 4-1. In simulation 4, the curvatures are multiplied by 0.7, resulting in a stiffer cable. Similar to the effect of the friction coefficient, this results in a higher damage. For simulation 5 the stiffness is reduced, resulting in a longer fatigue life. Figure 4-6 shows the damage along the cable. Comparing this to figure 4-5, it can be seen that the damage is more vulnerable to the same variation in standard deviation. This is as expected, since the sensitivity of the local analysis method directly influences the stiffness, whereas for the friction coefficient, the stiffness is indirectly influenced as a result of more traction between the layers.

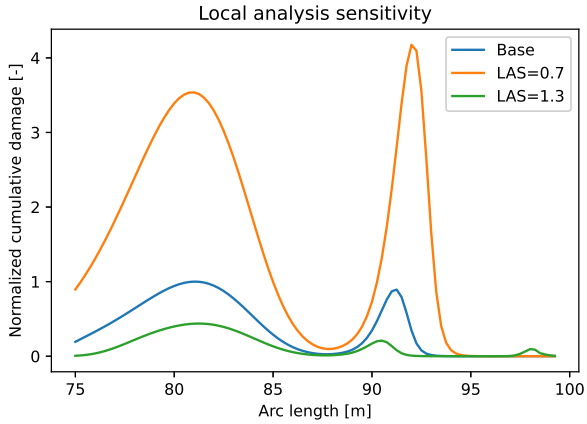

Figure 4-6: Damage along the DPC due to a variation in the local sensitivity

Soil stiffness

In section 3-3-1-2 the influence of the soil stiffness on the fatigue life at the touch down zone in illustrated. Due to a higher soil stiffness, a higher fatigue damage occurs. This same effect is seen in simulations 6 and 7. Simulation 6 has a lower soil stiffness than reference simulation 1, resulting in a lower fatigue damage. This holds vice versa for simulation 7, where the soil stiffness is higher than in simulation 1. The biggest effect of the variation in stiffness is on the seabed-induced peak (see figure 4-7). Interesting to note is that the fatigue damage is much more sensitive to a reduction in soil stiffness than to an increase in stiffness.

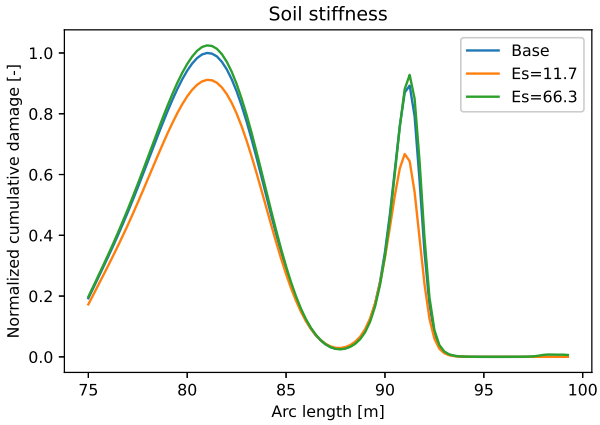

Figure 4-7: Damage along the DPC due to a variation in soil stiffness

Drag coefficient

In simulations 8 and 9 the drag coefficient for the dynamic power cable is decreased and increased respectively. Figure 4-8 shows the effect of the variation in drag coefficient. In line with logical reasoning, a higher drag coefficient, results in higher wave forces on the cable, resulting in higher fatigue damage. Supporting the statement that the left peak corresponds to wave induced fatigue, only the wave-induced peak in figure 4-8 is affected by the drag coefficient. This is more or less the opposite of what is seen for the soil stiffness.

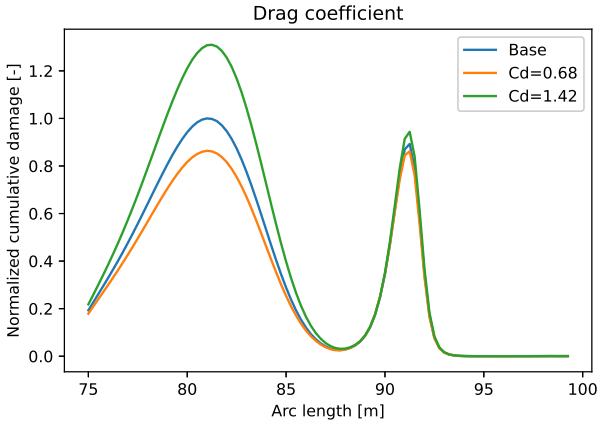

Figure 4-8: Damage along the DPC due to a variation in drag coefficient

Global analysis sensitivity

The last stochastic parameter used was the global analysis sensitivity, for simulations 10 and 11. The results for an increased sensitivity are straightforward. A higher uncertainty leads to higher stress, and thus a lower fatigue life.

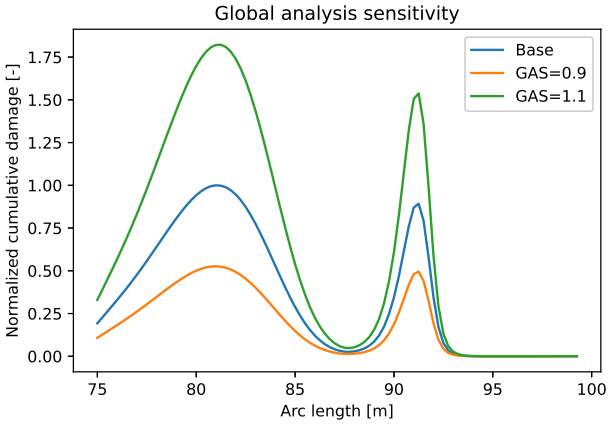

Figure 4-9: Damage along the DPC due to a variation in the global sensitivity

4-3 Reliability method

In the previous section, there is a clear distinction between the two visible peaks. It can be observed that different parameters have a different degree of influence on each respective peak. In order to get sensible results, it is important to make a clear distinction between the two peaks. Therefore, in this section results for the seabed-induced peak will be presented separately from the wave-induced peak.
Using the results from the global analysis, polynomial fits can be made, as described in section 2. As an example, the fit for the friction coefficient of the wave-induced peak is shown in figure 4-10, which can be observed to be close to linear. The full results of the polynomial fits are presented in appendix B. These fits are used in the First Order Reliability Method (FORM) analysis to evaluate the limit-state function at values other than the ones obtained from the Finite Element (FE) models. In appendix C the self written code used for the reliability analysis is presented.

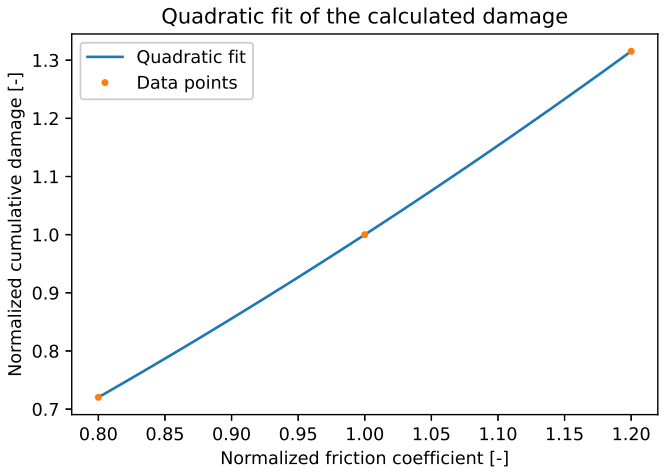

Figure 4-10: Polynomial fit for the friction coefficient of the left peak

In figure 4-11 the importance factors of both the wave-induced and seabed-induced peaks are shown. Comparison to the figures presented in the previous section can be made to judge the validity of the results of the FORM analysis. In figures 4-5 to 4-9, the influence of 2 times a standard deviation on the cumulative damage can be seen. The sensitivity of the local and global analysis models can clearly be identified as the most dominant. This is in line with figure 4-11, where these parameters are shown having the highest importance factors. Comparing figure 4-11a to 4-11b, it can be seen that the sensitivity of the local model is more dominant for the seabed-induced peak. This in turn corresponds to what is observed in figure 4-6.
The soil stiffness in figure 4-7 is showing little effect on the fatigue damage. This is also visible in the importance factors. It is in line with both figure 4-11 and 4-7 that the soil stiffness has a larger contribution on the uncertainty of the fatigue damage of the seabed-induced peak than on the wave-induced peak.
Vice versa, this holds for the drag coefficient. Figure 4-11a shows a significant contribution of the drag coefficient, in contrast with figure 4-11b, showing almost none. This corresponds

to the difference in peaks in figure 4-8.

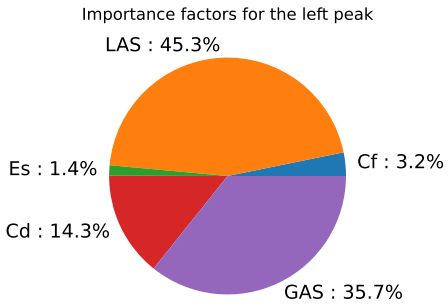

(a) Importance factors for the left peak

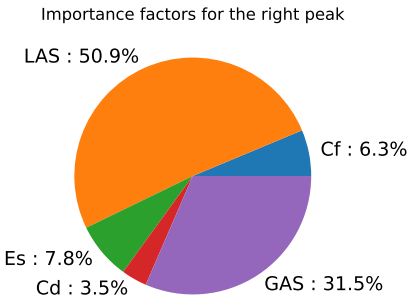

(b) Importance factors for the right peak

Figure 4-11: Importance factors from the FORM analysis

Having performed the FORM analysis, the effect of a Fatigue Safety Factor (FSF) can be investigated according to equation 4-1. By trying a number of different values for the FSF, and performing the FORM analysis, a continuous relation between the FSF and the Probability of failure (Pf) can be obtained.

$$g(\mathbf{X}) = 1 - \frac{D(\mathbf{X})}{FSF} \tag{4-1}$$

Again, the results are split up for the wave-induced and seabed-induced peaks, and are shown in figure 4-12, together with the probabilities of failure corresponding to the different safety classes, as prescribed by DNV [16].

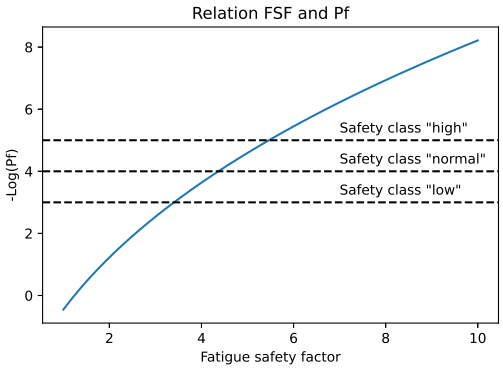

(a) FSF for the left peak

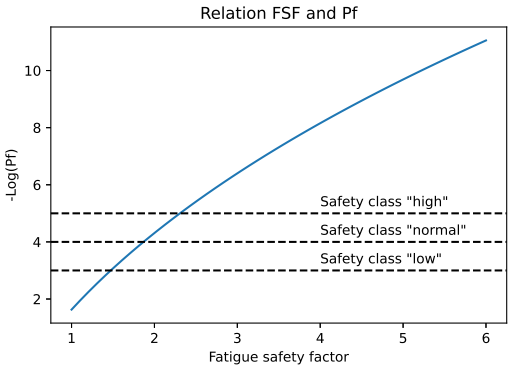

(b) FSF for the right peak

Figure 4-12: Relation between the fatigue safety factor and the probability of failure

From the results of the global analysis, it can already be seen that the wave-induced peak is the dominant peak, being more prone to fatigue failure. This can also be observed in figure 4-12, requiring a FSF of 3.5 to satisfy the low safety class, 4.4 for the medium one, and 5.5 for the high safety class. For the seabed-induced peak, the low safety class only needs a FSF

	Safety class		
	Low	Normal	High
	$Pf < 10^{-3}$	$Pf < 10^{-4}$	$Pf < 10^{-5}$
Wave-induced peak	3.5	4.4	5.5
Seabed-induced peak	1.5	1.9	2.3

Table 4-2: Required fatigue safety factor per peak per safety class

of 1.5, and the normal and high safety class are satisfied with a safety factor of 1.9 and 2.3 respectively. The full results are summarized in table 4-2.

The effect on the probability density function of the limit-state function can be seen in figure 4-13. Here the distance of the mean of the limit state function μ_g to the origin is denoted as $\beta\sigma_g$, which is the Hasofer-Lind (HL)-safety index multiplied by the standard deviation of the limit-state function. Because $\beta\sigma_g$ is the only thing changing, it is directly related to the probability of failure according to equation 4-2.

$$P_f = \Phi(-\beta) \tag{4-2}$$

Where Φ is the cumulative density function of the standard normal distribution.

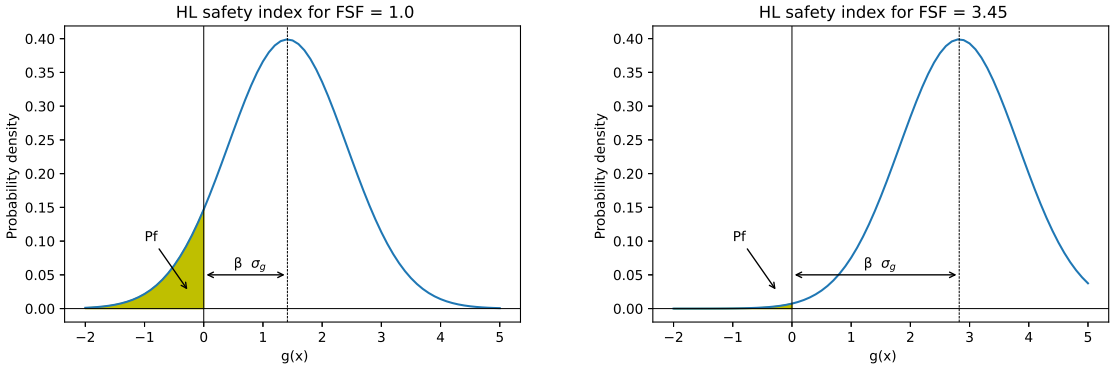

(a) Probability density function for FSF=1 **(b)** Probability density function for FSF=3.5

Figure 4-13: The effect on the probability density function of increasing the FSF

Chapter 5

Discussion

In this chapter, comparisons between the results presented in chapter 4 and available literature will be made. The goal is to judge how reliable the results presented are, and discuss what reason there is for any differences.

First, the evaluated importance factors will be discussed, and later on the evaluated fatigue safety factors.

5-1 Importance factors

The importance factors of the First Order Reliability Method (FORM) analysis for risers and umbilical are not widely discussed in the literature. Comparison will be made to [29] and [44], both discussing uncertainties in steel flexible pipes. Due to the different nature of the pipes, and the different choice in evaluated stochastic parameters, qualitative comparisons will be made, more so than quantitative.
In [29], stochastic parameters used in the analysis that are also used for the research in this paper are the drag coefficient, the sensitivity to the local analysis, and the sensitivity to the global analysis. Important to note is that for the drag coefficient, a different stochastic model is used, with a mean of 1.2 (instead of 1.05), and a standard deviation of 0.24 (instead of 0.175). All of the importance factors are shown in figure 5-1a. In this figure the importance factors that are also used in the research in this paper are emphasized, and plotted in an individual figure (5-1b) making for easier comparison.
The most interesting observations, about the matching importance factors, are that the drag coefficient is dominant in [29], and the sensitivity to the global analysis is almost negligible. In the case at hand, an analysis of a 1795m deep flexible riser is done. Due to the larger water-depth, combined with the inclusion of a current in the analysis, it is sensible that the drag coefficient plays a larger role. Unfortunately, very little detail about the scenario at hand is provided in the paper. Nothing is described about the riser configuration, what part is being evaluated, or how the sensitivity to the global model is being accounted for in the reliability analysis. The main conclusion that can be drawn from comparison to [29], is that

the local analysis method has a large influence on the uncertainty in the fatigue damage.

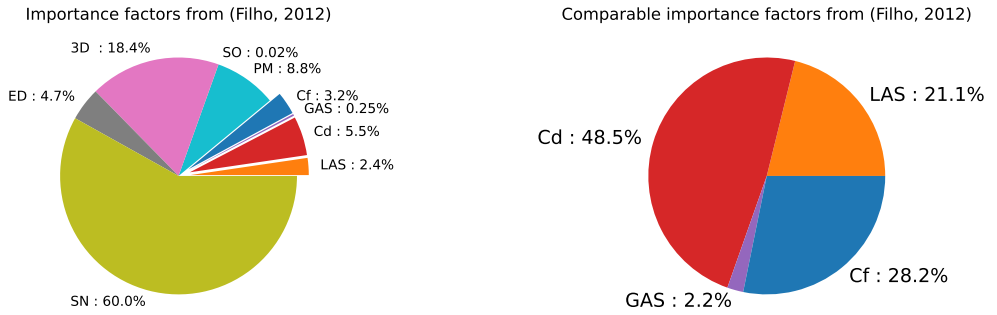

(a) All importance factors from [29] **(b)** Comparable importance factors from [29]

Figure 5-1: Importance factors from [29]

[44] evaluates two scenarios, for three different stochastic models. The first one focuses on the local stress analysis, the second one considers the global analysis, and in the third, the global and local sensitivities are combined, but eliminates the friction uncertainty.
Also here, other parameters are included in the model. For the sake of this discussion, the common parameters will be evaluated. These are the drag coefficient, the sensitivity to the local analysis , the sensitivity to the global analysis and the friction coefficient.
For the first case, the resulting importance factors are shown in figure 5-2. Here, a lazy-wave injection riser at 1450m water depth is being evaluated. Considering the shared importance factors, the sensitivity to the local model is observed as being dominant for both case one and three. The friction coefficient has a bit less than half the importance factor of the local sensitivity. In scenario two, when the local sensitivity to not being accounted for, the influence of the friction coefficient stays level, and factors having to do with the evaluation of the fatigue damage and the S-N curve become more dominant. Interestingly, the drag coefficient is not shown in the results by itself, meaning it has a contribution of less than 5%, and is grouped together with other parameters of little significance in the "others" group.

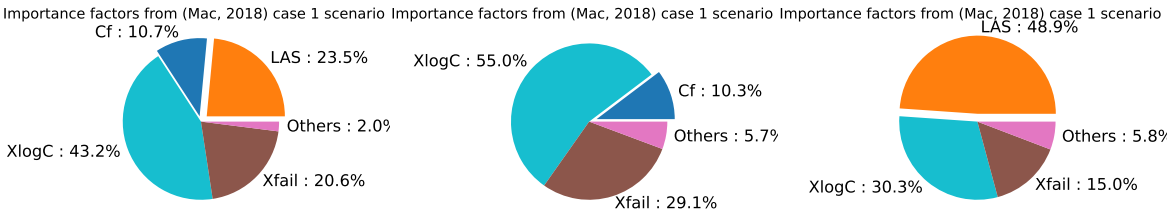

(a) Case 1 scenario 1 **(b)** Case 1 scenario 2 **(c)** Case 1 scenario 3

Figure 5-2: Importance factors from [44] case 1

Scenario 2, a pliant wave gas pipe at 395 meters water depth is considered. The importance factors for this scenario are shown in figure 5-3. Interesting to see here, making comparisons

to scenario 1, is that it seems like the shallower the water, the more significant the influence of the local analysis becomes. Furthermore, the sensitivity to the global model comes into play. Having no influence in the first scenario, in case 2 of the second scenario it accounts for almost 35% of the uncertainty. In scenario three, the global sensitivity is about one fourth of the local sensitivity.

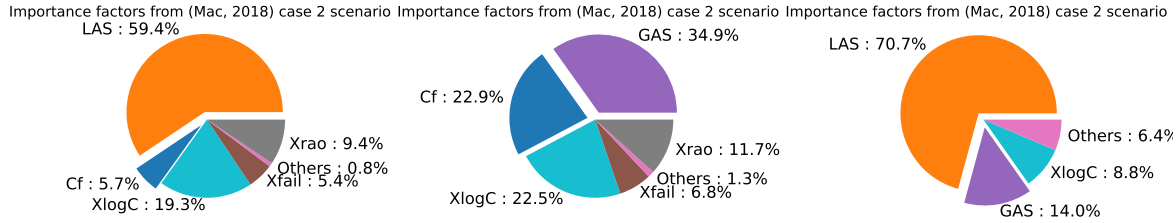

(a) Case 2 scenario 1 **(b)** Case 2 scenario 2 **(c)** Case 2 scenario 3

Figure 5-3: Importance factors from [44] case 2

Since the scenarios evaluated are so different from each other, no hard conclusions can be drawn from the above presented results. Yet, it is interesting to see that it seems like for shallower waters, the global and local analysis sensitivities become more important than the parameters having to do with damage evaluation. A possible explanation for this is that for shallower waters, the part of the loads induced by waves increases, since the effect of waves decreases for higher water-depths.
In summary, there seems to be somewhat of a consensus on the fact that the local analysis is very important, showing a large influence in both papers evaluated, as well as the case treated in this paper. Judging from the relation between water depth and the influence of the global analysis, it seems like the results presented for the global sensitivity in section 4 are following the trend found in the two papers. Friction is a bit harder to compare, since it is only considered in [44]. In the presented case study it always plays somewhat of a role, but definitely less than the local analysis sensitivity. The main point that remains is the effect of the drag coefficient, showing a significant contribution in [29], and being negligible in [44], despite both including a current in the analysis. Comparing this to the results from this paper, which are somewhere in between dominant and negligible, it is concluded that little consensus is to be observed about the importance of the drag coefficient.

5-2 Fatigue safety factor

The results for the Fatigue Safety Factor (FSF) are better documented than that of the importance factors. Again, only results for risers are found in the literature, belonging to a different safety class than power cables, but comparisons will be made to judge the results from chapter 4.
There are two interesting aspects to note about plots similar to figure 4-12. The value of the Probability of failure (Pf) at a FSF of 1, and the rate at which the Pf decreases as the FSF is increased. The former is an indication of the design life of a cable. For a cable designed for 30 years of service life, it is sensible that it would require a lower FSF than a cable designed for

20 years for a similar Pf in year 20. The latter indicates how sensitive the Pf is to a change in the FSF. For cables with a high degree of uncertainty, this slope will be gentle, whereas for cables with relatively little uncertainties in the fatigue life prediction, the slope will be steep.

[30] considers three different stages of operation of a riser at 300m. The cases of a dry annulus, a wet annulus with aerated water and a wet annulus with 10mbar H_2S are considered. The safety factors in their corresponding safety classes are shown in table 5-1. Comparing this to the results presented in this paper, it can be concluded that the riser has a longer fatigue life design than the Dynamic Power Cable (DPC), since it has a lower Pf for a FSF of 1 for all cases. Looking at the slope of the relation between the FSF and the Pf, the results for the DPC in this paper are comparable to that of the riser with a wet annulus with aerated water. Between every safety class there is an increase in the required FSF of around 1. For the dry annulus and the wet annulus with 10 mbar H_2S, a larger increase in the FSF is required to achieve the same decrease in the Pf, meaning a more gentle slope. What can be concluded from this, is that the presence of H_2S, or the absence of fluid in the riser increases the amount of uncertainty in the fatigue life prediction.

	Safety class		
	Low	Normal	High
	$Pf < 10^{-3}$	$Pf < 10^{-4}$	$Pf < 10^{-5}$
Dry annulus condition	1.10	2.80	6.10
Aerated water	1.45	2.45	3.75
10mbar H_2S	1.15	2.70	5.30

Table 5-1: Fatigue safety factors from [30]

5-3 Polynomial fits

In all of the literature consulted, three data points are used to make a quadratic fit for the normalized cumulative damage as a function of the normalized stochastic parameter. According to [30], the range between $\mu \pm 2\sigma$ "will cover the relevant variation range with a very high probability." In this section some attention is paid to the effect of using more than 3 data points in order to fit a polynomial.
In appendix B all of the quadratic fits are shown. The fits for the friction coefficient, the drag coefficient and the global analysis sensitivity all have a relatively low curvature, some could even be approximated as being linear. For the local analysis sensitivity and the soil stiffness this is not the case. The peak/valley of these parabolas can be observed to be in front of the last data point. This means that for the local analysis sensitivity, a lower value would give a higher damage. To check the effect of this possibly inaccurate polynomial fit, an extra simulation has been run, at $\mu_{LAS} + 4\sigma_{LAS}$. With this extra data point, two new polynomials can be plotted. Another quadratic fit using 4 data points, and a cubic fit.

Figure 5-4 shows these two plots, as well as the quadratic fit with N=3, for the wave induced peak, which has been used in this paper.

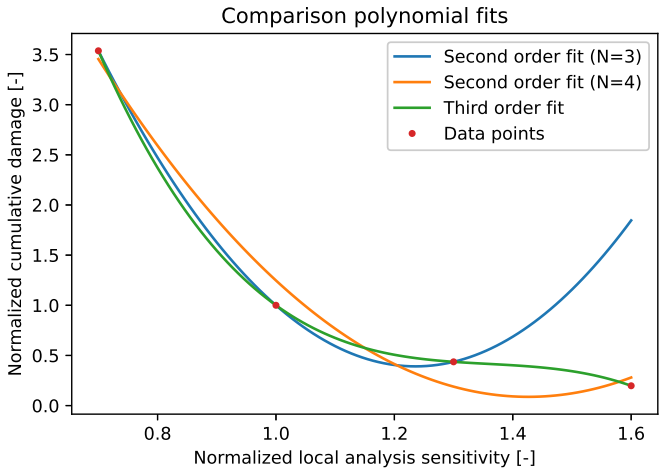

Figure 5-4: Comparison between a second and third order polynomial fit

It can be observed that for interpolation in the most occurring range ($\mu \pm 2\sigma$), already some deviations are present. For values outside this range, the quadratic fit with N=3 deviates from the other two fits significantly.
In order to really see the effect of these deviations, the FORM has been performed again, now also using the other two fits. Table 5-2 shows the effect on the required safety factors. It can be seen that for lower probabilities of failure, some difference in the results exists.

	Safety class		
	Low	Normal	High
	$Pf < 10^{-3}$	$Pf < 10^{-4}$	$Pf < 10^{-5}$
Second order fit (N=3)	3.4	4.4	5.5
Second order fit (N=4)	3.4	4.3	5.3
Third order fit (N=4)	3.4	4.4	5.6

Table 5-2: Fatigue safety factors calculated for different polynomial fits

In figure 5-5 the importance factors corresponding to the different polynomial fits are plotted. Interestingly the second order fit with N=3, and the cubic fit are almost identical, despite the big difference outside the $\mu \pm 2\sigma$ range. The second order fit with N=4 shows some more difference in the importance factors, having the local analysis sensitivity become less relevant, and the global analysis sensitivity becoming more dominant. This is in correspondence with the deviations observed in figure 5-4.

It can be concluded that $\mu \pm 2\sigma$ really does cover most of the variations, since the cubic fit and the quadratic fit with N=3 give almost identical results, despite deviating from each other between $\mu + 2\sigma$ and $\mu + 4\sigma$. The quadratic fit with N=4 already shows deviation inside $\mu \pm 2\sigma$, supporting the statement that most variations are covered in this range.

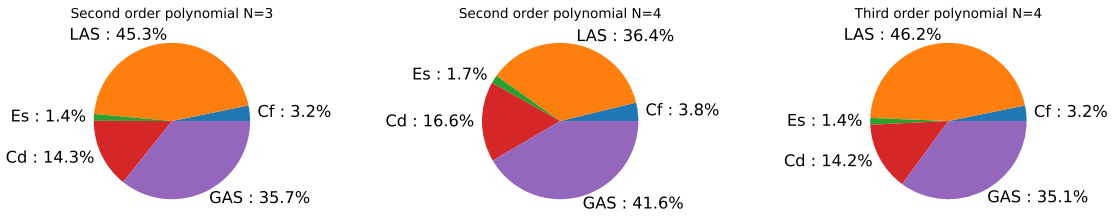

(a) Importance factors second order fit N=3

(b) Importance factors second order fit N=4

(c) Importance factors third order fit N=4

Figure 5-5: Importance factors for different polynomial fits

Chapter 6

Conclusion

In this section, first the main observations from the research will be discussed, aiming to provide concise answers to the research questions posed in section 1-4. Lastly, the validity of the results will be reflected on, looking back at the scope as defined in section 1-3.

6-1 Conclusions

The first point of attention was what a Fatigue Safety Factor (FSF) is, and what it is used for. Section 1-1-3 explain that due to uncertainties in the modeling of fatigue damage, safety factors are incorporated to account for this uncertainty. The higher the degree of uncertainty, the higher the safety factor needs to be. Since local stresses in dynamic power cables are dependent on many variables and complex interactions, there is a high degree of uncertainty in the evaluation of the fatigue damage.
It was found, that little to no effort has been made to identify what parameters are driving this uncertainty for dynamic power cables, and a value of 10 is adopted for the FSF. There is ambition from the industry to get a calibrated safety factor in order to reduce the Levelized Cost Of Energy (LCOE) of floating offshore wind. To facilitate this, DNV has set up a joint industry project focusing on reliability in floating offshore wind turbine design [13].

Next, a research into the evaluation methods for the FSF for comparable structures was done. Flexible risers and dynamic umbilicals, commonly used in the floating oil & gas sector, have close resemblance to dynamic power cables. For these structures, more effort has been made to calibrate a fatigue safety factor, and identify safety factor driving parameters. Two different methods are discussed in section 2-1. Both methods are said to be applicable to the analysis of other structures as well, but only one could be performed without the calibration of empirical constants [16]. For the sake of this research, is was deemed unfeasible to perform such a calibration. Despite the availability of methods to determine safety factors, it is interesting to see that standard values of 3, 6 and 10, as prescribed by DNV, still seem to be the standard. Seeing as the industry calls for calibrated safety factors for floating wind, it is

expected that calibration methods will have more impact in the floating wind sector.

Despite the resemblance between flexible risers/umbilicals and dynamic power cables, it would be presumptuous to say the results discussed in literature about the former can be directly applied to the latter. This is because, despite their similar appearance, there are two main differences between the cables used in the oil & gas sector, and the ones used in the offshore renewable sector.
Firstly, the dynamic excitation is different. Since oil rigs are different in size compared to floating wind turbines, they also have different responses to environmental loading. Moreover, due to their higher weight, oil rigs have lower natural periods than floating wind turbines. This means they likely have more low cycle stress ranges, as opposed to floating wind turbines, having more (relatively) high cycle stress ranges. Furthermore, the effect of wind plays a larger role on wind turbines. Due to the thrust load at hub height, an overturning moment is applied. Because of their height, this is a different kind of loading than an oil rig would experience.
Secondly, the cross-section is different. Risers are mostly hollow, to allow for the transportation of oil, and umbilicals are usually combinations of different wires and tubes. Due to this varying cross-section, components with different levels of stiffness are present. This causes stress concentrations to form in different locations. Moreover, umbilicals and risers may experience varying internal pressure, as a result of fluids being transported. This is an added parameter that is not at play in dynamic power cables.
So in summary, even though the analysis methods are comparable, the results most likely are not. Therefore, the methods from the oil & gas industry can be adopted and adapted to fit the case of dynamic power cables.

To demonstrate the implementation of the calibration of a FSF for a dynamic power cable, an adaptation of the reliability method from the literature is proposed in section 2. Here a local and global Finite Element (FE) model are set up to be implemented for a dynamic power cable.
To see the viability of the proposed method, a case study is conducted. For this case study, the aim is to provide a calibrated FSF, as well as identify what parameters are driving the safety factor. Details concerning the case are provided in section 3.
To answer what the required safety factor is for the studied case, a relation between the Probability of failure (Pf), and the corresponding safety factor is formed. This is done by evaluating the Pf for a number of different safety factors. The required safety factor can then be determined, based on the desired Pf. For this research, it was assumed that a Dynamic Power Cable (DPC) belongs in the safety category "low", meaning "failure implies insignificant risk of human injury and minor environmental and economic consequences"[15]. This category has a prescribed maximum probability of failure of 10^{-3} in the last year of service. This is commonly taken to be 20 years. The resulting FSF was 3.5, as opposed to the safety factor of 10, which is being recommended in [10]. This means that based on the parameters included in this research, a reduction by a factor of almost 3 is possible. Seeing as the cables are expected to account for almost 15% of the LCOE for floating offshore wind, this reduction in the FSF can have a significant influence on the economic feasibility of floating wind energy [20]. In section 5-2 two important observations about the relation between the FSF and the Pf are discussed. The first one being the value of the Pf at a FSF of 1. For the DPC

evaluated in this paper, the corresponding Pf is 0.078 (approximately 1/13). Comparing this to the risers evaluated in [30], it is a rather high Pf. This shows that the DPC was designed to have a fatigue lifetime close to 20 years. The slope of the relation between the FSF and the Pf is comparable to that of a riser filled with water, and steeper than that of a riser filled with H_2S or an empty riser. An important conclusion to be drawn from this, is that a lower degree of uncertainty is involved in the modeling of a DPC that in the modeling of a riser, for the parameters evaluated in this paper. This means that using the same safety factors for power cables as for risers leads to conservative results.

What can be concluded from the results about the importance factors, as well as the comparisons made in section 5-1, is that the local analysis model plays an important role in the uncertainty in the fatigue damage. In a lesser degree, the global analysis model is important. This is in line with comparable literature on the matter. Since the wave induced fatigue seems to be dominant for the cable, the soil stiffness has a negligible effect on the uncertainty of the fatigue damage. The third most important parameter is the drag coefficient, on which there does not seem to be a general consensus in the literature.
Conclusions for the industry to be drawn from these results are that detailed soil stiffness model will hardly influence the fatigue damage. Time and money that would be spent on this, is better put to use on the local stress analysis. Tailor made cross-sectional stress analysis software already exists, and this research goes to show that there really is an added benefit of having an accurate way of assessing local stress. It is important to validate these model results against test data, in order to be able to reduce the uncertainty in the fatigue life prediction. It can also be concluded that instead of relating the stress obtained from Orcaflex to an equivalent stress from Femap, which was deemed sufficiently accurate for the sake of this research, could have large consequences for the outcome of the predicted uncertainty in the fatigue life. A better way would be exporting a curvature and tension time series from the global model, and using that as input for the local model. Femap does not lend itself for these kind of operations so alternatives need to be looked at.
Lastly, the uncertainty in the drag coefficient is still up for debate. From comparing literature, there is a wide spread on how influential drag is. Since the drag is closely related to the marine growth on the cable, especially near the sea surface, a large variation can be expected over the lifetime. Either making a model that takes marine growth into account, or finding an efficient way of keeping the cables marine growth free can reduce the uncertainty here.

6-2 Reflection

For this research, being the first study looking into fatigue safety factors for dynamic power cables, a scope has been defined to be able to treat the subject at hand with adequate attention. In this section, the effect of the scope definition on the results will be discussed.

Firstly, the core of the cable has been left outside of the scope of this research. The implications of this are very dependent on what the main fatigue sensitive component will turn out to be. Based on currently available open literature, it is not possible to conclude if the core or the armoring is the most sensitive, or if it is case dependent.

Secondly, the environmental loading has been limited to wave loading. This implies that Vortex Induced Vibration (VIV) is not being considered. Effects of VIV are extensively discussed in literature, as well as ways to reduce/avoid it. In literature about the evaluation of Fatigue Safety Factor's (FSF's) for risers, VIV and wave-induced safety factors are often split up into two different analysis. This is done because different stochastic parameters are important for the two. Having performed both analysis, a most dominant loading type can be defined, of which the safety factor will be applied to the cable. Since here only wave-induced loading is being considered, it cannot be said with full confidence that this will be the real required safety factor, since VIV might be more dominant.

Thirdly, the chosen case largely effects the outcome of the research. For now, the case has been kept as simple as possible, in an attempt not to introduce components into the analysis about which assumptions need to be made. An example of this is a bend stiffener at the hang-off point. Because this is not included in the analysis, the touch-down zone has been investigated, not looking at stresses near the floater. Thus, results presented are not valid for the entire cable, but only for the investigated region. Moreover, a catenary shape is considered, so no floatation modules are included into the study. Looking at related literature, this is not the most common configuration.

Lastly, a limited number of stochastic parameters has been included. It was attempted to use parameters that were most interesting for power cables, not looking at, for example, parameters having to do with the uncertainties in the Miner's sum. This was done because these parameters have been discussed in literature before, and are not case specific. Due to the fact that parameters like this have been left out of the scope, and only 5 parameters have been included, other studies with more parameters, might show a higher degree of uncertainty.

The main take-away from this study is twofold. Firstly, it is expected that the calculated importance factors give a good idea of how significant the contributions of the individual parameters are in relation to each other. Since not all parameters are included, the presented importance factors are only part of the total uncertainty.
Secondly, it is important to realize that the value of the calculated FSF might be a bit optimistic due to the fact that simplifications have been made. However, the results do support that fact that adopting a safety factor of 10 from the oil & gas industry is not optimal. It goes to show that there is a need for a more elaborate, large scale research, in order to come up with a better founded recommend FSF.

Chapter 7

Further research

This chapter is split up into three sections. Each section discusses the potential further research of the associated part of the model.

7-1 Local model

In the local model, a simplified Dynamic Power Cable (DPC) has been modeled for this research. For further research, this model can be extended both in input parameters, output and validation.
For now only a bending moment has been applied. Since there will also be thermal loads in the cable, inclusion of this would be interesting. Commercial finite element software lends itself very well for this purpose, since heat transfer can be modeled using a similar set of equations as mechanical finite element equations. Furthermore, the inclusion of a detailed core is recommended. Both in order to see the effect of the core on the steel armor strands, as well as investigate stresses in the core itself.
As for the output of the local model, only bending stiffness was exported. This was the dominant parameter discussed in literature on the matter, but axial and torsional stiffness of course also play a role in the fatigue life. Another interesting effect is the coupling between axial tension in the cable, and the torsional and bending stiffness. Since tension in the armor layer changes the lay angle, also the bending stiffness will change. This is especially of interest in the hang-off region, where tension variations are most present.
Moreover, the validation of the model against a comparable dynamic power cable is required. For the lack of literature on the matter, the model has now been validated against a riser. To better calibrate the model, scale testing is necessary.
Lastly, it was shown that the accuracy of the local stress prediction is dominant on the uncertainty of the overall fatigue life of a cable. It is therefore deemed important to investigate the above mentioned points, to further reduce the uncertainty. Where commercial Finite Element (FE) software was used for this research, it is expected that tailor made cross-sectional analysis software will be more accurate in predicting these local stresses. For further research, the added value of software of this kind should be evaluated.

7-2 Global model

The global model can be extended in a variety of different ways to include more complexities. For now, the loading regime has been limited to wave loading only. For further research the effect of current and the inclusion of wind loads are recommended. The inclusion of current can help form a better understanding of the influence of the drag coefficient on the uncertainty of the fatigue life prediction.
In the literature there is a clear distinction between wave induced fatigue and Vortex Induced Vibration (VIV) induced fatigue. The same principle applied here to calculate a Fatigue Safety Factor (FSF) for wave induced fatigue, can be applied to calculate a safety factor for VIV induced fatigue, in order to see which of the two are driving in what scenarios.
The area of interest of this research was the touch-down zone, due to the lack of details available in the open literature about auxiliaries like bend stiffners and flotation units. In the design process of a DPC, when such details are available, the area in interest should be extended to provide a complete overview, covering the entire cable.
In order to get a more general FSF, not requiring one to be calculated for every new scenario, a wider range of configurations should be investigated. For now only a semi-submersible floater has been investigated, but Tension Leg Platform (TLP) or spar floaters can lead to different conclusions.

7-3 Reliability method

For the reliability method, the main point for further research is the inclusion of other parameters. For now literature study has come up with stochastic models for parameters that were of importance in the oil & gas industry, but more interesting would be the investigation of parameters specific for offshore renewable energy sources. Here one can think of the temperature in the cables due to friction and an electric current for example. This is varying depending on the wind conditions.
Furthermore, cross-validation between different parameters can be performed. For now it was assumed that all parameters are independent of one another, in line with similar studies in the literature. In further research this claim will need to to be (dis)proven.

Appendix A

Local results

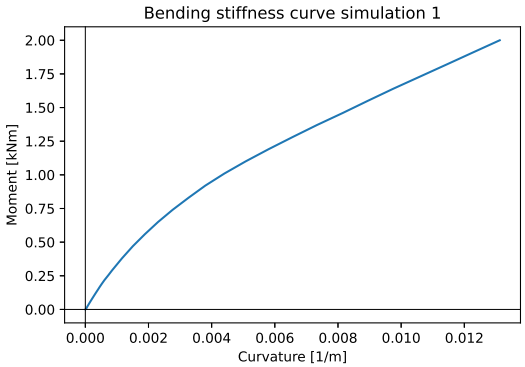

(a) Bending stiffness as obtained from Femap

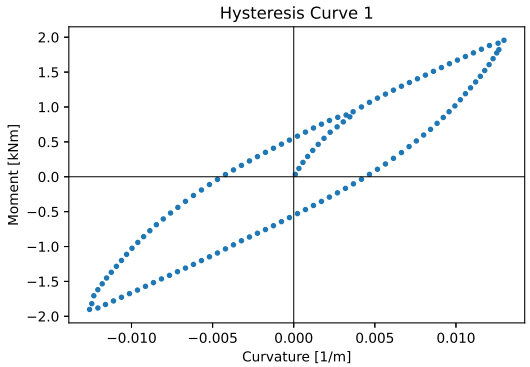

(b) Bending stiffness as read by Orcaflex

Figure A-1: Bending stiffness for simulation 1

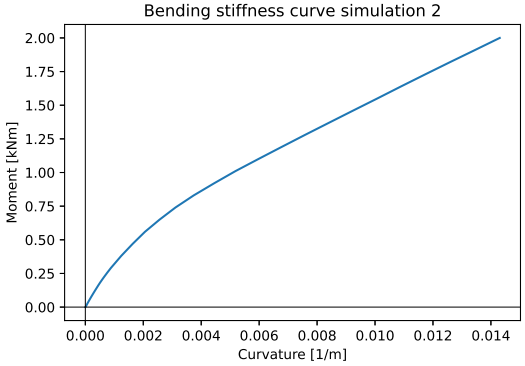

(a) Bending stiffness as obtained from Femap

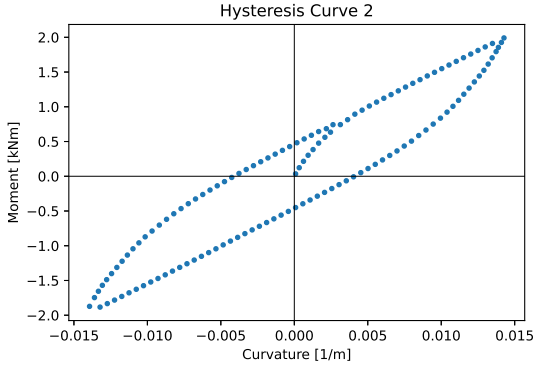

(b) Bending stiffness as read by Orcaflex

Figure A-2: Bending stiffness for simulation 2

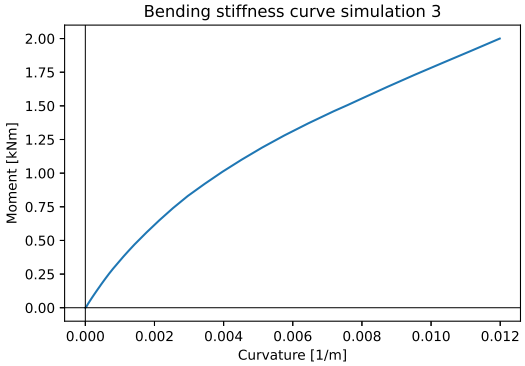

(a) Bending stiffness as obtained from Femap

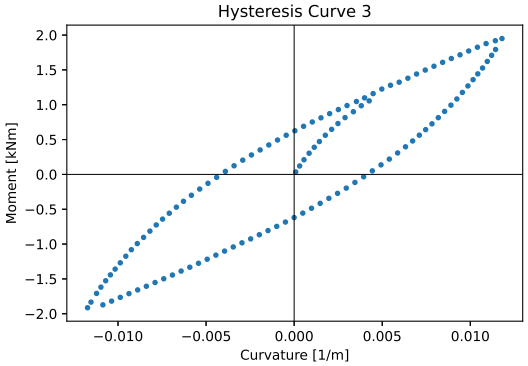

(b) Bending stiffness as read by Orcaflex

Figure A-3: Bending stiffness for simulation 3

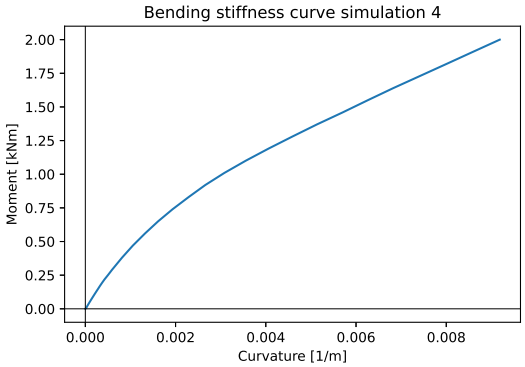

(a) Bending stiffness as obtained from Femap

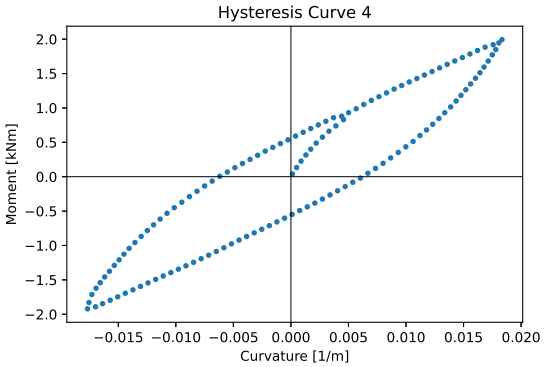

(b) Bending stiffness as read by Orcaflex

Figure A-4: Bending stiffness for simulation 4

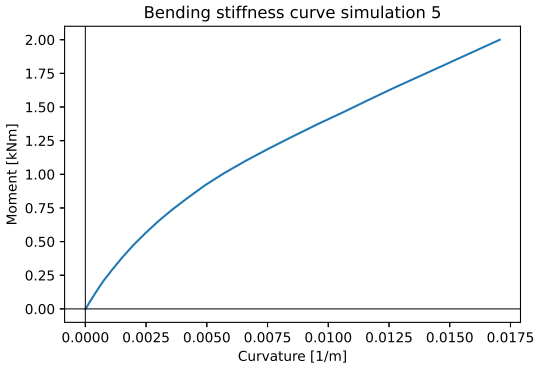

(a) Bending stiffness as obtained from Femap

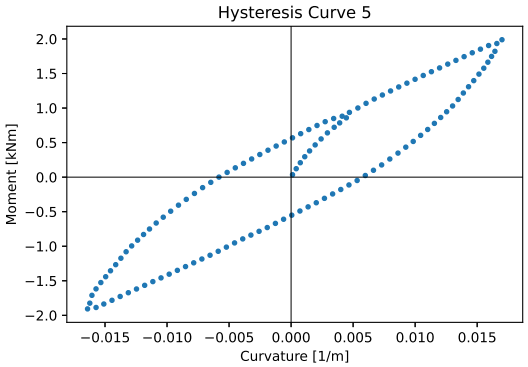

(b) Bending stiffness as read by Orcaflex

Figure A-5: Bending stiffness for simulation 5

Appendix B

Quadratic fits

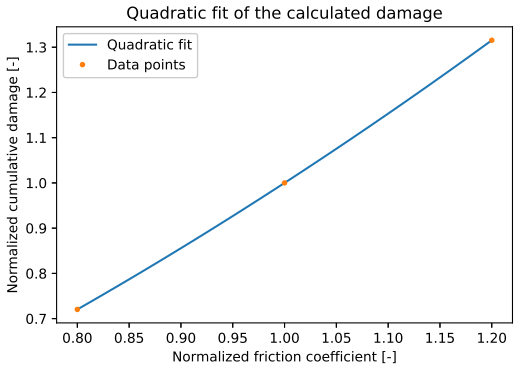

(a) Quadratic fit of the left peak

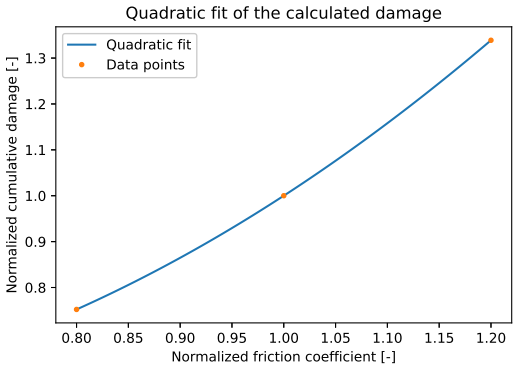

(b) Quadratic fit of the right peak

Figure B-1: Quadratic fit for the friction coefficient

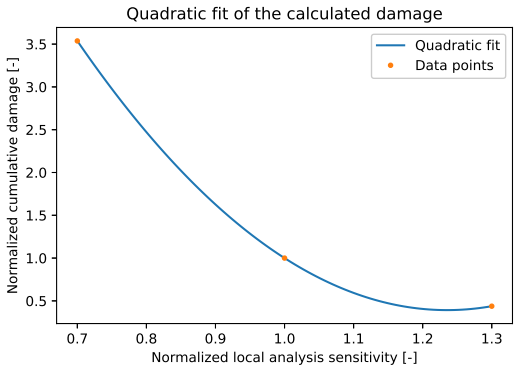

(a) Quadratic fit of the left peak

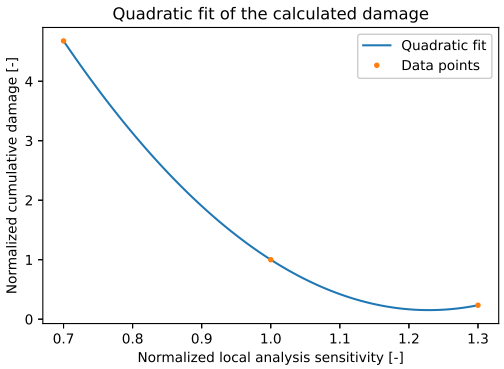

(b) Quadratic fit of the right peak

Figure B-2: Quadratic fit for the local analysis uncertainty

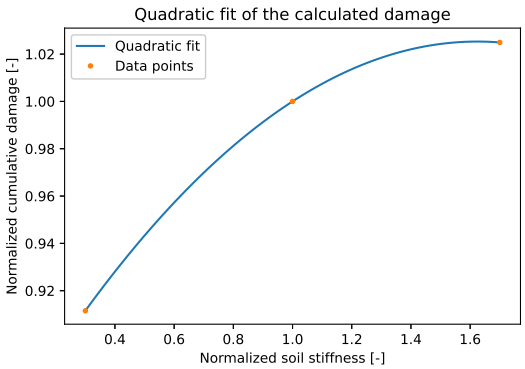

(a) Quadratic fit of the left peak

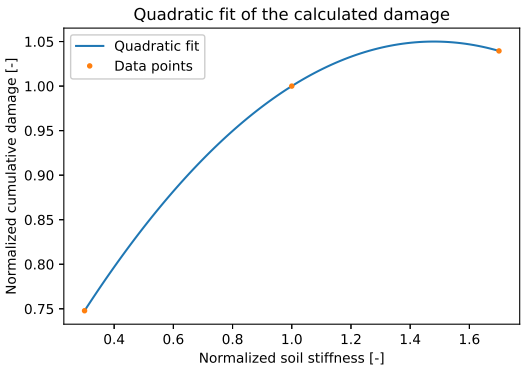

(b) Quadratic fit of the right peak

Figure B-3: Quadratic fit for the soil stiffness

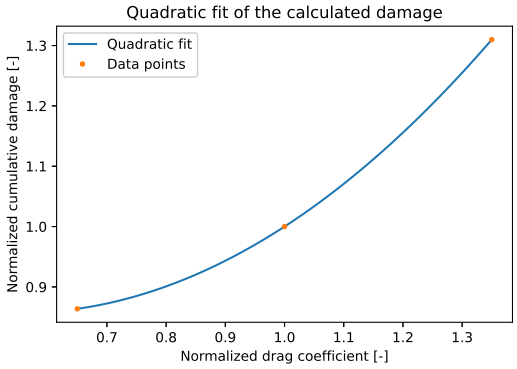

(a) Quadratic fit of the left peak

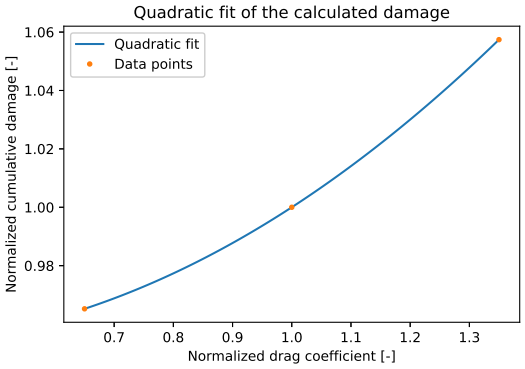

(b) Quadratic fit of the right peak

Figure B-4: Quadratic fit for the drag coefficient

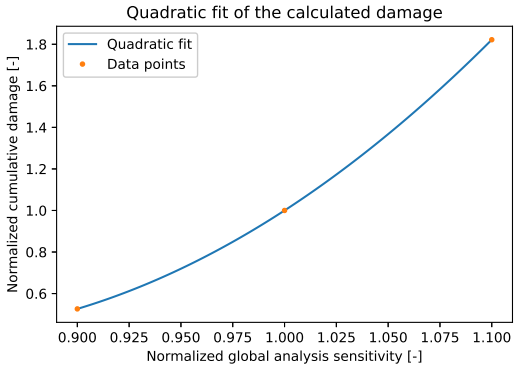

(a) Quadratic fit of the left peak

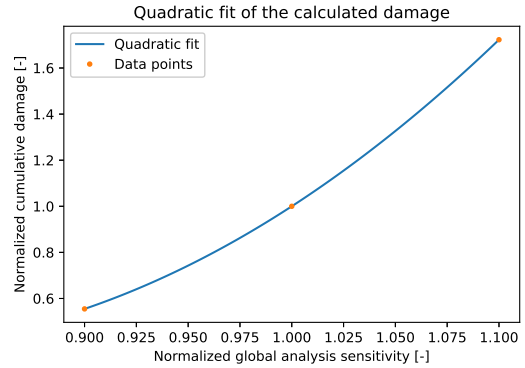

(b) Quadratic fit of the right peak

Figure B-5: Quadratic fit for the global analysis uncertainly

Appendix C

FORM code

C-1 Main

```
import numpy as np
import nDpolyfitCleaned
import pandas as pd
import FORMfun
import matplotlib.pyplot as plt


nVar=5 #Number of variables included in the analysis
LeftRightFull=1 #0 for left, 1 for right, 2 for full



#%% Read total damage for all 11 cases, for the left peak, the right peak and the maximum
FullDamage=pd.read_excel(r"C:\Users\OlivierdeJong\OneDrive - Mocean Offshore\Documenten\Olivier\Python\Form\FORM\DamageTable2.xlsx").to_numpy()[:,1:] #[3x11]

Damage=FullDamage[:,LeftRightFull]*10 #Damage for the peak of interest

#%% Define stochastic models [Mean, standard deviation, distribution type, abbreviation]
var1=[1, 0.1, 'LN', 'Cf']
var2=[1, 0.15, 'N', 'LAU']
var3=[1, 0.35, 'LN', 'Es']
var4=[1, 0.175, 'LN', 'Cd']
var5=[1, 0.05, 'N', 'GAU']

#%% Create df of all variables with distributions
listVar=[] #List containing Means, Standard deviations, Distribution type
```

```
27 for n in range(1,nVar+1):
28     templist=['var%s'%n]
29     data=globals()['var%s'%n]
30     templist.extend(data)
31     listVar.append(templist)
32 dfVar=pd.DataFrame(listVar)                                          #
       Convert list to pd. Dataframe
33 dfVar.columns=['variable', 'Mean', 'Std', 'Dist. type', 'VarName']  #Name
       the columns
34
35 Names=np.array(['Cf', 'LAS', 'Es', 'Cd', 'GAS'])
36
37 #%% Set up matrix with all combinations of variables used for the
       stochastic parameters
38 LSfun=np.zeros([nVar*2+1,nVar]) # [11x5] zeros matrix
39 for i in range(0,nVar):      #Fill with mean values
40     LSfun[:,i]=np.full((1,nVar*2+1),listVar[i][1])
41
42 stds=np.array([k[2] for k in listVar] )
43 for sig in stds: #Subtract and add 2*std add the required locations
44     ind=int(np.where(sig==stds)[0])
45     LSfun[2*ind+1,ind]=LSfun[2*ind+1,ind]-2*sig
46     LSfun[2*ind+2,ind]=LSfun[2*ind+2,ind]+2*sig
47
48 #%% Make limit state function interpretable for Python
49 Fullfit=nDpolyfitCleaned.nDpolyfitfun(dfVar, Damage, nVar)  #Coefficients
       2-11
50 temp=[]
51 for i in range(0,nVar):
52     Fullfit[i, 0]+='*'+str(Names[i])+'^2+'
53     Fullfit[i, 1]+='*'+str(Names[i])+'+'
54     temp.append('('+"".join(Fullfit[i,:])+')')
55     if i <4:
56         temp[i]+='*'
57
58 Fullformula="".join(temp)
59 Dx='('+Fullformula+')*20*'+str(Damage[0])
60
61 #%% Relationship FSF and Pf
62 listPf=[] # List containing probabilities of failure for different FSF
63 FSFs=np.linspace(1, 10, 10)
64 for FSF in FSFs:
65     print(FSF)
66     Gx='1-('+Dx+')/'+str(FSF)
67     Pf=FORMfun.FORM(Gx, Names.tolist(), FSF)
68     listPf.append(Pf)
69
70 #%% Plot relation FSF and Pf
71 plt.figure()
72 plt.title("Relation FSF and Pf")
73 plt.plot(FSFs, -np.log(listPf))
74 plt.axhline(y = 3, color = 'k', linestyle = 'dashed')
75 plt.text(4, 3.25, 'Safety class "low"')
```

```
76 plt.axhline(y = 4, color = 'k', linestyle = 'dashed')
77 plt.text(4, 4.25, 'Safety class "normal"')
78 plt.axhline(y = 5, color = 'k', linestyle = 'dashed')
79 plt.text(4, 5.25, 'Safety class "high"')
80 plt.xlabel('Fatigue safety factor')
81 plt.ylabel('-Log(Pf)')
```

C-2 Polyfit

```
1  import numpy as np
2  import pandas as pd
3  import matplotlib.pyplot as plt
4
5
6  def nDpolyfitfun(Var, Dx, nVar):
7      """
8      Function taking stochastim models, responses ot the limit-state
           function and the
9      number of variables, and returns quadratic fits for all parameters.
10
11
12     Parameters
13     ----------
14     Var     : Matrix containing [Means, standard deviations, distribution
           type, abbreviation]
15     Gx      : value of the limit state function evaluated at the means +-
           2std
16     nVar    : number of stochastic variables
17
18     Returns
19     -------
20     FullFit  : Linear regression object
21
22
23     """
24
25     df=pd.DataFrame({}) #Data frame containing the values used as input
           for the limit state function (means - 2std, mean, mean + 2 std)
26     for n in range(1,nVar+1):
27         temp=np.full((2*nVar+1), Var.at[n-1,'Mean'], dtype=float)
28         temp[n*2-1]-=2*Var.at[n-1,'Std']
29         temp[n*2]+=2*Var.at[n-1,'Std']
30         df['X%s'%n]=temp  #df containing all entries to the random
               variables,
31
32     df["g(x)"]=Dx
33
34     y, X = df["g(x)"],df.drop(["g(x)"], axis=1) #y contains values of g(x
           ) evaluated at X
35     names=['Friction coefficient', 'Local analysis uncertainty parameter'
           , 'Soil stiffness', 'Drag coefficient', 'Global analysis
           uncertainty']
```

```
36      #%% Fit polynomial
37
38      FullFit=np.zeros((5,3)).astype(str)
39      for i in range(0,nVar):
40          Xi=X.iloc[lambda X: [0, 2*i+1, 2*i+2],i].to_numpy()
41          yi=y.iloc[lambda y:[0, 2*i+1, 2*i+2]].to_numpy().astype(float)/y
                [0]
42          x=np.linspace(min(Xi),max(Xi),100)
43          modeli = np.poly1d(np.polyfit(Xi,yi, 2))
44          FullFit[i,:]=[str(i) for i in modeli.c]
45
46          # Plot polynomials
47          plt.figure()
48          plt.plot(x, modeli(x))
49          plt.plot([Xi[1], Xi[0], Xi[2]], [yi[1], yi[0], yi[2]],'.')
50          plt.legend(['Quadratic fit','Calculated damage'])
51          plt.xlabel(names[i])
52          plt.ylabel('Cumulative damage')
53          plt.title('Quadratic fit of the calculated damage')
54
55      return(FullFit)
```

Bibliography

[1] D. Young and O. Murphy, "Predicting dynamic subsea cable failure for floating offshore wind," 2018.

[2] R. Wiser, "Forecasting wind energy costs and cost drivers: The views of the world's leading experts," 2016.

[3] B. Fugløy and O. M. Akselsen, "Fatigue properties of corrugated sheathing for subsea power cables," 2017.

[4] T. Worzyk, "Submarine power cables: Design, installation, repair, environmental aspects (power systems)," 2009.

[5] R. Ross and W. S. Geurts, "Application of polyethylene sheath and swelling powder against water treeing," pp. 345–348, IEEE, 1998.

[6] "Recommendations for testing of long ac submarine cables with extruded insulation for system voltage above 30 (36) to 500 (550) kv," 2012.

[7] L. Resner and S. Paszkiewicz, "Radial water barrier in submarine cables, current solutions and innovative development directions," 2021.

[8] I. Lotsberg, "Fatigue design of marine structures," 2016.

[9] "Rainflow counting." https://community.sw.siemens.com/s/article/rainflow- counting. Accessed: 15-01-2022.

[10] "DNVGL-RP-F401 Electrical power cables in subsea applications ," standard, DNV GL, 2017.

[11] "ISO13628-5:2009 Petroleum and natural gas industries — Design and operation of subsea productionsystems Part 5: Subsea umbilicals ," standard, ISO, 2009.

[12] "IS0 13628-5:2002, Petroleum and natural gas industries-Design and operation of subsea production systems-Part 5: Subsea Umbilicals," standard, American Petroleum Institute, 2004.

[13] DNV, "Fow reliability joint industry project (jip) laying grounds for tomorrow's rules background and intro to jip scope," 2021.

[14] "DNVGL-ST-F201 Dynamic Risers ," standard, DNV GL, 2018.

[15] "DNV-OS-F101 Submarine Pipeline Systems," standard, DNV GL, 2012.

[16] "DNVGL-RP-F204 Riser fatigue," standard, DNV GL, 2017.

[17] "API17J API17J," standard, American Petroleum Institute, 2008.

[18] K. Mørk, "Enhanced risk based fatigue criterion," 2002.

[19] B. Stahl and H. Banon, "Fatigue safety factors for deepwater risers," 2002.

[20] M. Lerch, "Qualification of innovative floating substructures for 10mw wind turbines and water depths greater than 50m," 2019.

[21] "Experimental and finite element analysis of fatigue performance of copper power conductors," *International Journal of Fatigue*, vol. 47, pp. 244–258, 2 2013.

[22] "DNVGL-RP-C203 fatigue strength analysis of offshore steel structures," standard, DNV GL, 2001.

[23] M. Chezhian, D. Norske, V. Kim, M. Det, N. Veritas, N. S. Det, T. Stokka, M. Statoil, and B. Leira, "Risk based fatigue safety factors for deepwater risers," 2003.

[24] M. Chezhian, "Application of dnv-rp-f204 for determining riser viv safety factors," 2005.

[25] P. H. Wirsching and M. Asce, "Fatigue reliability for offshore structures," 1984.

[26] B. Leira, "Fatigue safety factors for flexible risers based on case specific reliability analysis," 2005.

[27] B. J. Leira, T. S. Meling, C. M. Larsen, V. Berntsen, B. Stahl, and A. Trim, "Assessment of fatigue safety factors for deep-water risers in relation to viv," *Journal of Offshore Mechanics and Arctic Engineering*, vol. 127, pp. 353–358, 11 2005.

[28] S. Choi, R. Grandhi, and R. Canfield, *Reliability-based Structural Design*. 2007.

[29] F. dos Santos Loureiro Filho and C. A. D. de Lemos, "Methodology for fatigue analysis in flexible pipes based on structural reliability considering s-n bi-linear curve," 2012.

[30] B. J. Leira, K. A. Farnes, R. T. Igland, J. M. Marintek, D. Percy, C. Lemos, R. Clements, and K. Nedrelid, "A framework for reliability-based fatigue safety factors for flexible risers," 2007.

[31] Siemens, "Simcenter femap: Siemens software."

[32] B. D. Edmans, D. C. Pham, Z. Q. Zhang, T. F. Guo, N. Sridhar, and G. Stewart, "An effective multiscale methodology for the analysis of marine flexible risers," *Journal of Marine Science and Engineering*, vol. 7, 10 2019.

[33] J. M. Leroy, T. Perdrizet, V. L. Corre, and P. Estrier, "Stress assessment in armour layers of flexible risers," vol. 5, pp. 951–960, 2010.

[34] J.-M. Leroy, Y. Poirette, and N. B. Dupend, "Assessing mechanical stresses in dynamic power cables for floating offshore wind farms," 2017.

[35] A. Bahtui, H. Bahai, and G. Alfano, "Numerical and analytical modeling of unbonded flexible risers," *Journal of Offshore Mechanics and Arctic Engineering*, vol. 131, pp. 1–13, 5 2009.

[36] J. Y. Li, Z. X. Qiu, and J. S. Ju, "Numerical modeling and mechanical analysis of flexible risers," *Mathematical Problems in Engineering*, vol. 2015, 2015.

[37] F. P. Nasution, S. Sævik, and J. K. Gjøsteen, "Finite element analysis of the fatigue strength of copper power conductors exposed to tension and bending loads," *International Journal of Fatigue*, vol. 59, pp. 114–128, 2014.

[38] "Orcaflex example files - simulation files amp; guidance documents," Jun 2019.

[39] Z. Tan, P. Quiggin, and T. Sheldrake, "Time domain simulation of the 3d bending hysteresis behaviour of an unbonded flexible riser," 2007.

[40] "Waveclimate from infoplaza." http://www.waveclimate.com/.

[41] J. R. M. D. Sousa, F. J. D. Sousa, M. Q. D. Siqueira, L. V. Sagrilo, and C. A. D. D. Lemos, "A theoretical approach to predict the fatigue life of flexible pipes," *Journal of Applied Mathematics*, vol. 2012, 2012.

[42] K. Bakken, "Fatigue of dynamic power cables applied in offshore wind farms," 2019.

[43] B. J. L. R. T and N. A. Y. E. Passano, "Fatigue safety factors for the tensile and pressure armours of flexible risers," 2007.

[44] D. H. Mac and P. Sicsic, "Uncertainties propagation within offshore flexible pipes risers design," vol. 213, pp. 708–719, Elsevier Ltd, 2018.

[45] 4COffshore, "Global offshore renewable map."

[46] "Offshore wind energy - draft sectoral marine plan: Regional locational guidance," Dec 2019.

[47] "DNVGL-RP-C205 environmental conditions and environmental loads," standard, DNV GL, 2014.

[48] P. R. Thies, L. Johanning, and G. H. Smith, "Assessing mechanical loading regimes and fatigue life of marine power cables in marine energy applications," vol. 226, pp. 18–32, 2 2012.

[49] M. Lynch, S. Doole, F. Borisade, F. Wendt, M.-A. Schwarzkopf, D. Matha, and L. R. S. Potestio, "corewind review of the state of the art of dynamic cable system design," 2020.

[50] E. Wong and W. Chin, "Certification of approval a study on the fatigue assessment of offshore steel catenary riser," 2016.

[51] Y. Yuan, M. Zheng, H. Xue, Z. Duan, and W. Tang, "Fatigue analysis of a steel catenary riser at touchdown zone with seabed resistance and hydrodynamic forces," *Ocean Engineering*, vol. 244, 1 2022.

[52] NKT, "World's first dynamic hv cable system."

[53] KOWL, "Kincardine offshore windfarm project cable plan kincardine offshore windfarm project," 2020.

[54] P. Group, "66 kv submarine cable systems for offshore wind."

[55] "Wire rope: Dry: Steel core: 10 mm."

[56] E. Gaertner, J. Rinker, L. Sethuraman, F. Zahle, B. Anderson, G. Barter, N. Abbas, F. Meng, P. Bortolotti, W. Skrzypinski, G. Scott, R. Feil, H. Bredmose, K. Dykes, M. Shields, C. Allen, and A. Viselli, "Definition of the iea wind 15-megawatt offshore reference wind turbine," 2020.

[57] C. Allen, A. Viselli, H. D. A. Goupee, E. Gaertner, N. Abbas, M. Hall, and G. Barter, "Definition of the umaine volturnus-s reference platform developed for the iea wind 15-megawatt offshore reference wind turbine," 2020.

[58] X. Bai, W. Huang, M. A. Vaz, C. Yang, and M. Duan, "Riser-soil interaction model effects on the dynamic behavior of a steel catenary riser," *Marine Structures*, vol. 41, pp. 53–76, 4 2015.

[59] X. Liu, G. Chen, J. Fu, J. Ji, Q. Song, and Y. Chang, "Analysis on the operation fatigue of deepwater drilling riser system," *Open Petroleum Engineering Journal*, vol. 9, pp. 279–287, 12 2016.

Glossary

List of Acronyms

FSF	Fatigue Safety Factor
FSF's	Fatigue Safety Factor's
CAPEX	Capital Expenditure
DPC	Dynamic Power Cable
DPC's	Dynamic Power Cable's
VIV	Vortex Induced Vibration
LCOE	Levelized Cost Of Energy
AC	Alternating Current
DC	Direct Current
FOSM	First Order Second Moment
FORM	First Order Reliability Method
SORM	Second Order Reliability Method
HL	Hasofer-Lind
MPP	Most Probable Point
RF	Rackwitz-Fiessler
FE	Finite Element
LCF	Low Cycle Fatigue
HCF	High Cycle Fatigue
XLPE	Cross-Linked Polyethylene
TLP	Tension Leg Platform
Pf	Probability of failure
Hs	Significant Wave-height
Tp	Peak Period
JONSWAP	Joint North Sea Wave Project